國立交通大學

應用化學研究所

博 士 論 文

高分子電解質中相行為，作用力機制以及

離子導電度之研究

Investigating Miscibility Behavior, Interaction Mechanisms and

Ionic Conductivity of Polymer Electrolytes

研 究 生：邱俊毅

指導教授：張豐志　教授

中 華 民 國 九 十 四 年 九 月

高分子電解質中相行為，作用力機制以及離子導電度之研究

Investigating Miscibility Behavior, Interaction Mechanisms and

Ionic Conductivity of Polymer Electrolytes

研 究 生：邱俊毅　　　　　Student：Chun-Yi Chiu

指導教授：張豐志　　　　　Advisor：Feng-Chih Chang

國 立 交 通 大 學

應用化學研究所

博 士 論 文

A Dissertation

Submitted to Department of Applied Chemistry

College of Science

National Chiao Tung University

in partial Fulfillment of the Requirements

for the Degree of

Doctor of Philosophy

in

Applied Chemistry

September 2005

Hsinchu, Taiwan, Republic of China

中華民國九十四年九月

高分子電解質中相行為，作用力機制以及離子導電度之研究

學生：邱俊毅　　　　　　　　　　　　　指導教授：張豐志 教授

國立交通大學應用化學研究所博士班

摘　　　要

近年來，高分子電解質（polymer electrolytes）一直被廣泛的研究，因其同時具有離子導電度與良好的機械性質，可以被應用於離子傳導之電子元件中。然而，完全固態（all-solid-state）的高分子電解質卻受限於低的離子導電度（ionic conductivity），而無法商業化。為了改善此一缺點，許多研究常會添加無機材料或是合成新結構之高分子主體，藉以提高高分子電解質的導電度，但是室溫下所得之離子導電度（$<10^{-4}$ S cm^{-1}）卻不盡理想，而無法實際應用於鋰電池（lithium battery）中。在致力於提高導電度的同時，往往忽略了探討離子傳導機制的重要性；在遭遇此種瓶頸時，我們必須轉向更基礎的研究討論，進一步去瞭解高分子主體與鹽類間複雜的作用力情形，從分析過程中，尋求改良離子導電度之途徑。因此，在本篇論文中，我們將藉由熱微分掃瞄卡計（DSC）、紅外線光譜儀（FTIR）、固態核磁共振光譜（Solid-state NMR）以及交流阻抗分析儀（ac Impedance）等儀器，觀察固態高分子電解質中，高分子相容行為（miscibility behavior）與高分子—鹽類間作用力機制（interaction mechanisms）對離子導電度之影響。而本論文可以分為三部分來討論：

(1) 由於 poly(ethylene oxide)（PEO）具有結構上的優勢，可幫助鹽類解離進而傳導離子，因此廣泛地應用於高分子電解質中。然而 PEO 中存在著高度結晶，會侷限離子傳導路徑，造成室溫的離子導電度極差。因此，我們加入

poly(ε-caprolactone)（PCL），藉由 PEO 與 PCL 間強大的相容性，降低 PEO 本身的結晶度，以提高離子導電度。

(2) 根據上述的研究結果得知，PEO 與 PCL 間高分子摻合的相容性極佳，因此可以預期 PEO-*b*-PCL 嵌段共聚高分子（ monomethoxypoly(ethylene glycol)-*block*-poly(ε-caprolactone) block copolymers）具有更佳的相容性，更有助於 PEO 結晶的破壞，而達到提高離子導電度之效果。

(3) 由於poly(methyl methacrylate)（PMMA）及poly(vinyl pyrrolidone)（PVP）均可做為高分子電解質中傳導離子的媒介，然而此兩種高分子分別有缺陷存在，使得它們在離子導電度的表現有所限制。所以，我們將擷取雙方面的優點，聚合PVP-*co*-PMMA無規則共聚高分子（poly(vinyl pyrrolidone-*co*-methyl metharcylate) random copolymers），並加入LiClO$_4$（lithium perchlorate）組成高分子電解質系統，藉由探討其間複雜的作用力，觀察離子導電度的改變情形。當PVP分子的存在時，其分子鏈上擁有高極性的官能基，可幫助鹽類解離；另一方面，PMMA分子的加入，可破壞PVP分子間強大的偶極—偶極力（dipole-dipole interactions）。上述兩種因素，均反映在離子導電度的提升。

Investigating Miscibility Behavior, Interaction Mechanism and Ionic Conductivity of Polymer Electrolytes

Student: Chun-Yi Chiu   Advisors: Dr. Feng-Chih Chang

Institute of Applied Chemistry
National Chiao Tung University

ABSTRACT

Solid state materials that exhibit high ion transport properties are of interest from both academic as well as applied points of view. Polymer electrolytes are materials of high technological perspective in several electrochemical applications. However, lithium-based polymer electrolytes exhibit several disadvantages that affect the commercialization of such cell; one major drawback is the low ionic conductivity of the electrolyte at ambient temperature. Although great efforts to enhance ionic conductivity have been made over the last 20 years, levels of ionic conductivity are persistently limited to a ceiling of around 10^{-4} S cm^{-1} at room temperature, which is insufficient for many lithium battery applications. In the face of such barriers in science, we must direct our attention to the fundamental research of polymer electrolytes, such as the complicated interaction mechanisms within the polymer electrolytes. In this study, therefore, we focused on investigating the effect of miscibility behavior and interaction mechanisms on ionic conductivity of polymer-salt complexes by means of differential scanning calorimetry (DSC), Fourier transform infrared (FTIR), solid-state ^{7}Li NMR, and alternating current (ac) impedance. The experimental work in this dissertation was divided into three sections as follows:

(a) The addition of poly(ε-caprolactone) (PCL) into poly(ethylene oxide) (PEO)-based electrolytes tends to suppress the crystallization of PEO due to the strong interaction between PEO and PCL, thus resulting in the increase of ionic conductivity for LiClO$_4$/PEO/PCL ternary blend systems-based polymer electrolytes.

(b) According to the above research, we subsequently synthesized monomethoxypoly(ethylene glycol)-*block*-poly(ε-caprolactone) (MPEG-*b*-PCL) block copolymers and studied the miscibility behavior based on polymer electrolytes consisting of LiClO$_4$ and MPEG-PCL. It is reasonable to us to expect that MPEG-PCL may be more miscible than the PEO/PCL binary blend.

(c) In the third part, we discussed the interaction mechanisms within the polymer electrolytes composed of LiClO$_4$ and poly(vinyl pyrrolidone-*co*-methyl methacrylate) (PVP-*co*-PMMA) random copolymers. The incorporation of MMA moiety tends to play an inert diluent role to reduce the self-association of PVP molecules. The more fraction of dissolved "free" ClO$_4^-$ of LiClO$_4$/PVP-*co*-PMMA blends can be detected than that of LiClO$_4$/PVP. Therefore, this factor is responsible for the observed increase in ionic conductivity of LiClO$_4$/PVP-*co*-PMMA blend.

ACKNOWLEDGEMENT

驪歌輕唱，轉眼間我的學生生涯即將畫上休止符。

回想大學畢業初期，似乎以為自己會得很多，然而，進入研究所後，讀得愈多，才愈發覺自己的渺小。四年多的研究生活，雖嫌匆促卻很充實，使我獲益良多，不僅豐富了我的學識，導正了我學習的態度以及研究的精神，更藉由實驗室的群體生活習得許多為人處事的道理。

在我的研究生涯裡，首先要感謝我的恩師，張豐志教授。感謝張老師在我大三下時，給我做專題的機會，讓我能順利甄試上應用化學所，並且進入張老師實驗室，在培養研究興趣的同時，更幸運的能在本實驗室逕讀博士班。張老師的學識淵博，在我研究遭遇瓶頸時，總能適時的給予我寶貴的意見，不厭其煩的指導我的論文及研究方向，並鼓勵我勇往直前；張老師亦提供良好的實驗環境，充裕的研究經費，於實驗上較能得心應手。另外，在張老師的帶領下，讓我培養「自動自發，積極進取」的研究精神，並深刻的體悟到，做學問，除了書本及老師能給的之外，更是需要靠自己努力探索得到的，也印證了一句俗語：「師父領進門，修行在個人」。

其次，特別感謝陳憲偉博士，謝謝學長從我專題生開始即引導我進入實驗室，在學長熱情及細心的教導下，使我習得實驗的技巧和數據分析的方法，奠定了我往後的研究基礎。此外，除了學術上的傳承，學長也常分享他人生的體會與處事的態度，並告誡我人生要有明確的目標。由於學長不遺餘力的教導和照顧，更加深我繼續攻讀博士班的決心。同時，我亦要感謝郭紹偉、黃智峰、蘇一哲與陳文億等學長，感謝你們在我論文的研究過程中，給予我許多寶貴的經驗，讓我少走了許多冤枉路。另外，我要感謝我的口試委員，中山大學蘇安仲教授，成功大學陳志勇教授，清華大學何榮銘教授，交通大學林宏洲、吳建興教授，台灣大學謝國煌教授，萬能科技大學黃介銘教授，台灣科技大學李俊毅教授，由於您們悉心的指教，並提供珍貴且精闢的意見，使得本論文更臻於完善。

再者，感謝我的同窗林振隆同學和葉定儒同學，同時也順便恭喜你們，大家

能一起畢業。感謝你們的陪伴，有你們一起互相扶持，四年的研究生活我們一路走來，雖然辛苦，卻不孤獨，這種能彼此砥礪，一起努力的感覺真的很好。林振隆同學更是和我從大學時期一直到研究所的好友兼室友，這難得的緣分很值得珍惜，更難得的是，我們竟然還能在同一個公司打拼（該說這是孽緣嗎？）；一直很欣賞你追求完美的態度，不得不鞭策自己向你看齊，讓我也能以嚴謹的態度從事研究。而葉定儒同學，長久的相處下來，總是覺得你沒什麼脾氣，人很好，拜託你的事很少拒絕，你樂觀進取的人生觀，亦是值得我學習的地方；你選擇了盡國民的應盡義務，所以在這裡先祝你當兵順利。

感謝婉君學妹兩年多的陪伴，有妳在身旁的鼓勵，不時的督促我積極認真，陪我分享快樂與悲傷，成為我努力的原動力，不管歡笑或是淚水，雖然，我銘感於心，我即將離開實驗室，未來還請妳多照顧自己。還有嚴英傑和徐文合學弟，感謝你們於實驗上的鼎力相助，我才能順利的完成實驗。

李欣芳、詹師吉和董寶翔學妹，感謝妳們帶來的歡樂，為苦悶的研究生活增添一股樂趣；還有實驗室其他同學，吳忠錫、鄭凱方、詹家明、詹嘉豪、王志逢、杜成偉、林漢清、賴芷伶、傅懷廣、辜佩儀、呂居樺、王怡婷、廖春雄，感謝你們對實驗室的付出，讓我們有良好的實驗環境。

當然還有我的大學好友，焙蓀、曜杉、智凱、震宇、怡翔、豪志、軍浩、衷核、志楠、昶慶，有你們陪我一起玩耍、嬉鬧，讓我在苦悶的研究生活之餘，得以放鬆自己的思緒，祝你們出社會的工作順利，還在當學生的，順利完成學業。

最後，由衷的感謝我的父母、姊姊和哥哥，謝謝你們在我求學過程中永遠給我最大的支持與鼓勵，讓我能沒有後顧之憂，專心完成學業，僅以此論文，獻給我親愛的家人。

鳳凰花開，學校生涯雖暫告一個段落，但出社會後，將是一個嶄新的體驗等著我去挑戰，期許自己能勇敢面對。

<div align="right">俊毅　于交大　94.9.13</div>

CONTENTS

Chapter 4 Miscibility Behavior and Interaction Mechanisms of Polymer Electrolytes
Comprising LiClO$_4$ and MPEG-*block*-PCL copolymers

LIST OF SCHEMES

LIST OF TABLES

XI

LIST OF FIGURES

CHAPTER 1

Introduction

Rechargeable Li-ion cells are key components of the portable, entertainment, computing and telecommunication equipment required by today's information-rich, mobile society. Despite the impressive growth in sales of batteries worldwide, the science underlying battery technology is often criticized for its slow advancement. A battery is composed of several electrochemical cells that are connected in series and in parallel to provide the required voltage and capacity, respectively. Each cell consists of a positive and a negative electrode separated by an electrolyte solution containing dissociated salts, which enable ion transfer between the two electrodes. Once these electrodes are connected externally, the chemical reactions proceed in tandem at both electrodes, thereby liberating electrons and enabling the current to be tapped by the user. The amount of electrical energy, expressed either per unit of weight (W h kg^{-1}) or per unit of volume (W h l^{-1}), that a battery is able to deliver is a both of which are linked directly to the chemistry of the system. Among the various existing technologies (Figure 1-1), Li-based batteries, because of their high energy density and design flexibility, currently outperform other systems, accounting for 63 % of worldwide sales values in portable batteries. This explains why they receive most attention at both fundamental and applied levels.

Solid electrolytes comprise a widely varied set of materials in which the ionic conductivity σ is far higher than that of typical ionic solids such as NaCl. The conductivity of typical solid electrolytes lies in the range ($10^{-6} \leq \sigma \leq 10^{-1}$ S cm^{-1}) characteristic of dilute aqueous ionic solutions. Solid electrolytes include refractory covalent solids such as β-alumina [(Na$_2$O)$_x$ · 11Al$_2$O$_3$] [1,2], soft ionic crystals such as AgI [3-5], glasses such as Ag$_2$GeSe$_3$, and among the most recently discovered and

investigated species, polymer-salt complexes.

Within the past 3 decades, the area of electroactive polymers has become one of the most challenging and fruitful realms of polymer science. Both electronically conductive polymers and polymeric electrolytes have been prepared and studied in a large number of laboratories, and a good deal of both synthetic and mechanistic knowledge about these new polymer materials bas been gained. While these species share some of the properties of more usual conductive systems such as metals, semiconductors, and ionic solutions, the polymeric structure provides a new set of conditions, so that a number of new features appear in the electrical response. Generally ionic conduction is associated with liquids, either solvents with high dielectric constants or molten salts. However, solids that can function as electrolytes also known as solid ionic conductors, fast ion conductors or solid electrolytes are exciting because of their wide ranging applications such as gas sensors [6,7], electrochemical display devices [8,9], high temperature heating elements [10], intercalation electrodes [11], power sources [12], fuel cells [13], solid state high energy density batteries [6,14] and so on.

In general, desirable battery properties are: energy content per unit volume and weight, discharge and charge characteristics at different rates and temperature, internal resistance, Ah and Wh efficiency, charge retention, life and mechanical stability. If not all most of these properties depend on the electrolytes that a battery is made up of. The choice of electrolyte for rechargeable batteries is governed by the following characteristics: (1) the electrolyte has to have negligent electronic conductivity (to prevent short circuiting) and favorable ionic conductivity, (2) the electrolyte should have a uni ion conduction, otherwise a concentration polarization in the cell may result, (3) the electrolyte must be electrochemically stable at least in the working potential range of the battery, (4) the electrolyte apart from being thermally

stable should be compatible with other cell components. A recent review summarizes the progress in ceramic solid electrolytes in general and Li^+ conducting solid electrolyte in particular. Table 1-1 categorizes the classes of solid electrolytes that have been extensively investigated. The classification is subjective; a number of intermediate situations occur and still other solid electrolytes do not fit into any of these categories.

According to Figure 1-2, the electrolyte serves as a medium to transport the ions involved in the charging/discharging cycle of the cell. In addition, a separator has to isolate the anode from the cathode electronically. While ceramic or polymeric separators have to be placed between the electrodes when liquid electrolytes are used, both functions, ion conduction and separation, can be realized in a single thin membrane when polymer electrolytes are used.

1-1 CONCEPT OF SOLID POLYMER ELECTROLYTES

Polymers that function as solid electrolytes (SPEs) are a subclass by themselves and are known as polymer electrolytes [15,16]. Besides the advantage of flexibility, polymers can also be cast into thin films and since thin films while minimizing the resistance of the electrolyte also reduces the volume and the weight, use of polymer electrolytes can increase the energy stored per unit weight and volume. In view of these attractive features, there has been considerable focus in recent years on the development of both inorganic and organic polymers as electrolytes for ion transport. In spite of the attractive features of conventional solid electrolytes in various applications, one of the main difficulties in their use in all solid state batteries is the loss of contact between electrodes and electrolyte during the charge-discharge-charge cycles of the battery. This is primary as a result of dimensional changes occurring at the electrodes during the charging or discharging mode. With conventional liquid

electrolytes such dimensional changes in the electrodes do not pose a problem, but with solid electrolytes, this leads to a loss of interfacial contact between the electrode and the electrolyte. In order to overcome this difficulty, batteries have to be operated at high temperatures so that the electrodes are molten. Alternatively the solid electrolyte should be a material that is flexible and therefore can deform with the electrodes to suit the dimensional changes that occur so that interfacial contact is maintained throughout the operation of the battery.

After Wright's discovery [17] of ionic conductivity in alkali metal salt complexes of poly(ethylene oxide) (PEO) in 1973, polymer electrolytes were proposed for batteries in 1978 because they combine the advantages of solid state electrochemistry with the ease of processing inherent to plastic materials [18]. Polymer electrolytes are solid solutions of alkali metal salts in polymers (not to be mixed up with *polyelectrolytes*, in which either the cation or the anion is covalently fixed to the polymer repeat unit). Since that time, the number of contributions to the field of SPEs has grown enormously, reflecting progress in the understanding of molecular and supramolecular architecture, which is prerequisite for fast ion transport in polymers [19].

Oligoethers seem to be a prerequisite for good solubility of alkali salts, since most of the polymer electrolytes contain these moieties as constitutive units either in their main or side chains. This is not surprising, since linear oligo(ethylene oxide)s form complexes with cations, and the cyclic oligomers (crown ethers) are well known for their excellent metal-complexing capabilities [20]. In order to facilitate, moreover, the dissociation of inorganic salts in polymer hosts, the lattice energy of the salt should be low and dielectric constant (ε) of the host polymer should be high. Consequently, the ionic conductivities of amorphous mixtures of Li salts with poly(propylene oxide) (PPO) are considerable smaller compared to equivalent

4

mixtures with PEO because PPO has a lower ε and its methyl groups hinder the complexation of Li^+. The ionic conductivity σ can be roughly expressed by the following equation:

$$\sigma = \sum_i n_i z_i \mu_i \qquad (1\text{-}1)$$

where n_i, z_i, and μ_i are the effective number of mobile ions, the elementary electric charge, and the ion mobility, respectively. Since the fraction of "free" ions that can be effectively transported is an important parameter, a high degree of dissociation of the salt in the polymer is a prerequisite for high conductivity. The degree of dissociation of the salts dissolved in the polymer host depends, however, on the total concentration of salt in the matrix. Generally, the degree of dissociation decreases with increasing salt concentration. As a consequence, the fraction of "free" ions has a maximumat an optimal salt concentration, which in many cases is located around Li/O = 0.04 (the molar ratio of lithium salt over oxygen (of ethylene oxide units)). Furthermore, another requirement is a high Li^+ transference number, i.e., a high ratio of the charge transported. The influence of the ion-ion and ion-polymer interactions on the ion transport in SPEs has been an important subject of research in recent years [19,21].

While in polymer electrolytes both the cations and anions may contribute to the ion conductivity, polyelectrolytes with the anions fixed to the polymer chain are "single-ion" conductors in which only the cations are mobile. Several kinds of Li^+ single-ion conducting polymers have been proposed, but the conductivities of such systems turned out to be only about 1 % that of ordinary SPEs. This is mainly attributed to the insufficient dissociation of Li^+ in such materials [22]. To date, no single-ion conducting polymers that possess sufficient conductivities to be useful in Li batteries are known.

Molecular dynamics simulations, as shown in Figure 1-3, suggest that the Li^+

ions are complexed to PEO through approximately five ether oxygens of a PEO chain, and that the mobility of the cations is decreased considerably by this complexation [23]. Consequently, the mobility of the Li^+ cations is related to the motions of the complexing segmental motion of the PEO matrix.

In conclusion, the polymer electrolyte is the key element in the SPE lithium battery's originality and specificity, and it constitutes a new approach to building a better storage battery. SPE makes it possible to manufacture all-solid-state cells without the difficulties generally associated with the use of rigid or liquid electrolytes. On the other hand, a large surface-to-thickness ratio is easily achieved with plastic materials. This compensates for the limited ion mobility. It has been shown that, in principle, SPEs can yield a power capability equivalent to that of molten-salt batteries if appropriate overall cell thickness and surface are selected. Such characteristics open the door to the production of large "power rolls" from which a variety of different cell sizes or shapes can be produced. Moreover, the polymer electrolyte plays three important roles in the SPE battery. Firstly, it is a lithium carrier that can be made very thin to improve the energy density. It is also a mechanical interelectrode separator, which eliminates the need for an inert porous separator. Finally, it is a binder and adhesive that ensures good mechanical and electrical contact, especially in the composite-cathode electrode but also with lithium electrode and current collectors.

1-2 GENERAL FEATURES FOR A POLYMER ELECTROLYTE

Since the polymer and the metal salt involved are both solid materials, the preparation of a polymer salt complex is achieved by the dissolution of the two materials in a common solvent such as acetonitrile, methanol or tetrahydrofuran (THF) followed by a slow removal of the solvent in vacuum. This results in either the bulk polymer-salt complex or a thin film depending upon the method of preparation. It is

essential to ensure that no traces of moisture are present and hence the operations are carried out by means of glove box methods. The polymer electrolytes with which we are principally concerned are complexes of alkali metal salts, denoted MX, with polymer hosts. Both the precursor salt and the neat polymer are solids, so that the complex-forming reaction [15]

$$m\mathrm{MX} + \left(-\,\mathrm{RY}\,-\right)_n \rightarrow (\mathrm{MX})_m \bullet \left(-\,\mathrm{RY}\,-\right)_n \tag{1-2}$$
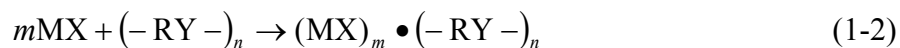
where (–RY–) denotes the polymer repeat unit, is a solid/solid reaction. As with most other reactions of this type, the kinetics of (1-2) are unfavorable, even when the complex is stable. Although other schemes for accelerating (1-2) have been employed, including intimate grinding/mechanical mixing [24], by far the most common method has been to dissolve or suspend both the MX salt and the host polymer in a common solvent and then to remove the solvent, producing the solvent-free polymer electrolyte in either bulk or thin-film form [25]. Care must be taken to purify the starting materials and to exclude water. Acetonitrile and methanol have been the solvents most commonly used. If the polymer-metal salt complex is partly crystalline, both the morphology and the transport properties of the electrolyte material produced may vary with choice of solvent.

Clearly, reaction (1-2) will be thermodynamically favorable (ΔG° negative) only if the Gibbs energy of salvation of the salt by the polymer is large enough to overcome the lattice energy of the salt. In general, one then expects a close relationship between the ability to form homogeneous complexes and the ability to monomer to dissolve the salt. Work by the Grenoble and Evanston groups has shown that for a given polymer host a fairly sharp demarcation line may be established between salts that can and cannot form complexes; the latter simply have too large lattice energies (compare Table 1-2). In addition to the very important lattice energy considerations, a number of other criteria that determine the possibility of forming

complexes have been described. As a result, three parameters are important for the control of salt/neutral molecule interactions: (a) electron pair donicity (DN), (b) acceptor number (AN) and (c) an entropy term. The DN term measures the ability of the solvent to donate electrons to solvate the cation, considered as a Lewis acid. Thus, the polymer which should function as a host in the polymer electrolyte should possess donor sites such as oxygen, sulfur or nitrogen either in the backbone or in a group attached in the form of a side chain to the polymer. Similarly, the AN term describes the possibility for anion (base) solvation. PEO, a polyether, which are quite strong donors and the donicity of PEO should be close to 20, similar to 1,2-dimethoxy ethane (DN,22; AN, 10.2) or even THF (DN, 20; AN, 8), as seen in Table 1-3 [26]. Ethers are, however, very poor acceptors, as they lack hydrogen bonding for anion salvation. Thus, PEO can effectively solvate cations possessing counter anions that are bulky delocalized anions such as I^-, ClO_4^-, BF_4^- or $CF_3SO_3^-$ which require little or no salvation. Moreover, the third term (entropy) has been related to the spatial disposition of the solvating unit and it has been shown that ethylene oxy (CH_2CH_2O) containing polymers such as PEO have the most favorable spatial orientation of the solvating units [27]. While small ions such as Li^+ which can be strongly solvated, lead to formation of polymer salt complexes even up to LiCl (lattice energy 853 kJ mol^{-1}) other larger cations, such as Na^+, K^+, require bulky counter anions such as I^-, SCN^- or $CF_3SO_3^-$ in order to be solvated by PEO [28].

Besides, it has also been recognized that the polymer should possess a low cohesive energy and a high flexibility in order to effectively solvate the ions. The former is characterized by lack of intermolecular interactions such as hydrogen bonding while the latter feature is indicated by a low glass transition temperature (T_g). Although polymers like polyamides contain oxygen and nitrogen atoms as donor sites in their backbone, these polymers are quite unsuitable as polymer hosts in polymer

electrolytes because of the presence of extensive intermolecular hydrogen bonding. Metal complexation with these polymers would cause the disruption of this energetically favorable situation. The second factor, i.e. the high torsional flexibility of the polymer, is indicated by a low T_g and is crucial for ion transport. Thus, large segmental motions of the polymer (either the backbone or the side chain) which is possible above its T_g can result in fast ion movement.

As a result, we can conclude as the following [28-32]: (1) A high concentration of polar (basic) groups on the polymer chain is needed to solvate the salt effectively. (2) The cohesive energy of the polymer cannot be too high, and its flexibility, as indicated by a low glass transition temperature, should be quite high, so that reorientation of the local coordination geometry, to achieve effective salvation, may be achieved.

In view of the above requirements, the polymers that have been studied as polymer electrolytes are either oxygen, nitrogen, or sulfur atoms-containing materials. The heteroatoms are either part of the backbone of the polymer or are present in the side chain attachments. Some important polymers include ethers in poly(ethylene oxide) and poly(propylene oxide) and polysiloxanes, carbonyl groups in poly(vinyl pyrrolidone) or poly(ethylene succinate), hydroxyls in poly(vinyl alcohol) nitrogen atoms in poly(ethylene imine) and sulfur atoms in poly(alkylene sulfides). Consequently, Table 1-4 [33-40] summaries the ionic conductivity data for polymer electrolytes containing linear polymers. In general, Lewis base character on the complexing host species is required to coordinate the cation of the salt and thus provide a favorable Gibbs energy of polymer-salt interaction [41].

1-3 CURRENT STATE OF PEO-BASED ELECTROLYTES

The first suggestion for the use of a poly(ethylene oxide) (PEO)-based

electrolyte have come in 1978 [42]. PEO-based complexes are thus the first solvent-free polymer electrolytes to have been reported and have received the extensive attention, especially after their generality was established [29,33].

PEO is obtained from the ring-opening polymerization of ethylene oxide. PEO is a linear polymer and the regularity of the unit allows a high degree of crystallinity involving ca. 70-85 % of the polymer. Pristine PEO adopts a helical configuration with sever monomer units and a thread of 1.93 nm per unit quadratic cell [43], as shown in Figure 1-4. The melting point (T_m) of the crystalline phase is ca. 65 °C while the glass transition temperature (T_g) of the amorphous is -60 °C. The dipole-dipole interactions are probably responsible for the higher value of T_g compared with polyethylene (PE, T_g = -100°C), since the energy barrier for rotation of the C-O bond (6.3 kJ) is lower than that of the C-C bond (12.6 kJ). However, the dielectric constant is still quite low (ca. 5), and this strongly influences the behavior of PEO-based electrolytes.

PEO-based electrolytes have presented the salient features as follows [28,29]:

(1) The salvation properties are due to the combination of the ether oxygen donicity and an optimal spacing of these heteroatoms along the polymer chain.

(2) Only the amorphous phase takes part in conductivity. Ion pairs and multiplets probably exist, but both anions and cations are mobile.

(3) The electrochemical characteristics of PEO meet those expected for the concept of thin film electrochemistry, and such applications may represent a breakthrough in reversible energy storage.

At present, PEO electrolytes have the drawback of low ionic conductivity at room temperature, and there is a considerable research effort aimed at finding substitutes with improved properties. As a result, Table 1-5 lists the chemical structure of the common PEO-derivative materials for solid polymer electrolytes [44-49]. Most

likely, new polymers will incorporate short PEO segments, as the solvating properties, stability and simple chemistry of ethylene oxide derivatives is unchallenged. An example is that of poly(bis(methoxyethoxyethoxy)phosphazene) [50] whose conductivity is close to 5×10^{-5} S cm^{-1} at 25 °C. In all cases, research in the field will benefit from the understanding of PEO-salt complex behavior. In addition, owing to the readily available of PEO, solid electrolytes can now be made very simply in any laboratory.

1-4 GEL TYPE POLYMER ELECTROLYTES

A variety of dimensionally stable solid electrolytes consisting of a mixture of organic plasticizer (summarized in Table 1-6), such as ethylene carbonate (EC) and propylene carbonate (PC), along with structurally stable polymers such as poly(acrylonitrile) (PAN), poly(vinyl sulfone) (PVS), poly(vinyl pyrrolidone) (PVP) and poly(vinyl chloride) (PVC) and several lithium salts have been tested and found to have excellent ionic conductivities ranging between 10^{-4} and 10^{-3} S cm^{-1} at ambient temperatures [51-57]. In these gel-type electrolytes the primary role of the polymers PAN, PVS, PVP or PVC is to immobilize the lithium salt solvates of the organic plasticizer liquids. Studying the ionic conductivity based on plasticized polymer electrolyte systems has shown that the ion motion is decoupled from the polymer motion and therefore salvation by the polymer host loses its importance once a plasticizer is introduced. However, it is worth to note that there may be a level of competition for salvation between the polymer host and plasticizing solvent, giving some degree of polymer-ion interaction in those PAN gelled electrolytes. The main role of small molecules in a gelled electrolyte plays to be a plasticizer for the polymer host, improving flexibility and segmental motion in the host polymer chains and to solvate the cation, thus reducing ion-ion interactions.

11

Watanabe prepared for the first time solid electrolytes comprising PC and LiClO$_4$ in PAN and reported a maximum conductivity of 2×10^{-4} S cm^{-1} [51]. Abraham and Alamgir prepared Li$^+$ conductive polymer electrolytes with extremely high ambient temperature conductivities of 4×10^{-3} S cm^{-1} [52,53]. These electrolytes are composed of Li salts, such as LiClO$_4$, dissolved in organic solvents EC and PC and immobilized in a polymer network of PAN or PVP. Moreover, Matsumuto, Rutt and Nishi described gel-type polymer electrolytes possess high ionic conductivities (10^{-3} S cm^{-1}) and good mechanical strength [54-57]. Another typical example for gel-type polymer electrolyte is prepared by swelling poly(acrylontrile-*co*-butadiene) (NBR) / poly(styrene-*co*-butadiene) (SBR) / LiClO$_4$ latex films with an organic solvent, γ-butyrolactone (BL) [54]. The authors suggest that these gel-type polymer electrolyte systems (NBR/SBR/LiClO$_4$/BL) possess dual ion conductive channels, one which is the fused NBR-latex phase and the other is the LiClO$_4$ phase present at the interface of SBR/NBR latex particles. The pure SBR phase is non polar and therefore is not impregnated and merely provides mechanical support. Table 1-7 summarizes the conductivity data for some of gel-type polymer electrolytes.

1-5 RESEARCH MOTIVATION

Polymer electrolytes have attracted considerable attention due mainly to the possibility of their application in various electrochemical devices such as rechargeable lithium batteries. According to the above-mentioned introduction to polymer electrolytes, there remains intense interest in developing solid polymer electrolytes, free from low molecular weight plasticizer and with a sufficiently high ionic conductivity for application in all-solid-state rechargeable lithium batteries. For such applications, conductivities above the present maximum of 10^{-4} S cm^{-1} are required. Gel-type electrolytes, in which a liquid electrolyte is entrapped in a polymer matrix,

possess levels of ionic conductivity that are sufficient for application in lithium batteries. These materials will lead to the first commercialization of polymer batteries. Nevertheless, such electrolytes did not get rid of the problems, which are many of disadvantages associated with liquid electrolytes still retained in the gel.

Great progress has been made over the last 30 years in increasing the level of ionic conductivity exhibited by polymer electrolytes. However, despite innovative designs of flexible polymers and the addition of inorganic materials to form polymer composite capable of suppressing crystallinity, levels of ionic conductivity are persistently limited to a ceiling of around 10^{-4} S cm^{-1} at room temperature. Such a level is insufficient for many lithium battery applications.

When such barriers are reached in science, it is time to change the way we think. Our version is that we must direct our attention to the phase behavior and interaction mechanism of polymer electrolytes. It is of vital importance to optimize the performance of the ionic conductivity through understanding of the fundamentals of ionic interaction mechanism and phase behavior in full detail within polymer electrolytes.

Poly(ethylene oxide) (PEO)-based polymer electrolytes are still among the most extensively studied polymer ionic conductor owing to their structures are beneficial for facilitating fast ion transport. Unfortunately, a high content of a crystalline phase limits the conductivity of PEO-based electrolytes. It is an important challenge to develop practical methods for preparing the SPEs for that have higher conductivity and dimensional stability. In this regard, the preparation of polymer electrolytes by blending them with other appropriate polymers is of interest. Polymer blend is a quick and economical alternative method for obtaining materials that have optimized properties and for the easy control of their physical properties by compositional change. Therefore, the introduce of poly(ε-caprolactone) (PCL) into PEO-based

polymer electrolytes tends to suppress the crystallization of PEO and results in higher ionic conductivity. In Chapter 3, we employed differential scanning calorimetry (DSC), Fourier transform infrared (FTIR), solid-state ^{7}Li NMR, and alternating current (ac) impedance to investigate the miscibility and related conductivity behaviors of this LiClO$_4$/PEO/PCL ternary blend system. Subsequently, we synthesize monomethoxypoly(ethylene glycol)-*block*-poly(ε-caprolactone) (MPEG-PCL) block copolymers and blend them with LiClO$_4$ salt to study the influences that the miscibility behavior and interaction mechanisms have on the variation of ionic conductivity, which was discussed in Chapter 4.

Finally, since poly(vinyl pyrrolidone) (PVP) and poly(methyl methacrylate) (PMMA) both possess their own advantages to act as polymer electrolyte, we are interested in studying the polymer electrolyte incorporating lithium perchlorate with PVP and PMMA. However, PVP/PMMA blends tend to be immiscible, therefore, PVP-*co*-PMMA random copolymer was synthesized by free radical polymerization. It seemed reasonable to us to expect that the gel-type polymer electrolyte based on PVP-*co*-PMMA may not only sustain the mechanical properties of PMMA-based gel polymer electrolyte but also increase the dissolubility of the lithium salt due to the strong withdrawing group within PVP molecules. As a result, Chapter 5 investigated the interaction behavior and related conductivity of all-solid-state polymer electrolyte based on LiClO$_4$/PVP-*co*-PMMA blend systems.

1-6 REFERENCES

1. Weber, N.; Kummer, J. T. *Proc. Annu. Power Sources Conf* **1967**, *21*, 37.

2. Whittingham, M. S.; Huggins R. A. *J. Chem. Phys*. **1971**, *54*, 414.

3. Owens, B. B.; Argue, A. G. *Science* **1967**, *157*, 308.

4. Takahashi, T.; Ikeda, S.; Yamamoto, O. *J. Electrochem. Soc*. **1972**, *119*, 477.

5. Tatsumisago, M.; Shinkuma, Y.; Minami, T. *Nature* **1991**, *354*, 217.

6. Nicholson, P. S.; Whittingham, M. S.; Farrington, G. C.; Smeltzer, W. W.; Thomas J., Eds. *Solid State Ionics*; North-Holland: Amsterdam, 1992.

7. Chowdari, B. V. R.; Chandra, S.; Singh, S.; Srivastava, P. C., Eds. *Solid State Ionics*, *Materials and Appications*; North-Holland; Amsterdam, 1992.

8. Bange, K.; Gambke, T. *Adv. Mater*. **1990**, *2*, 10.

9. Visco, S. J.; Liu, M.; Doeff, M. M.; Ma, Y. P.; Lampert, C.; De Jonghe, C. *Solid State Ionics* **1993**, *60*, 175.

10. Hagenmuller, P.; Van Gool, W., Eds. *Solid Electrolytes*, *General Principles*, *Characterization*, *Materials*, *Applications*; Academic Press: New York, 1978.

11. Vincent, C. A.; Bonino, F.; Lazzari, M.; Scrosati, B., Eds. *Modern Batteries*; Edward Arnold: London, 1983.

12. Gabano, F., Ed. *Lithium Batteries*; Academic Press: London, 1983.

13. Rickert, H. *Angew. Chem. Int. Ed. Engl*. **1978**, *17*, 37.

14. Bonino, F.; Ottaviani, M.; Scrosati, B. Pistoia, G. *J. Electrochem. Soc*. **1998**, *135*, 12.

15. Ratner, M. A.; Shriver, D. F. *Chem. Rev*. **1988**, *88*, 109.

16. Gray, F. M. Ed. *Solid Polymer Electrolytes*: *Fundamentals and Technological Applications*; VCH: New York, 1991.

17. Fenton, D. E.; Parker, J. M.; Wright, P. V. *Polymer* **1973**, *14*, 589.

18. Armand, M.; Duclot, M. *French Patent* **1978**, *7832976*.

19. Armand, M. *Solid State Ionics* **1994**, *69*, 309.

20. Vögtle, F.; Weber, E. In *Crown Ethers and Analogs*, Patai, S., Rappoport, Z., Eds.; Wiley: New York, 1989.

21. Bruce, P. G.; Vincent, C. A. *Faraday Discuss. Chem. Soc.* **1989**, *88*, 43.

22. Takeoka, S.; Ohno, H.; Tsuchida, E. *Polym. Adv. Technol.* **1993**, *4*, 53.

23. Müller-Plathe, F.; Van Gunsteren, W. F. *J. Chem. Phys.* **1995**, *103*, 4745.

24. Gray, F. M.; MacCallum, J. R.; Vincent, C. A. *Solid State Ionics* **1985**, *18–19*, 282.

25. LaNest, J. F.; Cheradame, H.; Dalard, F.; Deroo, D. *J. Appl. Electrochem.* **1986**, *16*, 75.

26. Gutmann, V., *The Donor Acceptor Approach to Molecular Interactions*; Plenum Press: New York, 1978.

27. Shotenshtein, A. I.; Petrov, E. S.; Yokovlevla, E. A. *J. Polym. Sci.*, Part *C* **1967**, *16*, 1799.

28. Vincent, C. A.; MacCallum, J. R. In *Polymer Electrolyte Reviews*; Mac Callum, J. R., Vincent, C. A., Eds., Elsevier: London, 1987.

29. Armand, M. B.; Chabagno, J. M.; Duclot, M. J. In *Fast Ion Transport in Solids*; Duclot, M. J., Vashishta, P., Mundy, J. N., Shenoy, G. K., Eds.; North-Holland: New York, 1979.

30. Shriver, D. F.; Papke, B. L.; Ratner, M. A.; Dupon, R.; Wong, T.; Brodwin, M. *Solid State Ionics* **1981**, *5*, 83.

31. Paper, B. L.; Ratner, M. A.; Shrever, D. F. *J. Phys. Chem. Solids* **1981**, *42*, 493.

32. Paper, B. L.; Ratner, M. A.; Shrever, D. F. *J. Electrochem. Soc.* **1982**, *129*, 1694.

33. Armand, M. B. *Solid State Ionics* **1983**, *9–10*, 745.

34. Watanabe, M.; Rikukawa, M.; Sanui, K.; Ogata, N.; Kato, H.; Kobayashi, T.; Ohtaki, Z. *Polymer J.* **1983**, *15*, 65.

35. Watanabe, M.; Togo, M.; Sanui, K.; Ogata, N.; Kobayashi, T.; Ohtaki, Z.

Macromolecules **1984**, *17*, 2908.

36. Watanabe, M.; Rikukawa, M.; Sanui, K.; Ogata, N.; Kato, H.; Kobayashi, T.; Ohtaki, Z. *Macromolecules* **1984**, *17*, 1902.

37. Dupon, R.; Papke, B. L.; Ratner, M. A.; Shriver, D. F. *J. Electrochem. Soc.* **1987**, *131*, 586.

38. Armstrong, R. D.; Clarke, M. D. *Electrochim. Acta.* **1984**, *29*, 1443.

39. Harris, C. S.; Shriver, D. F.; Ratner, M. A. *Macromolecules* **1986**, *19*, 987.

40. Clancy, S.; Shriver, D. F.; Ochrymomycz, L. A. *Macromolecules* **1986**, *19*, 606.

41. Angell, C. A.; Liu, C.; Sanchez, E. *Nature* **1993**, *362*, 137.

42. Armand, M. B.; Chabagno, J. M.; Duclot, M. J. In *Extended Abstract Second International Meeting on Solid Electrolytes*, St Andrews, Scotland, 20–22 Sept., 1978.

43. Takahashi, Y.; Takadoro, H. *Macromolecules* **1983**, *6*, 672.

44. Nagaoka, K.; Naruse, H.; Shinohara, I. Watanabe, M. *J. Polym. Sci.*, *Polym. Lett. Ed.* **1984**, *22*, 659.

45. Hall, P. G.; Davis, G. R.; McIntyre, J. E.; Ward, I. M.; Banister, D. J.; Le Brocq, K. M. F. *Polym. Commun.* **1986**, *27*, 98.

46. Fish, D.; Khan, I. M.; Smid, J. *Macromol. Chem. Rapid Commun.* **1986**, *7*, 115.

47. Fish, D.; Khan, I. M.; Smid, J. *Br. Polym. J.* **1988**, *20*, 281.

48. Blonsky, P. M.; Shriver, D. F.; Austin, P.; Allcock, H. R. *J. Am. Chem. Soc.* **1984**, *106*, 6854.

49. Inoue, K.; Nishikawa, Y.; Tanigaki, T. *Marcomolecules* **1991**, *24*, 3464.

50. Blonsky, P. M.; Shriver, D. F. *J. Am. Chem. Soc.* **1984**, *106*, 6854.

51. Watanabe, M.; Kanba, M.; Nagaoka, K.; Shinohara, I. *J. Polym. Sci.*, *Polym. Phys. Ed.* **1983**, *21*, 939.

52. Abraham, K. M.; Alamgir, M. *J. Electrochem. Soc.* **1990**, *137*, 1657.

53. Abraham, K. M.; Alamgir, M. *Solid State Ionics* **1994**, *70*, 20.

54. Matsumoto, M.; Rutt, S. J.; Nishi, S. *J. Electrochem. Soc.* **1995**, *142*, 3052.

55. Matsumoto, M.; Ichino, T.; Rutt, S. J.; Nishi, S. *J. Electrochem. Soc.* **1993**, *140*, L151.

56. Matsumoto, M.; Ichino, T.; Rutt, S. J.; Nishi, S. *J. Electrochem. Soc.* **1994**, *141*, 1989.

57. Matsumoto, M.; Ichino, T.; Rutt, S. J.; Nishi, S. *J. Polym. Sci.*, *Polym. Chem. Ed.* **1994**, *32*, 2551.

Table 1-1. Classes of Solid Electrolytes

ceramic framework materials		soft framework materials		polymers[a]	
crystalline species	glasses	crystalline species	glasses	partly crystalline	amorphous
LiAlSiO$_4$	LiAlSiO$_4$ (glass)	AgI	AgCl/AgI/CsCl		
β-alumina [(Na$_2$O)$_x$ $\cdot$ 11Al$_2$O$_3$]	Ag$_{2x}$GeSe$_{2+x}$	Ag$_2$HgI$_4$		LiSCN $\cdot$ PEO	LiSCN-MEEP
		PbI$_2$		NaCF3SO3 $\cdot$ PEI	
Na$_2$SO$_4$					NaCF3SO3 $\cdot$ PPO

[a] PEO = poly(ethylene oxide), PEI = poly(ehylenimine), MEEP = poly(bis(methoxyethoxyethoxy)phosphazene), and PPO = poly(propylene oxide).

Table 1-2. Salts That Form Complex Polymeric Electrolytes with PEO[a]

	Li$^+$	Na$^+$	K$^+$	Rb$^+$	Cs$^+$
F$^-$	no	no	no	no	no
	1036	923	821	785	740
Cl$^-$	yes	no	no	no	no
	853	786	715	689	659
Br$^-$	yes	yes	no	no	no
	807	747	682	660	631
I$^-$	yes	yes	yes	yes	yes
	757	704	644	630	604
SCN$^-$	yes	yes	yes	yes	yes
	807	682	619	616	568
CF$_3$SO$_3^-$	yes	yes	yes	yes	yes
	725	650	605	585	550

[a] The numbers reported are the lattice energies of the salts (in kJ/mol). "Yes" indicates polymer-salt complex formation and "no" indicates the lack of complex formation. The stair-step line indicates the division between complex formation and separate phases.
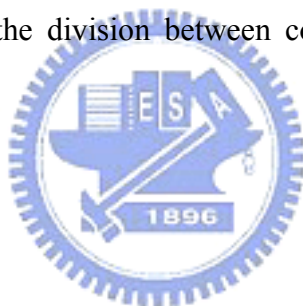
Table 1-3. The Important Parameter for Salt Solubilities
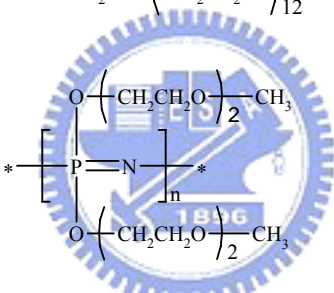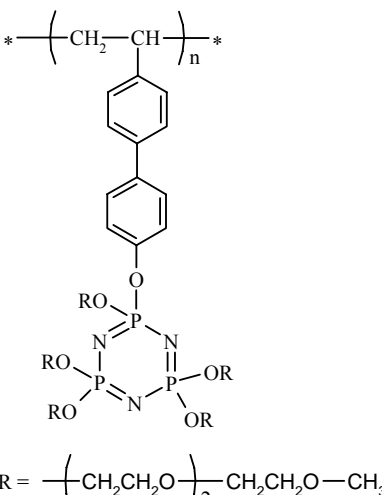
common solvents	DN	AN
Acetonitrile	14.1	18.9
Propylene carbonate	15.5	18.3
Methanol	19.1	41.5
1,2-Dimethoxyethane (glyme)	22.0	10.2
Tetrahydrofuran (THF)	20.0	8.0
Water	16.4	54.8

Table 1-4. Conductivity Data for Polymer Electrolytes Containing Linear Polymers [33-40]

polymers	metal salts	O/Li ratio	maximum conductivity, S cm^{-1}	reference
1. poly(propylene oxide)	LiBr, LiI	9/1	$\sim 10^{-6}$	[33,34]
	NaB(C$_6$H$_5$)$_4$		$\sim 10^{-6}$	
	LiCF$_3$SO$_3$		2.2×10^{-5} (312)[a]	
	NaCF$_3$SO$_3$		$\sim 10^{-6}$	
2. poly(β-propiolactone)	LiClO$_4$	20/1	3.5×10^{-6}	[35]
3. poly(ethylene succinate)	LiClO$_4$	33/1	$\sim 10^{-5}$ (363)	[36,37]
	LiBF$_4$	12/1	3.4×10^{-6} (288.2)	
4. poly(ethylene adipate)	LiCF$_3$SO$_3$	16/1	$\sim 10^{-6}$	[38]
5. poly(ethylene imine)	NaCF$_3$SO$_3$	6/1[b]	$\sim 10^{-7}$	[39]
6. poly(alkylene sulphide)	AgNO$_3$	4/1[c]	9×10^{-7} (318)	[40]

[a] The number in the bracket indicates the measured temperature in Kevin unit. [b] O/Na ratio. [c] O/Ag ratio.
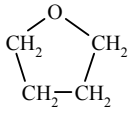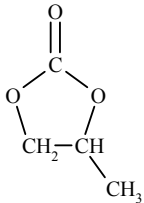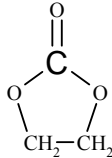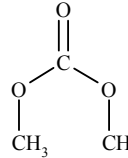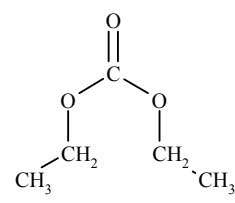
Table 1-5. Chemical Structures of Common PEO-derivative Materials for Solid Polymer Electrolytes [44-49]

compounds	molecular structure	reference
1		[44]
2		[45,46
3		[47]
4 (MEEP)[a]		[48]
5		[49]

[a] MEEP = poly(bis(methoxyethoxyethoxy)phosphazene)

Table 1-6. The Properties of Common Use of Organic Solvents for Gel-type Polymer electrolytes

Characteristic	THF	PC	EC	DMC	DEC
Structure formula					
Boiling temperature, °C	65 ~ 67	240	248	91	126
Melting temperature, °C	-109	-49	39 ~ 40	4.6	-43
Density, g/cm^3	0.887	1.198	1.322	1.071	0.98
Solution conductivity, S/cm	2.1×10^{-7}	2.1×10^{-9}	$< 10^{-7}$	$< 10^{-7}$	$< 10^{-7}$
Viscosity at 25 °C, cP	0.48	2.5	1.86 (at 40 °C)	0.59	0.75
Dielectric constant at 20 °C	7.75	64.4	89.6 (at 40 °C)	3.12	2.82
Molecular weight	72.1	102.0	88.1	90.1	118.1

[a] THF = tetrahydrofuran, PC = propylene carbonate, EC = ethylene carbonate, DMC = dimethyl carbonate, DEC = diethyl carbonate.

Table 1-7. Conductivity Data for Gel-type Polymer Electrolytes [51-57]

gel polymers	Li salt	maximum conductivity, S cm^{-1}	reference
NBR/SBR/BL[a]	LiClO$_4$	1.2×10^{-3} (298)[e]	[54]
PAN/EC[b]/PC[c]	LiClO$_4$	1.7×10^{-3} (293)	[53]
PAN/PC	LiClO$_4$	2.0×10^{-4} (293)	[51]
EC/PC/PAN/PEGDA[d]	LiClO$_4$	4.0×10^{-4} (263); 1.2×10^{-3} (293)	[55]
EC/PC/PAN	LiCF$_3$SO$_3$	4.0×10^{-4} (263); 1.4×10^{-3} (293)	[56]
EC/PC/PVP	LiCF$_3$SO$_3$	4.0×10^{-5} (263); 5.0×10^{-4} (293)	[57]

[a] BL = γ-butyrolactone, [b] EC = ethylene carbonate, [c] PC = propylene carbonate, [d] PEGDA = poly(tetra ethylene glycol diacrylate), [e] The number in the bracket indicates the measured temperature in Kevin unit.
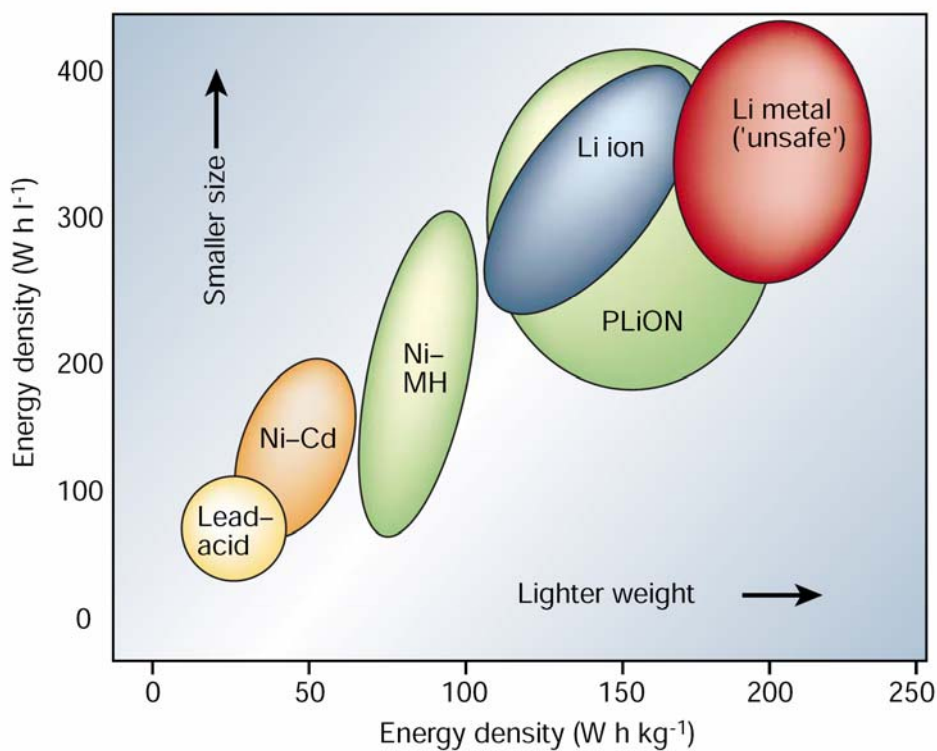
Figure 1-1. Comparison of the different battery technologies in terms of volumetric and gravimetric energy density. The share of worldwide sales for Ni-Cd, Ni-MeH and Li-ion portable batteries is 23, 14, 63 %, respectively. The use of Pb-acid batteries is restricted mainly to SLI (starting, lighting, ignition) in automobiles or standby applications, whereas Ni-Cd batteries remain the most suitable technologies for high-power applications.

anode reaction: Li_xC_6 $\Leftrightarrow$ $xLi^+ + xe^- + C_6$

cathode reaction: $xLi^+ + xe^- + Li_{1-x}Mn_2O_4$ $\Leftrightarrow$ $LiMn_2O_4$
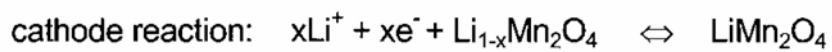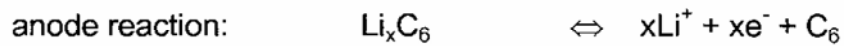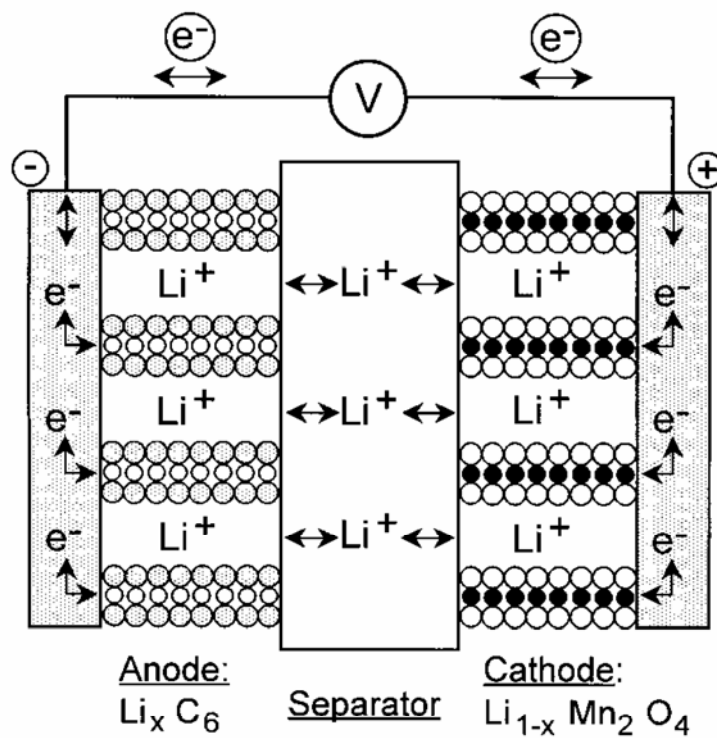
                                                  charging $\Leftrightarrow$ discharging

Figure 1-2. Schematic illustration of a lithium rocking chair battery with graphite and spinel as intercalation electrodes and its electrode reactions.
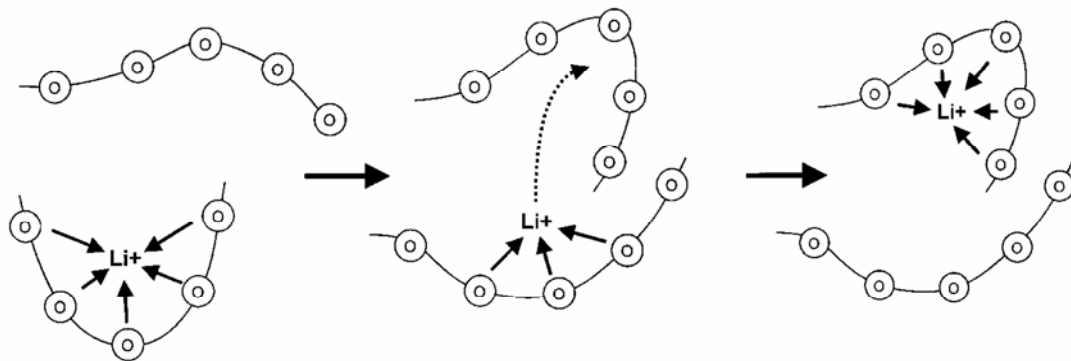
Figure 1-3. Schematic of the segmental motion assisted diffusion of Li$^+$ in the PEO matrix. The circles represent the ether oxygen atoms of PEO.
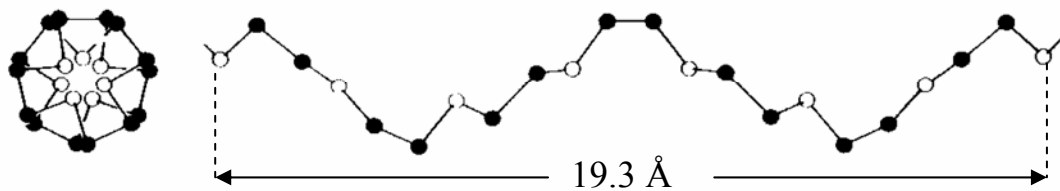
Figure 1-4. The helical structure of PEO molecule [43].

CHAPTER 2

Background and Theorems

2-1 BACKGROUND

2-1-1 The Development of High-Energy-Density Batteries

The significance of the SPE battery and its potential impact on the development of high-energy-density batteries can best be grasped from an overview of past and present systems. Representative batteries [1] that have already reached or are close to commercial production will be discussed briefly while milestones in the development of the related technologies are summarized in Table 2-1.

Furthermore, the development of secondary (or rechargeable) batteries has often been intertwined with that of primary batteries since they frequently share common electrolytes and technologies, e.g. alkaline or organic electrolyte cells. In some cases, it is even difficult to distinguish between a "primary" and a "rechargeable" cell. By contrast, SPE appear especially well adapted to the solution of major problems associated with the development of high-energy-density rechargeable batteries. Consequently, most of the discussions and the comparisons with existing technologies will refer to rechargeable systems [2].

2-1-1-1 Aqueous Systems

Ever since Volta's initial work in 1800, water-based electrolytes have represented the choice medium for most primary- and secondary- battery developments. This can be explained, in part, by the large volume of knowledge accumulated on these electrolytes and, also, by manufacturers' greater familiarity with aqueous electrochemistry. Nowadays, water-based electrolytes account for most manufactured batteries and a traditional system like the starting-lighting-ignition (SLI)

lead/acid battery is still expected to offer the best performance/cost ratio in the foreseeable future. Aqueous batteries fall into three broad categories according to the type of electrolyte used, namely: water containing dissolved ionic salts, acids and alkalis. Table 2-1 lists the principal events in the evolution of primary and secondary batteries.

(a) Neutral Electrolytes: These electrolytes, made by dissolving ionic salts in water, are what Volta himself used in his original cell. However, the best known battery of this category is the Liclanché (or carbon-zinc) cell, which is still in use.

(b) Acid Electrolytes: The lead/acid battery is the most famous representative of this category and the oldest known rechargeable battery. This system, first discovered by Planté in 1859, is still the most widely used.

(c) Alkaline Electrolyte: Two major applications of alkaline electrolytes, usually KOH solutions, have been extensively developed, the alkaline manganese dioxide primary cell and the nickel-cadmium rechargeable battery. Recently, the markets for cylindrical primary cells have become increasingly dominated by alkaline MnO2 batteries, whereas the small sealed nickel-cadmium battery is at present opening new consumer-oriented markets for rechargeable batteries, mostly in portable-equipment applications.

2-1-1-2 Alkali Metal Systems

Today's aqueous batteries represent a mature technology, usually optimized with respect to performance and cost, and they generally satisfy most of the markets they have created. Other markets could be expanded or created if better batteries in terms of stored-energy capacity, cycle life and cost were to become available. One such market can be envisaged for the electric propulsion battery, which offers tremendous interest from the energy and environmental standpoints. The major drawback of

today's aqueous rechargeable batteries, which restricts their marketability, is their low energy density.

The energy density (Wh kg^{-1}) of a battery is directly related to the free energy variation ($\Delta G°$) of the global chemical reaction and to the weight of all chemical reactants ($\sum wt_r$):

$$\left(-\Delta G^0\right)\big/3600\sum wt_r = \text{n.F.E}\big/3600\sum wt_r \qquad (2\text{-}1)$$

Light electropositive metals such as alkaline or alkaline-earth metal are therefore choice elements for a high-energy-density battery. Water-based electrolytes, however, are not sufficiently stable with such reducing metals nor with many of the highly oxidant cathode materials and, apart from a few projects to develop metal-are of zinc-halogen batteries, most research on high-energy-density batteries with water-based systems has been redirected towards modest improvements to existing technologies. Consequently, early this century, research was initiated to develop electrolytes compatible with alkali (or alkaline-earth) metals.

(a) Liquid Electrolytes: Liquid organic and inorganic electrolytes that are kinetically stable in contact with alkali metals, especially lithium, have been identified. Key events in the evolution of lithium batteries towards successful commercialization of small primary cells are reported in Table 2-1, along with more modest developments of the rechargeable lithium battery. An important element behind the recent surge of interest in the rechargeable lithium battery is the identification of ion-inserting structures operating reversibly, and at high temperature, with lithium ions.

(b) Molten Salts: Only molten-salt electrolytes offer true thermodynamic stability towards alkali (or alkaline earth) metals. They also enable high power capability to be achieved because of their excellent ionic conductivity. Unfortunately,

however, a high operating temperature, associated with thermal-management and corrosion problems, has restricted their potential applications to relatively large battery installations.

(c) Solid Electrolytes: For Practical reasons, combination of the ion-conduction and mechanical-separator functions in a solid electrolyte has always been an attractive notion but high ionic conductivity in the solid state (crystalline or amorphous) is still difficult to achieve. So far, only a handful of materials have been identified and even these have led to only very limited applications such as pacemakers (Figure 2-1). Another major hurdle in the use of rigid electrolytes in batteries is the difficulty in establishing and maintaining electrode/electrolyte contact during successive discharge/charge cycles. An initial solution was the sodium-sulfur-type battery, in which the ceramic (or glass) electrolyte is in contact with liquid (or molten) electrolytes, as well as the usual problems associated with a high operating temperature, have limited the development of this high-energy-density rechargeable battery. The use of SPEs with alkali-ion reversible electrodes was proposed as a means of taking advantage of the best of both worlds: a reliable "solid" electrolyte separator and electrolyte deformability and flexibility, in order to maintain the electrode/electrolyte contact and accommodate volume variations of the electrodes during cell cycling.

2-1-2 Historical Developments in Li-battery Research

As seen above, the SPE lithium battery is a direct outcome of research and reflections on solid ionic conductors. It combines the use of thin-film lithium-ion-conducting polymer electrolytes with lithium-ion reversible electrodes. The schematic in Figure 2-1 illustrates the main differences between the SPE lithium-rechargeable battery and existing aqueous systems. The concept, proposed by

Armand [3], involves an all-solid rechargeable generator made of two lithium-reversible electrodes, one acting as a source of lithium ions during discharge, the other as a corresponding sink, the two being separated by a thin-film polymer electrolyte acting as a lithium cation carrier.

The motivation for using a battery technology based on Li metal as anode relied initially on the fact that Li is the most electropositive (-3.04 V versus standard hydrogen electrode) as well as the lightest (equivalent weight $M = 6.94$ g mol^{-1}, and specific gravity $\rho = 0.53$ g cm^{-3}) metal, thus facilitating, the design of storage systems with high energy density. The advantage in using Li metal was first demonstrated in the 1970s with the assembly of primary (for example, non-rechargeable) Li cells [4,5]. Owing to their high capacity and variable discharge rate, they rapidly found applications as power sources for watches, calculators or for implantable medical devices. Over the same period, numerous inorganic compounds were shown to react with alkali metals in a reversible way. The discovery of such materials, which were later identified as intercalation compounds, was crucial in the development of high-energy rechargeable Li systems. Like most innovations, development of the technology resulted from several contributions. By 1972, the concept of electrochemical intercalation and its potential use were clearly defined [6,7], although the information was not widely disseminated, being reported only in conference proceedings. Before this time, solid-state chemists had been accumulating structural data on the inorganic layered chalcogenides [8,9], and merging between the two communities was immediate and fruitful.

In 1972, Exxon [10,11] embarked on a large project using TiS_2 as the positive electrode, Li metal as the negative electrode and lithium perchlorate ($LiClO_4$) in dioxolane as the electrolyte. TiS2 was the best intercalation compound available at the time, having a very favorable layered-type structure. As the results were published in

readily available literature, this work convinced a wider audience. But in spite of the impeccable operation of the positive electrode, the system was not viable. It soon encountered the shortcomings of a Li-metal/liquid electrolyte combination-uneven (dendritic) Li growth as the metal was replaced during each subsequent discharge-recharge cycle (Figure 2-2 a), which led to explosion hazards. Substituting Li metal for an alloy with Al solved the dendrite problem [12] but, as discussed later, alloy electrodes survived only a limited number of cycles owing to extreme changes in volume during operation. In the meantime, significant advances in intercalation materials had occurred with the realization at Bell Labs that oxide, besides their early interest for the heavier chalcogenides [13,14], were giving higher capacities and voltages. Moreover, the previously held belief that only low-dimensional materials could give sufficient ion diffusion disappeared as a framework structure (V_6O_{13}) proved to function perfectly [15]. Later, Goodenough [16,17], with Li_xMO_2 (where M is Co, Ni, or Mn), would propose the families of compounds that are still used almost exclusively in today's batteries.

To circumvent the safety issues surrounding the use of Li metal several alternative approaches were pursued in which either the electrolyte or the negative electrode was modified. The first approach [18] involved substituting metallic Li for a second insertion material (Figure 2-2 b). The concept was first demonstrated in the laboratory by Murphy et al. [19] and then by Scrosati et al. [20] and led, at the end of the 1980s and early 1990s, to the so-called Li-ion or rocking-chair technology. The principle of rocking-chair batteries had been used previously in Ni-MeH batteries [21,22]. Because of the presence of Li in its ionic rather that metallic state, Li-ion cells solve the dendrite problem and are, in principle, inherently safer than Li-metal cells. To compensate for the increase in potential of the negative electrode, high-potential insertion compounds are needed for the positive electrode, and

emphasis shifted from the layered-type transition-metal disulfides to layered- or three-dimensional-type transition-metal oxides [16]. Metal oxides are more oxidizing than disulfides (for example, they have a higher insertion potential) owing to the more pronounced ionic character of "M-O" bonds compared with "M-S" bonds. Nevertheless, it took almost ten years to implement the Li-ion concept. Delays were attribyted to the lack of suitable materials for the negative electrode (either Li alloys or insertion compounds) and the failure of electrolytes to meet − besides safety measures − the costs and performance requirements for a battery technology to succeed. Finally, capitalizing on earlier findings [23,24], the discovery of the highly reversible, low-voltage Li intercalation-deintercalation process in carbonaceous material [25] (providing that carefully selected electrolytes are sued), led to the creation of the $C/LiCoO_2$ rocking-chair cell commercialized by Sony Corporation [26] in June 1991. This type of Li-ion cell, having a potential exceeding 3.6 V (three times that of alkaline systems) and gravimetric energy densities as high as 120-150 W h kg^{-1} (two to three times those of usual Ni-Cd batteries), is found in most of today's high-performance portable electronic devices.

The second approach [27] involved replacing the liquid electrolyte by a dry polymer electrolyte (Figure 2-3 a), leading to the so-called Li solid polymer electrolyte (Li-SPE) batteries. But this technology is restricted to large systems (electric traction of backup power) and not to portable devices, as it requires temperatures up to 80 °C. Shortly after this, several groups tried to develop a Li hybrid polymer electrolyte (Li-HPE) battery [28,29], hoping to benefit from the advantages of polymer electrolyte technology with out the hazards associated with the use of Li metal. 'Hybrid' meant that the electrolyte included three components: a polymer matrix, as shown in Figure 2-3 b, swollen with liquid solvent and a salt. Companies such as Valence and Danionics were involved in developing these

polymer batteries, but HPE systems never materialized at the industrial scale because Li-metal dendrites were still a safety issue.

With the aim of combining the recent commercial success enjoyed by liquid Li-ion batteries with the manufacturing advantages presented by the polymer technology, Bellcore researchers introduced polymeric electrolytes in a liquid Li-ion system [30]. They developed the first reliable and practical rechargeable Li-ion HPE battery, called plastic Li ion (PLiON), which differs considerably from the usual coin-, cylindrical-, or prismatic-type cell configurations (Figure 2-4). Such a thin-film battery technology, which offers shape versatility, flexibility and lightness, has been developed commercially since 1999, and has many potential advantages in the continuing trend towards electronic miniaturization. Finally, the 'next generation' of bonded liquid-electrolyte Li-ion cells, derived from the plastic Li-ion concept, are beginning to enter the market place. Confusingly called Li-ion polymer batteries, these new cells use a gel-coated, microporous poly-olefin separator bonded to the electrodes (also gel-laden), rather than the P(VdF-HFP)-based membrane (that is, a copolymer of vinylidene difluoride with hexafluoropropylene) used in the plastic Li-ion cells.

Having retarded almost 30 years of scientific venture leading to the development of the rechargeable Li-ion battery, we now describe some of the significant issues and opportunities provided by the field by high lighting the various areas in need of technological advances.

2-1-3 Present Status and Remaining Challenges

Whatever the considered battery technology, measures of its performance (for example, cell potential, capacity or energy density) are related to the intrinsic property of the materials that form the positive and negative electrodes. The cycle-life and

lifetime are dependent on the nature of the interfaces between the electrodes and electrolyte, whereas safety is a function of the stability of the electrode materials and interfaces. Compared with mature batteries technologies, such as lead-acid or Ni-Cd, rechargeable Li-based battery technologies are still in their infancy, leaving much hope for important over the next decade. Such improvements should arise from changes in battery chemistry and cell engineering. Advances in active chemistry are left to the solid-state chemists' creativity and innovation in the design and elaboration of new intercalation electrodes. At the same time, they must bear in mind that it is impossible to predict the demands that might be placed on tomorrow's portable devices, which in turn places different requirements on the active material chemistry. For instance, with respect to the lower operating voltages of emerging electronics, much debate has focused on whether we should develop a low-voltage active chemistry or rely entirely on electronics and persist in searching for high-voltage active Li chemistry. Finding the best-performing combination of electrode-electrolyte-electrode can be achieved only through the selective use of exciting and new materials as negative and positive electrodes, and of the right electrolyte combination, so as to minimize adverse reactions associated with the electrode-electrolyte interface, the critical phase of any electrochemical system.
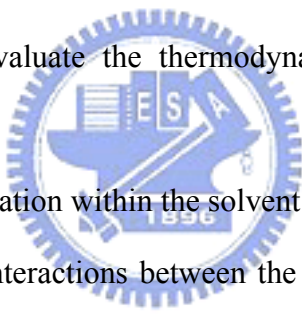
As a result, the choice of the positive electrode depends on whether we are dealing with rechargeable Li-metal or Li-ion batteries [31] (Figure 2-5). For rechargeable Li batteries, owing to the use of metallic Li as the negative electrode, the positive electrode does not need to be lithiated before cell assembly. In contrast, for Li-ion batteries, because the carbon negative electrode is empty (no Li), the positive one must act as a source of Li, thus, requiring use of air-stable Li-based intercalation compounds to facilitate the cell assembly. Although rechargeable Li-SPE cells mainly use Li-free V_2O_5 or its derivatives as the positive electrode, $LiCoO_2$ is most widely

used in commercial Li-ion batteries, deintercalating and intercalating Li around 4 V.

2-2 THEOREMS

2-2-1 Ion-Molecule Interactions

The solubility of a salt in a particular solvent is determined by the energy and entropy changes associated with the transfer of its constituent ions from the crystal lattice to their equilibrium positions in solution [32]. Form the point of view of energy, salts will dissolve only if the lattice energy is compensated by exothermic ion-solvent interactions. The entropy of salvation is determined largely by specific short-range ion-solvent forces, which cause a net ordering of the solvent molecules by the ions, except in the case of highly structured solvents such as water. The terms which must be considered in order to evaluate the thermodynamic parameters of electrolyte salvation include:

(a) energy of cavity formation within the solvent host;

(b) sort-range specific interactions between the ions and the solvent molecules or solvating groups within their immediate neighborhood, for example hydrogen bonding, coordinating bond formation, etc.; and

(c) long-range electrostatic forces.

In the polymer electrolytes so far reported, the "solvent" is a macromolecular array of Lewis bases of low polarity. These are commonly based on the oxygen atoms of a polyether or a polyester, or on the nitrogen atoms of a polyaziridene. Only two types of force are considered to contribute significantly to ion salvation in such systems: (1) general electrostatic interaction of which the principal components are ion-dipole, ion-quadrupole and dipole-dipole forces, and (2) non-electrostatic interactions which, in addition to van der Waal's dispersion forces, may include energy associated with the formation of strained conformations in the polymer

backbone caused by main chain rotations required to accommodate the coordinating groups around the ions.

In protic media, hydrogen bonding plays an important role in specific anion salvation in addition to being responsible for long-range solvent structural effects. In dipolar aprotic solvents such as the low molecular weight ethers there is considerable evidence to indicate that specific anion salvation is effectively absent. Thus even for small anions, conductance experiments show that anion mobility is a simple inverse function of crystal radius [33]. Differences in the general salvation energies of anions do, however, occur as the dielectric constant of the solvent is varied. Most anions are destabilized on passing from polar (and especially protic) solvents to less polar media, and this destabilization is directly related to the charge density and basicity of the ion [34]:

$$CH_3COO^- > Cl^- > Br^- > I^- \approx SCN^- > ClO_4^- \approx CF_3SO_3^- > BF_4^- \tag{2-2}$$
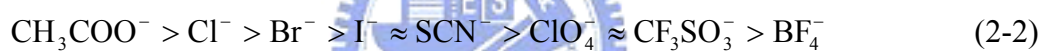
It may be concluded that the most suitable anions for polymer electrolytes based on dipolar aprotic repeat units will be large, "soft" ions such as BF_4^- or ClO_4^-. Such ions have low ion-dipole stabilization energies, but the ion-solvent interactions due to mutual polarizability are relatively large.

The term which undoubtedly dominates the energetics of solvation in polymer electrolytes is that arising from the solvation of the cation. The latter can occur by simple electrostatic interaction between the positive charge on the ion and the negative end of the solvent dipole, or by a partial sharing of a lone pair of electrons leading to the formation of a coordinate bond. For low molecular weight ethers, spectroscopic evidence shows poor correlation of solvent effects with dielectric constant, thus implying that specific cation solvation via Lewis acid-base interactions is important [35].

A more general point may be made concerning the entropy of solvation in polymer media: the loss of translational entropy will normally be much smaller than in low molecular weight solvents (especially if the ion is solvated by neighboring coordination sites on the same chain). Therefore, the entropy of solvation will be positive, and of similar magnitude for most salts. Differential solubility of salts is thus largely controlled by (a) the lattice energy of the salt, and (b) the solvation energy of the cations.

2-2-2 Measurement of Ion Transport

In the characterization of the electrical properties of a solid electrolyte the most basic and useful information is the total conductivity and the fraction of this conductivity that is attributable to each charge carrier. In the electrolyte materials with which we are now dealing, conductivity occurs by the migration of ions. The measurement of ionic conductivity, or ion transport as it is often called, is nontrivial, because of resistance to ion flow at the electrode-electrolyte interface. In general, it is much more difficult to establish a low-resistance interface for ion flow than for electron flow [36,37]. It is adequate, thus, to note that the measurements are often made with the electrolyte sandwiched between a pair of electrochemically inert electrodes (Figure 2-6); a sinusoidal potential is applied and magnitude (*A*) and phase shift (*ϕ*) of the current (*I*) are measured. Thus the sinusoidal dependence of the current with time (*t*) is given by

$$I = A \sin (\omega t + \phi) \tag{2-3}$$

This measurement is repeated at a series of frequencies which typically may range as low as 10^{-4} Hz to as high as 10 MHz. From these data it is possible to extract the conductivity and dielectric constant of the bulk electrolyte sample. Information on the resistance to interfacial charge transport also can be determined. This analysis

follows along lines originally proposed by Cole and Cole [36] and developed in detail

by Macdonald [37,38]. The raw data referred to above can be used to express the ac

current vector (I^*) in terms of real (I') and imaginary (I'') parts:

$$I^* = I' + jI'', \qquad j = \sqrt{-1} \tag{2-4}$$

and a similar expression applies to the ac potential:

$$E^* = E' + jE'' \tag{2-5}$$

The ac impedance, $Z^* = E^*/I^*$, also can be expressed as a real and imaginary part:

$$Z^* = Z' + jZ'' \tag{2-6}$$

In a Cole-Cole plot, Figure 2-7 [39] presents that, now commonly referred to as an

impedance spectrum, the real part of the impedance (Z') is plotted against the

imaginary part (Z'') for data collected at a series of frequencies. In favorable cases

various features of the impedance spectrum can be interpreted in terms of the

response of the bulk polymer whereas other features arise from the

electrode-electrolyte interface. The bulk resistance of the electrolyte (R_b) is one of the

quantities that can be derived from such a plot. The value for the resistance of the

sample (R_b) along with thickness of the sample and electrode area yields the

resistivity of the sample or its inverse, the conductivity. As shown in the following

equation (2-7):

$$\sigma = L/A \times R_b \tag{2-7}$$

where σ is the conductivity, L is the thickness of the electrolyte film, A is the section

area of the stainless-steel electrode, and R_b is the bulk resistance. Table 2-2 presents

some typical values for the total ionic conductivity for a range of electrolytes, as well

as some more familiar electronic conductors, which are included to put the

electrolytes into perspective.

The identity of the charge carriers and the fraction of the current carried by each

is a more subtle issue that is still not well resolved in most studies of solvent-free polymer electrolytes. This issue was addressed by physical chemists around the turn of the century for liquid electrolytes. They devised simple but elegant methods for the determination of transference numbers, which are generally designated as t_+ or t_- for the fraction of the current carried by the cation and anion, respectively [40]. The measurement of transference numbers, or transport numbers as they are also called, is experimentally more difficult with the solid electrolytes than their solution counterparts [41], but measurements of fair quality have been made and the general picture for a variety of polymer electrolytes is that somewhat over half of the current is carried by the anion and therefore less than half by the cation. A major issue that is not yet well resolved is the nature of the mobile species. With monovalent ions in dilute aqueous solution the isolated cation and anion are the charge carriers. But the much lower dielectric constant of the polymer host in the solvent-free polymer electrolytes should be conductive to strong Coulombic interaction between ions. In the salt concentration range generally studied in polymer electrolytes, the primary charge carriers may well be ion triplets, quintets, and so on. A recent detailed study of ion transport in fluid solutions of short-chain poly(ethylene oxide) provides strong evidence for the importance of ion clusters in the solid electrolytes [42].

2-2-3 Interpretation of Ionic Conductivity

The temperature dependence of the conductivity of polymer electrolytes indicates an activated process. Thus the conductivity increases with increasing temperature, and Arrhenius behavior often provides a good representation of the data [43], as shown in Figure 2-8. On closer inspection, changes in slope and curvature of the log σ vs $1/T$ plots are often observed. An abrupt change in slope can generally be traced to a phase change in polymer-salt complex [27]. It is clear form Figure 2-9 [44]

41

that higher conductivity occurs in the amorphous phase that is metastable at room temperature. The multiphase behavior presents complications for fundamental studies and for applications. To gain fundamental insight into the mechanisms of ionic motion in polymer electrolytes, we consider fully homogeneous amorphous polymer-salt complexes. These materials are in fact now of primary interest in the study of polymeric electrolytes.

The conductivity of any material can be expressed in terms of the mobility m by the relationship [43]:

$$\sigma = \sum_i \mu_i n_i z_i \qquad (2\text{-}8)$$

Where σ, μ_i, n_i, and z_i are respectively conductivity, the mobility of the i species, the concentration of carriers of the i species, and the charge of the i species. The polymer electrolytes contain no significant conjugation within the polymer backbone, and the salts on which they are based have negligible electronic conductivities. Thus one might suspect, and indeed several experimental measurements have shown [45], that electrons or electron holes do not contribute to the summation in eq (2-8). Both cations and anions do, however, contribute and as discussed above, important questions concerning the relative mobility (transference numbers) of the cationic and anionic carriers remain. Once again, this represents a complication in the simple interpretation of the temperature dependence of conductivity.

Experimentally, one observes fairly straigntforward behavior of the temperature dependence of the conductivity in homogeneous electrolytes. The straight or curved lines observed when the conductivity is plotted in Arrhenius coordinates (Figure 2-8) can be fit, respectively, to the Arrhenius and VTF (Vogel-Tamann-Fulcher) [46] forms:

$$\sigma T = \sigma_0 \exp\left(- E_A / kT\right) \qquad (2\text{-}9)$$

$$\sigma T = \sigma_0 \exp(-B/k(T - T_0)) \qquad\qquad (2\text{-}10)$$

In the Arrhenius form, E_A is the usual activation energy, whereas in the VTF form, T_0 is a parameter to be determined (in many cases, however, it is found that T_0 is very close to T_g, the glass transition temperature), and B is a constant, whose dimensions are in fact energy and called the pseudo activation energy, but which is not simply interpreted as an activation term (E_A); k is Boltzmann's constant. The early investigations of the groups in Grenoble [27,47-49] generally showed curved plots, corresponding to VTF type behavior. Consequently, Cheradame and co-workers [48-52] discussed these plots in terms of the chain segment mobility of the polymer host material. They used the relationship, very common in discussion of polymer dynamics, of polymer chain viscosity to glass transition temperature that is summarized in the Williams-Landel-Ferry (WLF) relationship [53]:

$$\log\left[\frac{\sigma(T)}{\sigma(T_s)}\right] = \log a_T = \frac{-C_1(T - T_s)}{C_2 + (T - T_s)} \qquad\qquad (2\text{-}11)$$

Where T_s is an arbitrary reference temperature, a_T is called the mechanical shift factor, and C_1 and C_2 are "universal" constants.

2-3 REFERENCES

1. Gauthier, M.; Bélanger, A.; Kapfer, B.; Vassort, G.; Armand, M. In *Polymer Electrolyte Reviews*; Mac Callum, J. R., Vincent, C. A., Eds., Elsevier: London, 1987.

2. Hooper, A.; Gauthier, M.; Bélanger, A. In *Electrochemical Science and Technology of Polymers*; Linford, R. G. Ed., Elsevier: London, 1988.

3. Armand, M. B.; Chabagno, J. M.; Duclot, M. J. In *Fast Ion Transport in Solids*; Vashista, P., Mundy, J. N., Shenoy, G. K. Eds., Elsevier: New York, 1979.

4. Tarascon, J. M.; Armand, M. *Nature* **2001**, *414*, 359.

5. Ikeda, H.; Saito, T.; Tamura, H. In *Proc. Manganese Dioxide Symp. Vol. 1*; Kozawa, A., Brodd, R. H., IC sample Office: Cleveland, 1975.

6. Steele, B. C. H. In *Fast Ion Transport in Solids*; Van Gool, W., Ed., North-Holland: Amsterdam, 1973.

7. Armand, M. B. In *Fast Ion Transport in Solids*; Van Gool, W., Ed., North-Holland: Amsterdam, 1973.

8. Rouxel, J.; Danot, M.; Bichon, M. *Bull*. *Soc*. *Chim*. **1971**, *11*, 3930.

9. Di Salvo, F. J.; Schwall, R.; Geballe, T. H.; Gamble, F. R.; Osieki, J. H. *Phys*. *Rev*. *Lett*. **1971**, *27*, 310.

10. Whittingham, M. S. *Science* **1976**, *192*, 1226.

11. Whittingham, M. S. *US Patent 4009052*, **1976**.

12. Rao, B. M. L.; Francis, R. W.; Christopher, H. A. *J. Electrochem*. *Soc*. 1977, *124*, 1490.

13. Broahead, J.; Butherus, A. D. *US Patent* **1978**, *3791867*.

14. Broahead, J; DiSalvo, F. J.; Trumbore, F. A. *US Patent* **1978**, *3864167*.

15. Murphy, D. W.; Christian, P. A. *Science* **1979**, *205,* 651.

16. Mizushima, K; Jones, P. C.; Wiseman, P. J. Goodenough, J. B. *Mat*. *Res*. *Bull*.

1980, *15*, 783.

17. Thackeray, M. M.; David, W. I. F.; Bruce, P. G.; Goodenough, J. B. *Mat. Res. Bull.* **1983**, *18*, 461.

18. Armand, M. B. In *Materials for Advanced Batteries*; Murphy, D. W., Broadhead, J., Steele, B. C. H. Eds., Plenum: New York, 1980.

19. Murphy, D. W.; Disalvo, F. J.; Carides, J. N.; Waszczak, J. V. *Mat. Res. Bull.* **1978**, *13*, 1395.

20. Lazzari, M.; Scrosati, B. *J. Electrochem. Soc.* **1980**, *127*, 773.

21. Will, F. G. *US Patent* **1975**, *3874958*.

22. Percheron-Guegan, A.; Achard, J. C.; Sarradin, J.; Bronoël, G. *French Patent* **1975**, *7516160*.

23. Guérard, D.; Hérold, A. *C. R. Acad. Sci. C* **1972**, *275*, 571.

24. Basu, S. *US Patent* **1983**, *4423125*.

25. Mohri, M. *J. Power Sources* **1989**, *26*, 545.

26. Nagaura, T.; Tozawa, K. *Prog. Batteries Solar Cells* **1990**, *9*, 209.

27. Armand, M.; Chabagno, J. M.; Duclot, M. J. In *Fast Ion Transport in Solids Electrodes and Electrolytes*; Vashishta, P., Moundy, J. N., Shenoy, G. K. Eds., North-Holland: Amsterdam, 1979.

28. Kelly, I. E.; Owen, J. R.; Steel, B. H. *J. Power Sources* **1935**, *14*, 13.

29. Kelly, I. E.; Owen, J. R.; Steel, B. H. *Interfacial Electrochem.* **1984**, *168*, 467.

30. Tarascon, J. M.; Gozdz, A. S.; Schmutz, C.; Shokoohi, F.; Warren, P. C. *Solid State Ionics* **1996**, *86-88*, 49.

31. Guyomard, D. In *New Trends in Electrochemical Technology: Energy Storage Systems for Electronics*; Osaka, T., Datta, M. Eds., Gordon & Breach Science Publishers, 2000.

32. MacCallum, J. R.; Vincent, C. A. In *Polymer Electrolyte Reviews*; Mac Callum, J.

R., Vincent, C. A., Eds., Elsevier: London, 1987.

33. Parker, A. J. *Quart. Rev.* **1962**, *16*, 163.

34. Marcus, Y. *Ion Solvation*; Wiley: Chichester, 1985.

35. Garst, J. F. In *Solute-Solvent Interactions*; Coetzee, J. F., Ritchie, C. D. Eds., Dekker: New York, 1969.

36. Cole, K. S.; Cole, R. H. *J. Chem. Phys.* **1941**, *9*, 341.

37. Macdonald, J. R. *J. Chem. Phys.* **1973**, *58*, 4982.

38. Macdonald, J. R. In *Superionic Conductors*; Mahan, G. D., Roth, W. L. Eds.; Plenum Press: New York, 1976.

39. Lee, I. J.; Song, G. S.; Lee, W. S.; Suh, D. H. *J. Power Sources* **2003**, *114*, 320.

40. Smedley, S. *The Interpretation of Ionic Conductivity in Liquids*; Plenum: New York, 1980.

41. LeNest, J. F.; Cheradame, H.; Dalard, F.; Deroo, D. *J. Appl. Electrochem.* **1986**, *16*, 75.

42. Vincent, C. A. *Electrochim. Acta.* **1995**, *40*, 2035.

43. Ratner, M. A.; Shriver, D. F. *Chem. Rev.* **1988**, *88*, 109.

44. Jannasch, P. *Chem. Mater.* **2002**, *14*, 2718.

45. Dupon, R.; Whitmore, D. H.; Shriver, D. F. *J. Electrochem. Soc.* **1981**, *128*, 716.

46. Fulcher, G. S. *J. Am. Ceram. Soc.* **1925**, *8*, 339.

47. Armand, M. B.; Chabagno, J. M.; Duclot, M. *Extended Abstracts*, *Second International Conference on Solid Electrolytes*, St. Andrews, Scotland, 1978.

48. Killis, A.; LeNest, J. F.; Cheradame, H. *Makromol. Chem.*, *Rapid Commun.* **1980**, *1*, 595.

49. Killis, A.; LeNest, J. F.; Gandini, A.; Cheradame, H. *J. Polym. Sci.*, *Polym. Phys. Ed.* **1981**, *19*, 1073.

50. Killis, A.; LeNest, J. F.; Gandini, A.; Cheradame, H.; Cohen-Addad, J. P. *Solid*

State Ionics **1984**, *14*, 231.

51. Killis, A.; LeNest, J. F.; Gandini, A.; Cheradame, H. *Makromol. Chem.* **1982**, *183*, 1087.

52. Killis, A.; LeNest, J. F.; Cheradame, H.; Gandini, A. *Makromol. Chem.* **1982**, *183*, 2835.

53. William, M. L.; Landel, R. F.; Ferry, J. D. *J. Am. Chem. Soc.* **1955**, *77*, 3701.

Table 2-1. Principal Events in the Development of Primary and Secondary Batteries [1]

AQUEOUS BATTERIES

Water electrolytes	*1800* Zn-Ag Invention by Volta →	*1866* Leclanché cell invention →	*1888* First production of C-Zn cells →	*1945-1955* Heavy-duty C-Zn cell by electrolyte and MnO_2 optimization →	*1960 ~ present* Market decline due to competition
Acid Electrolytes	*1859* Lead-acid battery discovery by Planté →	*1881* Development of Pb-Sb alloy grids →	*1935* Development of Pb-Ca alloy grids →	*1970-1980* Development of small sealed batteries →	*1988 ~ present* Market dominated by SLI motor vehicle application

	Alkaline Electrolytes					
Primary MnO_2-Zn batteries	*1981-1912* Scientific papers describing MnO_2 alkaline cells →		*1947-1950* First production for special applications →		*1970-1988* Development of large markets	
Rechargeable Ni-Cd batteries	*1899* Ni-Cd battery invention (Jungner, Edison) →	*1909* Pocket plate development for vented battery production →	*1944* Sintered plate development for vented battery production →	*1950* Sealed Ni-Cd battery development →	*1985 ~ present* Market development of small portable sealed batteries

ALKALI-METAL BATTERIES

	Liquid Electrolytes					
1912 Determination of Li electrode potential in organic liquid	*1945-1960* Research on liquid organic electrolytes for alkali metal batteries →	*1960-1970* Development of primary Li battery for special applications →	*1967-1970* Li-CuO production Li-$SoCl_2$, $LiSO_2$ research →	*1973-1976* Li-CF_x, Li-MnO_2 commercialization →	*1978 ~ present* Rapid market growth	
	~ 1958 Initial research on solid cathodes for Li rechargeable batteries →	*1973* Solid-state Li-insertion cathode invention →	*1977* Li-MoS_2 initial studies →	*1978* Brief production of LiAl-FeS_x batteries →	*~ 1983* Rechargeable Li-$SO2$ research →	*1987* Industry production of Li-MoS_2 Moli^R cells

Molten-salts Electrolytes			*1968* Rechargeable Li-S, Li-Se cells with LiCl-KCl eutectic →	*1973-1988* LiAl-FeS_x research and engineering →	*1987* Research on low-temperature molten-salts cells
Solid Electrolytes	*1950-1960* Research on crystalline halide batteries →	*1960* First commercial batteries based on $RbAg_4I_5$ →	*1966* Na-S, β-$Al2O_3$ battery invention →	*1970-1975* Commercial development of solid Li-I batteries for pacemakers →	*1978* Li rechargeable SPE battery invention → *1984 ~ present* Determination of SPE cyclability and room temperature operation

Table 2-2. Typical Conductivities[a]

material	conductivity, S cm^{-1}
P(EO)$_{12}$LiClO$_4$	5.6 ×10^{-6}
P(PO)$_9$LiCF$_3$SO$_3$	2.2 ×10^{-5}
(MEEP)$_4$LiCF$_3$SO$_3$	1.0 ×10^{-4}
RbAg$_4$I$_5$	6.0 ×10^{-1}
Ge[b]	5.0 ×10^{-2}
Cu[b]	5.6 ×10^5

[a] The experimental condition is at 312 K. [b] Electronic conductivity.

Lead–acid battery
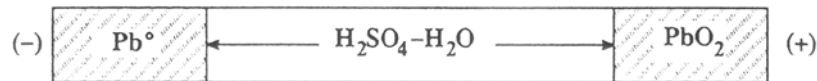
N.B. Electrolyte participation in electrode reactions.
Overall reaction: $Pb + PbO_2 + 2H_2SO_4 \rightleftharpoons 2PbSO_4 + 2H_2O$
Energy density (Wh/kg): 250 (theoretical), ~25–35 (practical, ~1/8).
Secondary reaction: $H_2O \rightarrow H_2 + \frac{1}{2}O_2$
% Efficiency (Ah and Wh): 85 and 70–75%.
Cycling characteristic (full discharges): short cycle life (300 cycles).
Operating-temperature range: −20 to 40°C (−40°C for SLI use).

Nickel–cadmium battery
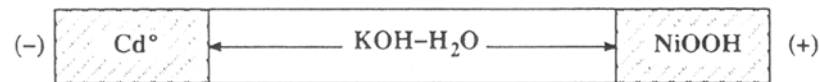
N.B. Water participation in electrode reactions.
Overall reaction: $Cd + 2NiOOH + 2H_2O \rightleftharpoons 2Ni(OH)_2 + Cd(OH)_2$
Energy density (Wh/kg): 245 (theoretical), ~35 (practical, ~1/7).
Secondary reaction: $H_2O \rightarrow H_2 + \frac{1}{2}O_2$
% Efficiency (Ah and Wh): 70 and 60–65%.
Cycling characteristic: good cycle life (500–1000 cycles), memory effect.
Operating-temperature range: −40 to 50°C.

SPE lithium battery
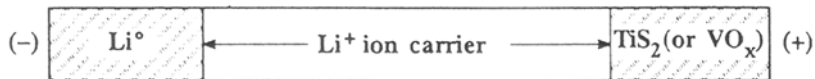
N.B. SPE is simply a Li^+ ion carrier that can be made ultra-thin.
Overall reaction: $TiS_2 + xLi^0 \rightleftharpoons Li_xTiS_2$
Energy density (Wh/kg): 480 (theoretical), ~120 (practical, ~1/4).
No secondary reaction.
% Efficiency (Ah and Wh): ~100 and 85–95%.
Cycling characteristic: full discharge capability (600 cycles).
Operating-temperature range: −10 to 130°C.

Figure 2-1. Main differences between the SPE lithium-reversible battery and exist aqueous systems (lead-acid and nickel-cadmium batteries).
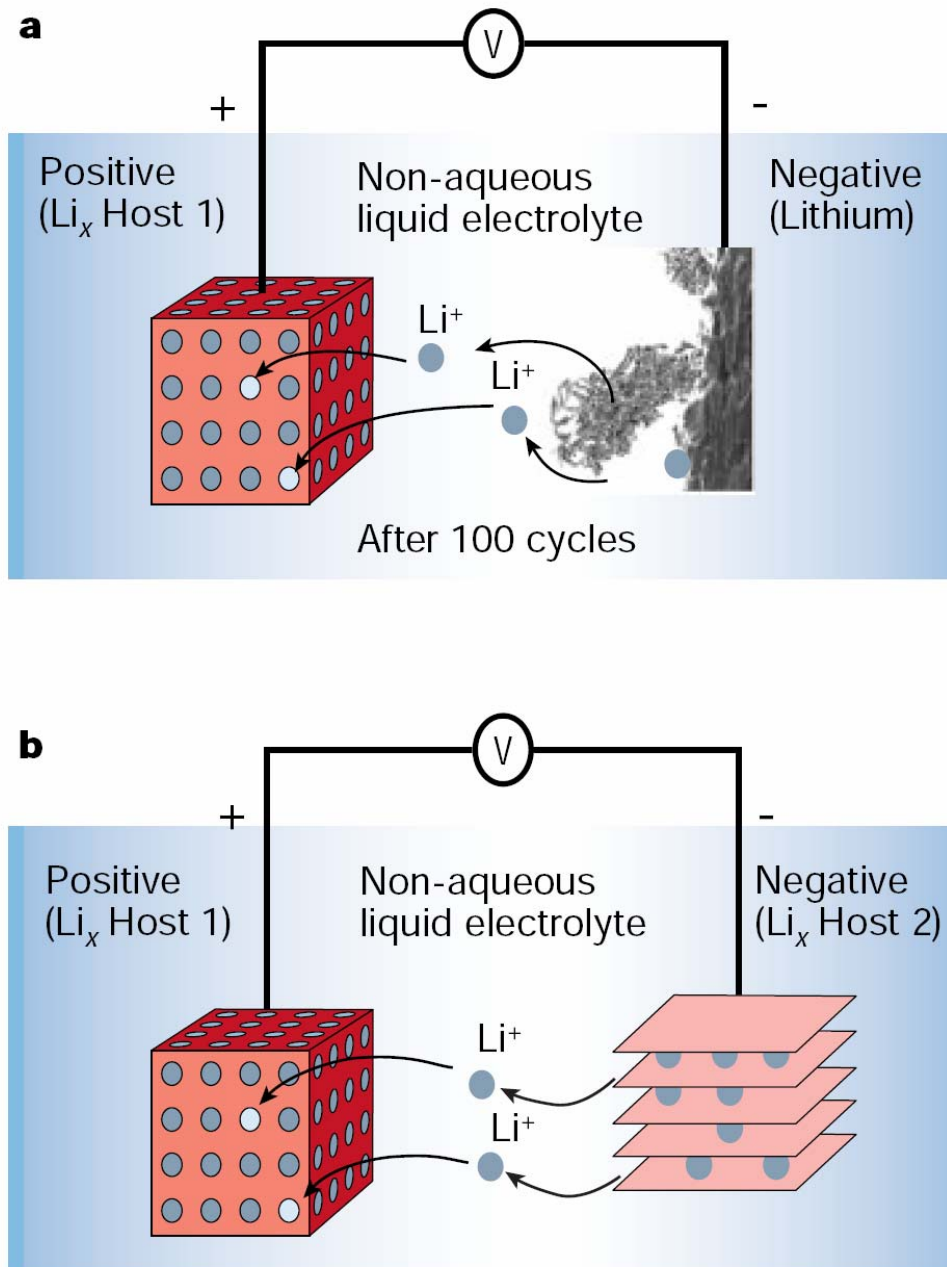
Figure 2-2. Schematic representation and operating principles of Li batteries. (a) Rechargeable Li-metal battery. (b) Rechargeable Li-ion battery.
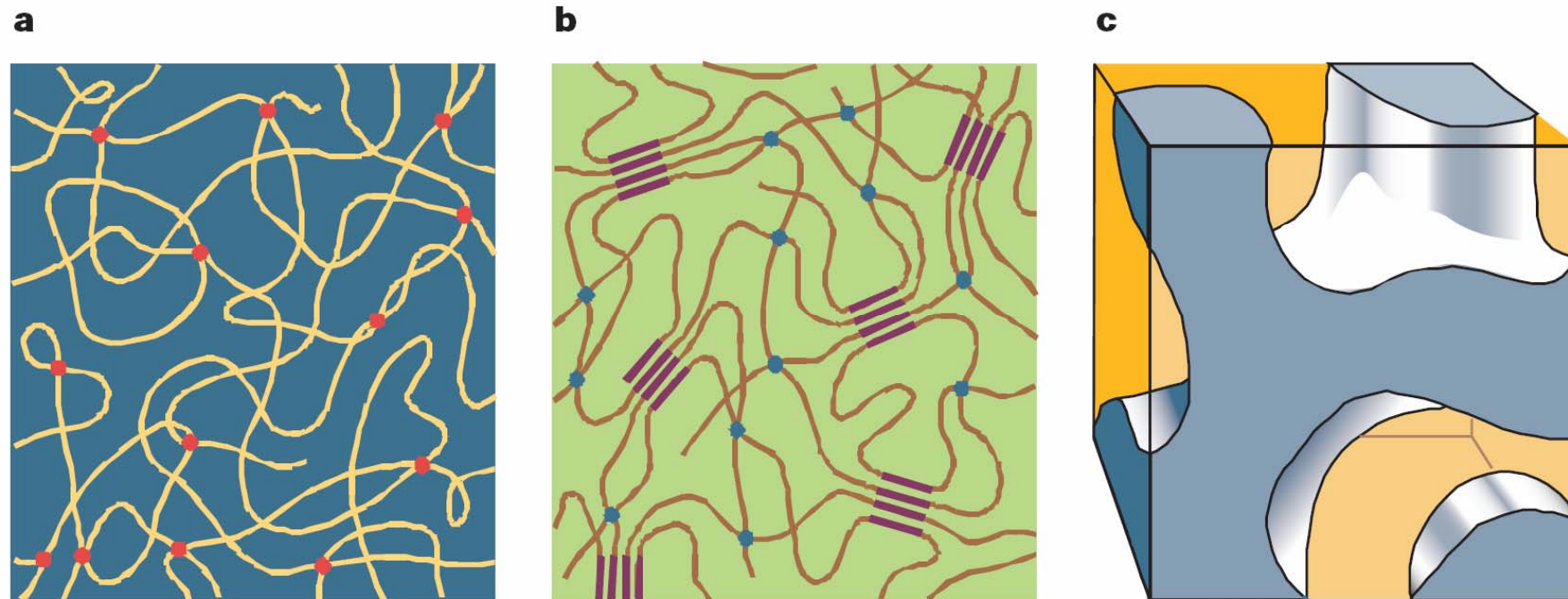
Figure 2-3. Schematic representations of polymer electrolyte networks. (a) Pure (dry) polymer consisting of entangled chains, through which the Li ions (red points) move assisted by the motion of polymer chains. (b) A hybrid (gel) network consisting of a semicrystalline polymer, whose amorphous regions are swollen in a liquid electrolyte, while the crystalline regions enhance the mechanical stability. (c) A poly-olefin membrane in which the liquid electrolyte is held by capillaries.
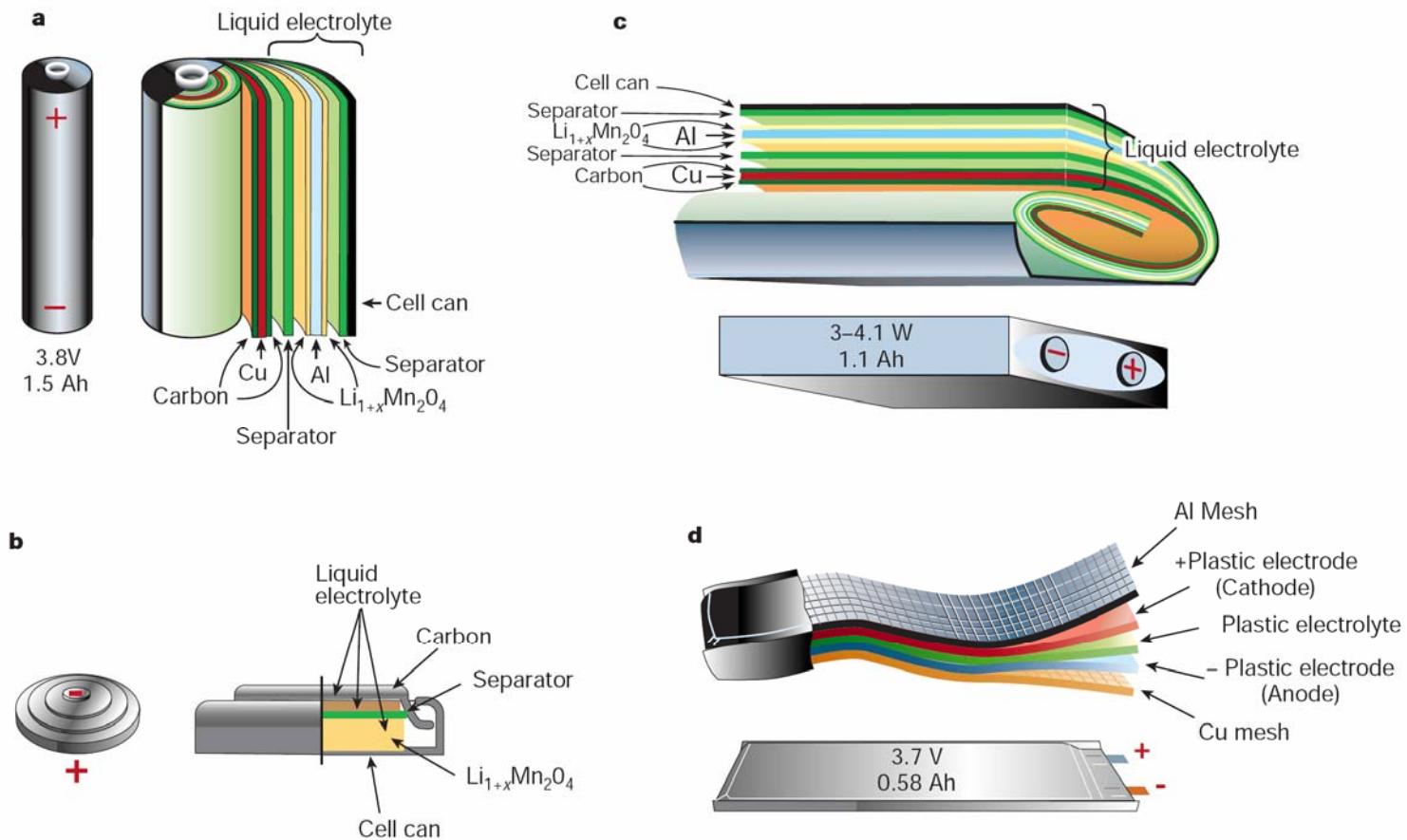
Figure 2-4. Schematic drawing showing the shape and components of various Li-ion battery configurations. (a) cylindrical; (b) coin; (c) prismatic; and (d) thin and flat. Note that the unique flexibility of the thin and flat plastic LiION configuration; in contrast to the other configurations, the PLiION technology does not contain free electrolyte.
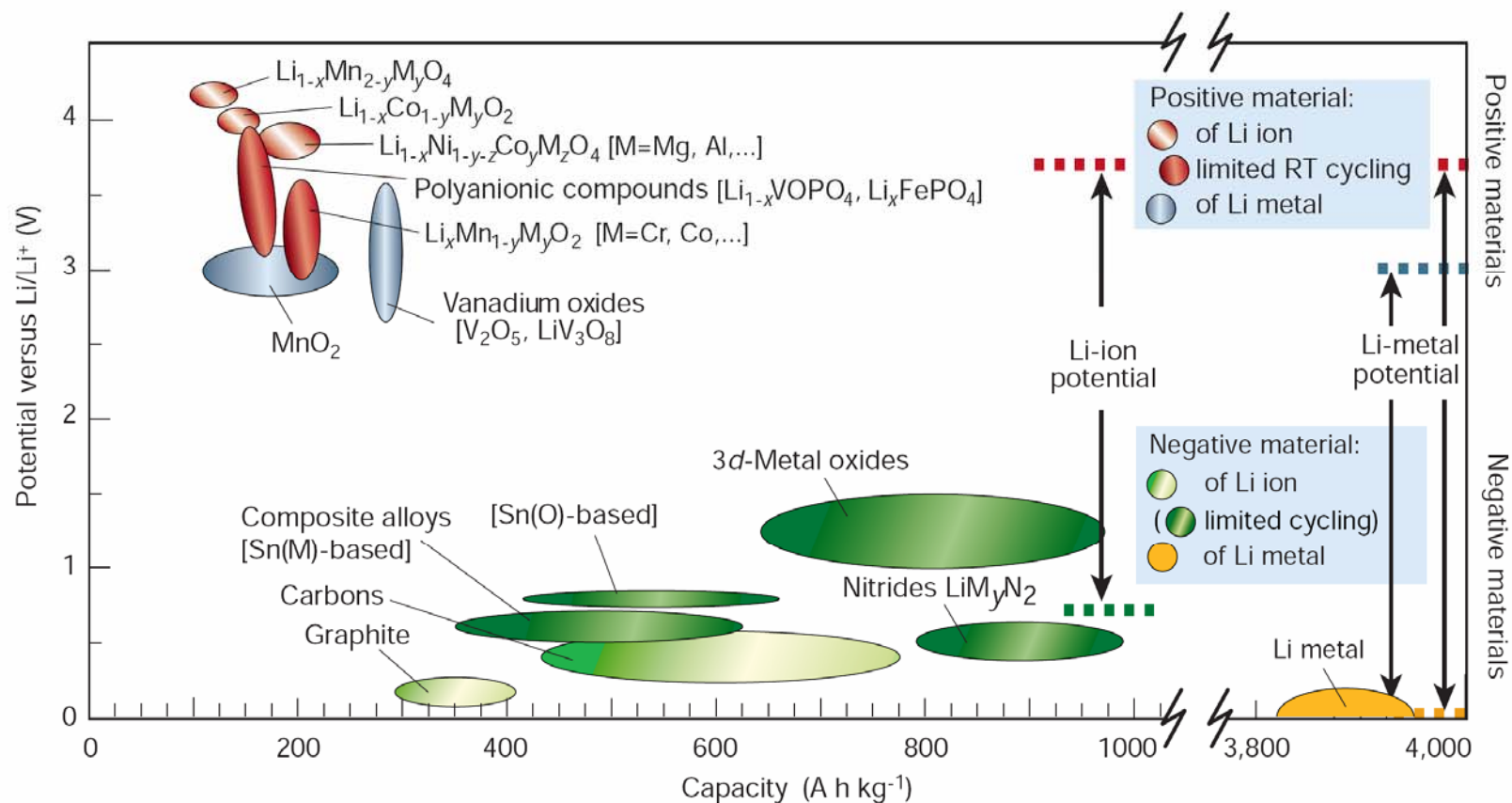
Figure 2-5. Voltage versus capacity for positive and negative electrode materials presently used or under serious considerations for the next generation of rechargeable Li-based cells. The output voltage values for Li-ion cells or Li-metal cells are represented.
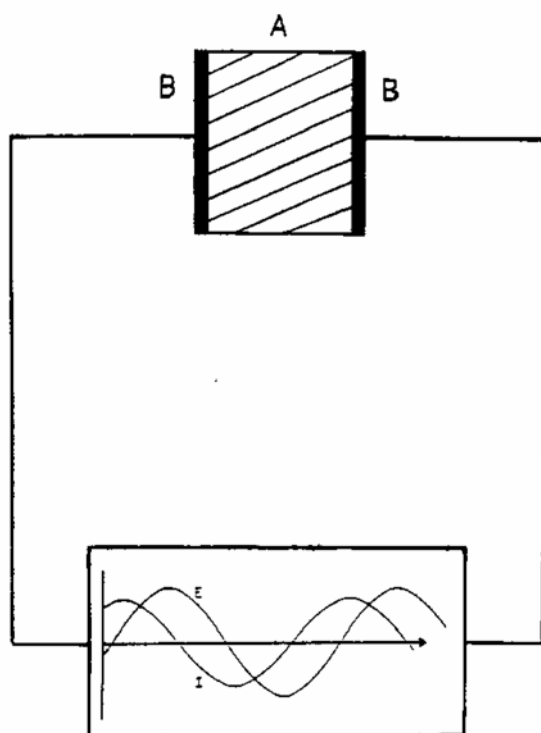
Figure 2-6. Schematic of an ac impedance experiment. B = electrode, A = polymer electrolyte, E = imposed potential, and I = measured current response.
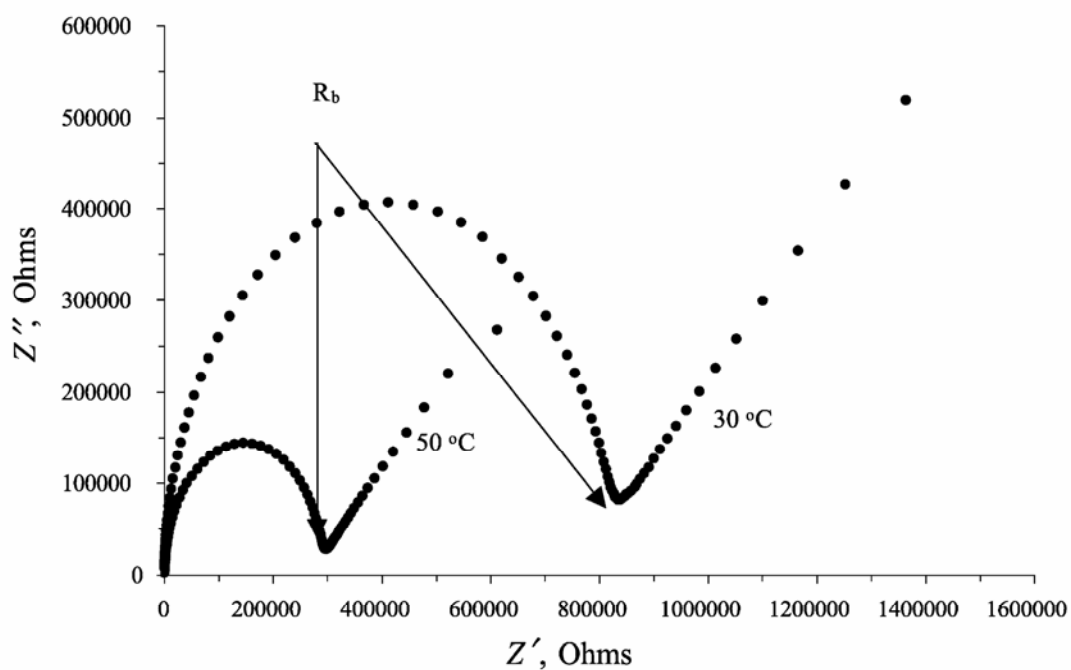
Figure 2-7. Complex impedance spectrum (Cole-Cole plot) of D_4D_2-40 complex with [CN]:[Li$^+$] ratio of 16:1 at 30 and 50 °C (taken from ref. 39). R_b represents the bulk resistance of the electrolyte sample.
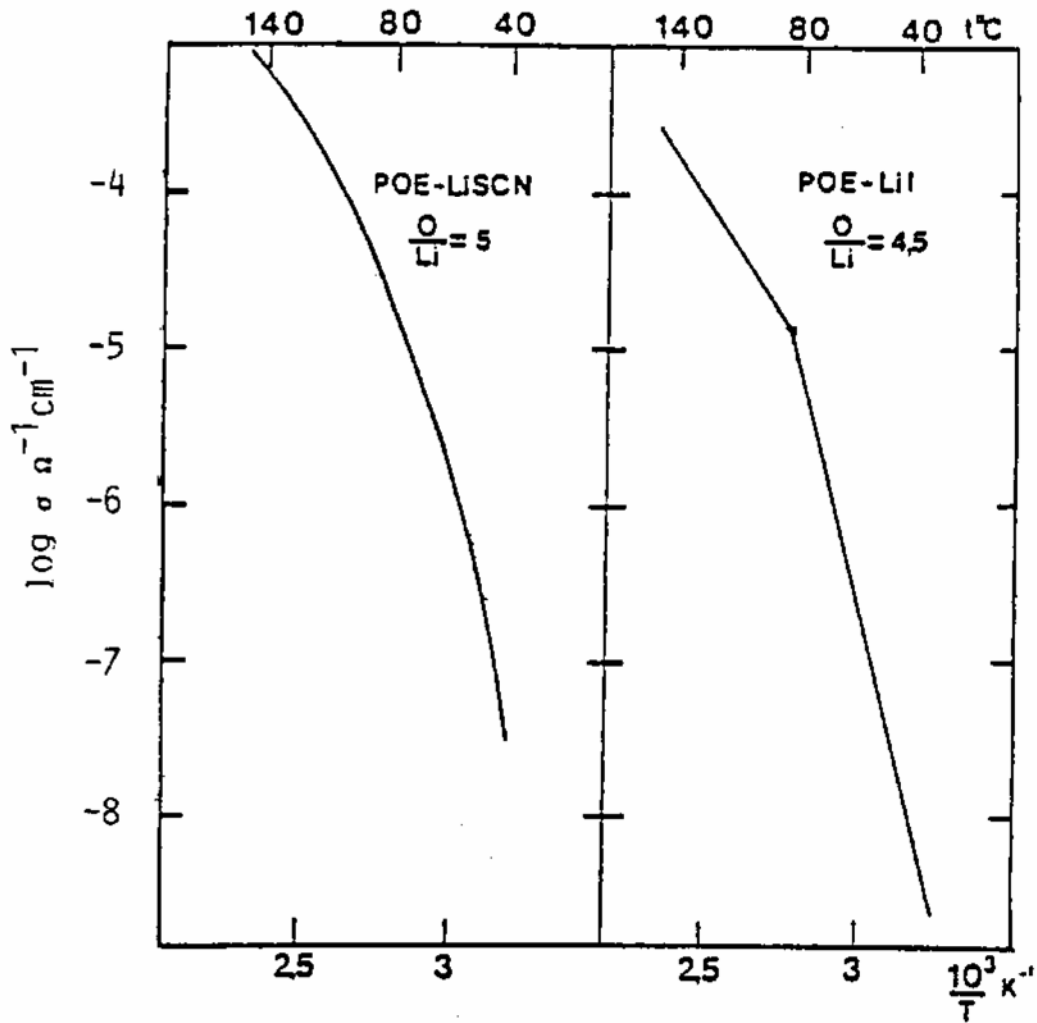
Figure 2-8. Arrhenius-type plots for log σ versus T^{-1} for PEO complexes of LiI and LiSCN. The curved behavior for PEO/LiSCN fits the VTF relation of eq. (2-10). The double Arrhenius behavior from PEO/LiI corresponds to the conduction of the partially crystalline and elastomeric phases.
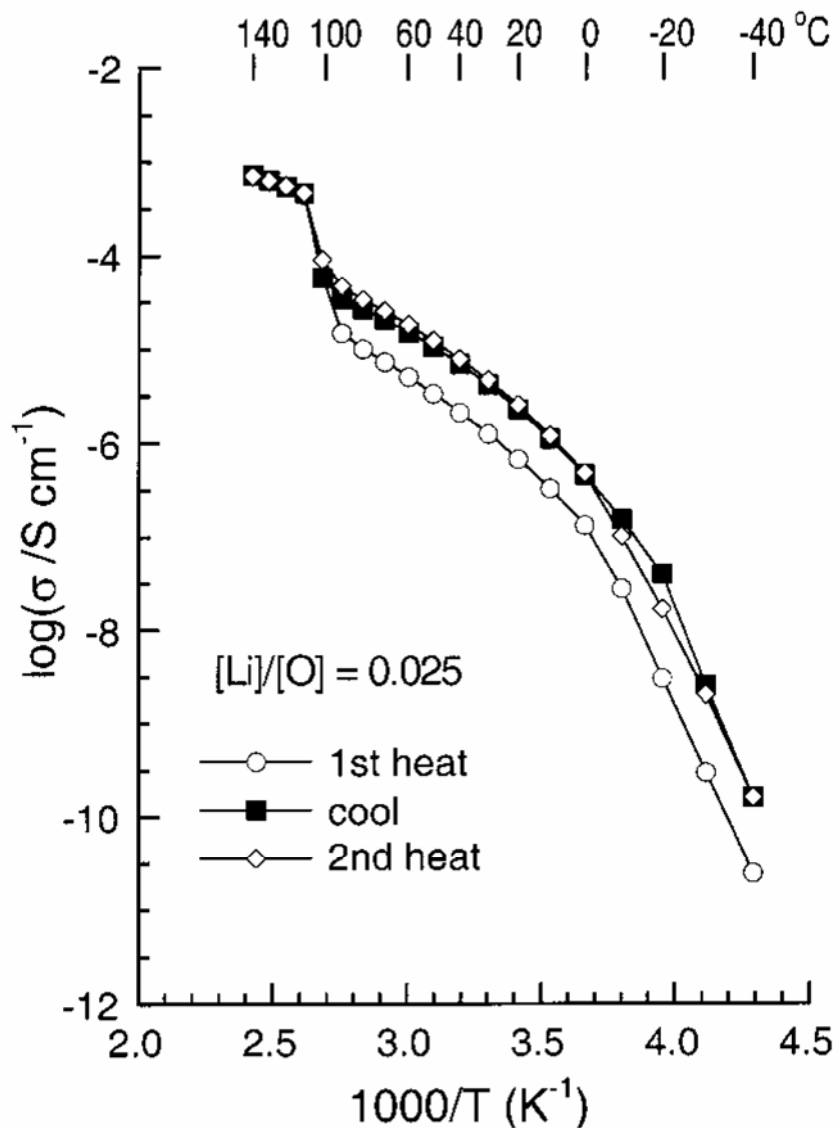
Figure 2-9. Temperature versus conductivity plots showing thermal hysteresis effects of σ for solid polymer electrolyte based on PEO-PEOPO-PEP triblock copolymer [44] with LiTFSI at $[Li^+]/[O] = 0.025$. The conductivities were evaluated by impedance spectroscopy during the temperature scan: -40 $\rightarrow$ 140 $\rightarrow$ -40 $\rightarrow$ 140 °C.

CHAPTER 3

Investigating the Effect of Miscibility on the Ionic Conductivity of LiClO$_4$/PEO/PCL Ternary Blends

ABSTRACT

In this paper, we demonstrate that miscibility affects the ionic conductivity of ternary polymer blends of lithium perchlorate (LiClO$_4$), poly(ethylene oxide) (PEO), and poly(ε-caprolactone) (PCL). Although individually these three binary blends are fully miscible, a closed immiscibility loop exists in the ternary blend phase diagram as a result of the complicated interactions among LiClO$_4$, PEO, and PCL. The addition of PCL suppresses the crystallization of PEO and results in higher ionic conductivity. FTIR spectroscopy studies indicate that an excess PCL content causes immiscibility, which results in PCL being excluded from the ternary blends. Consequently, the maximum ionic conductivity ($6.3 \times 10^{-7} \mathrm{Scm}^{-1}$) at ambient temperature of ternary blends having a fixed LiClO$_4$ content (25 wt%) is at a composition of 25/60/15 (LiClO$_4$:PEO:PCL).

3-1 INTRODUCTION

Solid polymer electrolytes (SPEs), which are complexes of solvent-free polymers and metal salts, are prepared by dissolving salts in high-molecular-weight polar polymer hosts. Polymer electrolytes have been studied extensively during the past two decades because of their potential applications, which include high-energy density batteries and fuel cells [1-5]. Ionic transport occurs in the amorphous regions of the polymer and very often is the result of a coupling between the ions and segmental motions of the polymer chains. Poly(ethylene oxide) (PEO)-based polymeric electrolytes are still among the most extensively studied polymer ionic conductors because their structures are beneficial for supporting fast ion transport. Unfortunately, a high content of a crystalline phase limits the conductivity of PEO-based electrolytes. Efforts to enhance the ionic conductivity of PEO based SPEs have focused on suppressing its crystallinity by incorporating an inorganic filler, such as clay, to form composite polymeric electrolytes [6], by copolymerizing PEO with macromonomers [7], and by blending with other polymers into PEO-based electrolytes [8]. It is an important challenge to develop practical methods for preparing the SPEs that have higher ionic conductivity and dimensional stability. In this regard, the preparation of polymeric electrolytes by blending them with other appropriate polymers is of interest. Polymer blend is a quick and economical alternative method for obtaining materials that have optimized properties and for the easy control of their physical properties by compositional change.

PEO/PCL (poly(ε-caprolactone)) blends are miscible over their entire range of compositions [9]. The existence of strong interaction between PEO and PCL tends to suppress the crystallinity of PEO. Furthermore, because PCL possesses low T_g (-60 °C), PEO/PCL blend systems generally maintain the polymer chain mobility and flexibility. Nevertheless, the immiscible phenomenon occurs upon the addition of

certain compositions of lithium perchlorate ($LiClO_4$) into a ternary $LiClO_4$/PEO/PCL blend system, even though any pair of its components is miscible. Amorphous PEO complexes with $LiClO_4$ are suitable for achieving reasonably high and stable conductivity [1,10,11]. Because the addition of PCL into an electrolyte system based on $LiClO_4$/PEO tends to retard or inhibit the PEO crystallization, we expected that this ternary blend, $LiClO_4$/PEO/PCL, would have higher ionic conductivity than previously reported electrolyte systems based on $LiClO_4$/PEO binary blends.

To our knowledge, there has been no previous study of the influence of the miscibility behavior and interaction mechanism on the variation of ionic conductivity in polymer electrolytes. In this study, we employed differential scanning calorimetry (DSC), Fourier transform infrared (FTIR), solid-state ^{7}Li NMR spectroscopy and alternating current (ac) impedance to investigate the miscibility and related conductivity behaviors of this $LiClO_4$/PEO/PCL ternary blend system. Furthermore, we have presented a more convenient method to suppress the crystalline phase of PEO and obtain a higher ionic conductivity by adding PCL in $LiClO_4$/PEO-based electrolyte system.

3-2 EXPERIMENTAL

3-2-1 Materials

The poly(ethylene oxide) (PEO) with M_v = 10,000 and poly(ε-caprolactone) (PCL) with M_w = 65,000 were purchased from Aldrich Co. Lithium perchlorate (LiClO$_4$; Aldrich) was dried in a vacuum oven at 80 °C for 24 h and stored in a desiccator prior to use. Acetonitrile was distilled at a suitable temperature under nitrogen atmosphere prior to use.

3-2-2 Sample Preparations

Polymer electrolytes of LiClO$_4$/PEO/PCL in various ternary blend compositions were prepared by solution casting. Desired amounts of PEO, PCL, and LiClO$_4$ salt were dissolved in dry acetonitrile, and stirred continuously for 24 h at 60 °C. The solution was cast onto a Teflon dish and maintained at 50 °C for an additional 24 h to remove the solvent, and then the dish was further dried under vacuum at 80 °C for 2 days. To prevent its contact with the air and moisture, the polymer electrolyte was transferred to a glovebox under a nitrogen atmosphere.

3-2-3 Differential Scanning Calorimetry (DSC)

Thermal analyses were performed using a DSC instrument (DuPont TA 2010). The sample was heated from -100 to 150 °C under dry nitrogen. The glass transition temperature (T_g) was obtained as the inflection point of the heat capacity jump recorded at a scan rate of 20 °C /min.

3-2-4 Fourier Transform Infrared Spectroscopy (FTIR)

The conventional potassium bromide (KBr) disk method was employed to measure the infrared spectra of the blend films. All polymer films were prepared

under a N_2 atmosphere. The acetonitrile solution was cast onto a KBr disk, from which the solvent was evaporated under vacuum at 70 °C for 48 h. All IR spectra were obtained within the range of 4000-400 cm^{-1} using a Nicolet AVATRR 320 FTIR Spectrometer (Nicolet Instruments, Madison, WI) operating at a resolution of 1 cm^{-1}.

3-2-5 Solid-State NMR Spectroscopy

The solid-state ^{7}Li magic angle spinning (MAS) NMR spectra were recorded at 300 K on a Bruker DSX-400 NMR Spectrometer equipped with a 7 mm double-resonance probe, operating at 400.13 MHz for ^{1}H nucleus and 155.27 MHz for ^{7}Li nucleus. Typical experimental conditions used to obtain the solid-state NMR spectra: π/2 duration, 2 μs ; recycle delay, 8 s; ^{1}H decoupling power, 65 kHz; spinning speed, 2 kHz. A 1 M aqueous LiCl solution was used as an external chemical shift reference (0 ppm).

3-2-6 Conductivity Measurements

Ionic conductivity measurements with alternation current were conducted on an AUTOLAB designed by Eco Chemie within the frequency range from 10 MHz to 10Hz. The electrolyte film was sandwiched between stainless-steel blocking electrodes (diameter: 1 cm). The specimen thickness varied from 0.8 to 1.2 mm; the impedance response was gauged over the range from 20 to 120 °C. The bulk resistance was derived from the Cole-Cole plot of the complex impedance data of the blend where the imaginary impedance is zero [12-14]. Conductivity was calculated from the bulk resistance according to the equation

$$\sigma = L/A \times R_b$$

where σ is the conductivity, L is the thickness of the electrolyte film, A is the section area of the stainless-steel electrode, and R_b is the bulk resistance.

3-3 RESULTS AND DISCUSSION

3-3-1 DSC Studies

The DSC analysis is one of the most convenient methods for determining the miscibility in polymer blends. T_gs of the pure polymers used in this study, PEO and PCL, are both ca. -60 °C. Figure 3-1 presents the conventional second-run DSC thermograms of various LiClO$_4$/PEO/PCL ternary blends. Each system (Figures 3-1 (a) ~ (e)) contains a fixed fraction of lithium perchlorate, but the PEO/PCL ratios vary; either single T_g or two T_g's are identified in all blends. A single T_g strongly suggests that these blends are fully miscible and exist as a homogeneous amorphous phase. Meanwhile, a ternary blend with two T_g's implies is considered immiscible or partially miscible in the amorphous phase. In PEO/PCL binary blends, however, a single T_g or two T_g's can not be identified from the DSC thermograms because T_gs of PEO and PCL are so close. Therefore, the miscibility between PEO and PCL can not be determined simply based on the appearance of one or two T_g's in the DSC thermogram. Kuo et al. have reported [9], however, that the binary blends of PEO/PCL at various ratios are miscible in their amorphous phase. Therefore, the phase diagram of this ternary LiClO$_4$/PEO/PCL blend system at room temperature based on its DSC analyses is present in Figure 3-2. A closed-loop, phase-separated region exists in this three-component the phase diagram. This observed phenomenon indicates that these complicated interactions, which can be grouped into LiClO$_4$/PEO, LiClO$_4$/PCL, and PEO/PCL pairs, exist in this ternary blend system and that these interactions compete with each other. Interestingly, even though these three individual binary blends (LiClO$_4$/PEO, LiClO$_4$/PCL and PEO/PCL) are all miscible in the amorphous phase, immiscibility exists within certain compositions of the ternary system.

Figure 3-3 displays the effect that the LiClO$_4$ content has on the glass transition

temperatures of (a) LiClO$_4$/PEO and (b) LiClO$_4$/PCL blends. In both of these systems, the T_gs increase upon increasing the LiClO$_4$ content, but they tend to decrease for concentrations of LiClO$_4$ above 20-25 wt%. It has been suggested that the initial increase in T_g is due to the interaction between the polymer chains and the salt whereas the decrease is due to the repulsion between the free anions or the dilution effect of salt aggregation [15,16]. Within the range of 10-20 wt% of LiClO$_4$, the T_g increment of the LiClO$_4$/PEO system is greater than that of the LiClO$_4$/PCL system, implying that the interaction between LiClO$_4$ and PEO is stronger than that between LiClO$_4$ and PCL.

When we look at the changes in T_g (Figure 3-3) on the molar basis, though the two T_g elevation patterns look similar, the elevation maximum in LiClO$_4$/PEO takes place at Li/O mole ratio of 1/9.7, whereas in LiClO$_4$/PCL it occurs at Li/ester group = 1/2.8. It is understandable because PEO interacts stronger with lithium ions than that of PCL. Moreover, the distance between ether oxygens in PEO is shorter than that between ester groups in PCL. It has been suggested that the lithium ion is able to coordinate with more functional groups of the polymer chain in PEO than that in PCL. As a result, higher content of LiClO$_4$ salt is needed to achieve maximum T_g in LiClO$_4$/PCL system.

3-3-2 FT-IR Spectroscopy

Figure 3-4 shows infrared spectra recorded at room temperature, displaying the bands representing the carbonyl stretching (a) and CH$_2$ wagging (b) of a series of PEO/PCL binary blends. As shown in Figure 3-4 (a), two carbonyl stretching bands appear for the pure PCL at 1734 and 1724 cm^{-1}; these bands correspond to the absorptions of the amorphous and crystalline conformations, respectively. The relative peak area of the crystalline conformation of PCL (1724 cm^{-1}) decreases upon

increasing the PEO content in this binary PEO/PCL blend system. Figure 3-4 (b) shows infrared spectra of the CH_2 wagging vibration, in the region 1320-1380 cm^{-1}, of the pure PEO and various PEO/PCL binary blends. The pure PEO has two bands, at 1360 and 1343 cm^{-1}, that represent its crystalline phase [17]. The crystalline conformation of PEO is partially destroyed when the PCL content in this binary blend is increased. As a result, we confirm that the interaction between PEO and PCL tends to decrease the fraction of the crystalline phases of both PEO and PCL.

Figure 3-5 presents Infrared spectra recorded at room temperature, that display the carbonyl stretching (a) and CH_2 wagging (b) regions of a series of ternary $LiClO_4$/PEO/PCL blends containing the $LiClO_4$ content fixed at 10 wt%. In the carbonyl group vibration region (Figure 3-5 (a)), the spectrum of the blend $LiClO_4$/PCL = 10/90 possesses a shoulder band at 1700 cm^{-1}, which reflects the interaction between the lithium cation and the carbonyl group of PCL. This shoulder peak disappears upon the addition of PEO, even at a content of as low as 18 wt%, indicating that the interaction between Li^+ cation and PEO is much stronger than that between Li^+ and PCL. The crystalline phase of PCL nearly disappears at low PCL concentration (compositions of $LiClO_4$/PEO/PCL = 10/85.5/4.5 and 10/81/9; Figure 3-5 (a)). By comparing these spectra with those in Figure 3-4 (a), the fraction of the crystalline PCL phase in this ternary blend is relatively higher than that in the binary blend at the same PEO/PCL ratio. The addition of $LiClO_4$ in PEO/PCL binary blend tends to promote PCL's phase separation and crystallization; the lithium perchlorate prefers to coordinate with PEO rather than with PCL. The bands of crystalline PEO still exist in the ether group vibration region displayed in Figure 3-5 (b), which suggests that the crystalline phase of PEO is only partially destroyed because of the relatively lower content of $LiClO_4$ (10 wt%) in these ternary blends.

Figure 3-6 shows infrared spectra of these $LiClO_4$/PEO/PCL ternary blends

containing a fixed and relatively higher lithium perchlorate content (25 wt%). We observe the same trends with respect to the appearance of the carbonyl group vibration as appear in Figure 3-5 (a), but Figure 3-6 (b) indicates that the crystalline PEO phase disappears totally when the PEO content is 71.25 wt% or less. This finding implies that at a high $LiClO_4$ content (25 wt%) in these ternary blends, $LiClO_4$ interacts with or complexes to essentially all of the available PEO, which, thus, retards its crystal formation.

Infrared spectra recorded an even higher $LiClO_4$ content (40 wt%) are shown in Figure 3-7. At compositions of 40/12/48 and 40/0/60 (Figure 3-7 (a)), the spectra of the bands representing the carbonyl group indicate that the crystalline PCL phase is destroyed completely while a strong shoulder peak appears at 1700 cm^{-1}, which corresponds to the interaction between the lithium cation and the carbonyl group of the PCL. This content of $LiClO_4$ (40 wt%) is high enough to interact with essentially all of the PEO, and portion of the PCL, in the 40/12/48 blend. Further addition of the PEO component to 24 wt% or more, the peak at 1700 cm^{-1} disappears completely while the crystalline phase of PCL appears. In other words, no free PEO or free $LiClO_4$ salt is left and available to interact with PCL and this situation results in the PCL's phase separation and crystallization. Figure 3-7 (b) shows that PEO is totally amorphous at all compositions in these ternary blends containing 40 wt% $LiClO_4$, indicating that excess $LiClO_4$ tends to coordinate with all of the PEO present.

3-3-3 ^{7}Li MAS NMR Spectroscopy

Solid-state ^{7}Li NMR spectroscopy has been used widely to study the interaction between the lithium ions and the polymer hosts [18-20] since the strong receptivity of the Li$^+$ ion makes it a very attractive analytical tool. Figure 3-8 (a) shows the ^{7}Li NMR spectra, recorded at 300 K, of ternary $LiClO_4$/PEO/PCL blends having a $LiClO_4$

concentration at fixed 10 wt%. One single peak appears for all of the blends at this low $LiClO_4$ concentration. The peak at high field (ca. -1.1 ppm) is assigned as the interaction between PEO and Li cation, whereas the peak at low field (ca. -0.4 ppm) is assigned to the coordination of Li^+ with PCL; the latter peak appears only at a composition of 10/0/90, i.e., where PEO is absent. This result indicates that the lithium cation coordinates much more preferably with PEO than with PCL. This result also demonstrates that the ability of PCL to donate its electron to Li^+ is significantly poorer than that of PEO. Figure 3-8 (b) displays the ^7Li MAS NMR spectra of various $LiClO_4$/PEO/PCL ternary blends containing a fixed $LiClO_4$ content of 25 wt%. Unlike the spectra displayed in Figure 3-8 (a), there is no longer only a single peak in each ^7Li NMR spectrum; a new shoulder signal is present at compositions of 25/45/30, 25/30/45, and 25/15/60. After curve fitting, a new peak appears at ca. -1.6 ppm (Peak III) in addition to two peaks mentioned above (Peak I at ca. -0.4 ppm and Peak II at ca.-1.1 ppm). Peak III has been assigned as representing the ion pairs of the lithium salt or its aggregates [19,21]. The relative intensity of Peak III increases as the PCL content increases. Because PEO tends to interact with PCL, as a result of the strong miscibility between PEO and PCL, there is not enough free PEO available to dissolve the $LiClO_4$ and, thus, the Li^+ ion re-coordinates with its counter ion (ClO_4^-) or the salt aggregates. Upon further addition of PCL, a decrease in the relative intensity of Peak III accompanies an increase in the relative intensity of Peak I; these observations result from the dissolution of $LiClO_4$ salt in PCL. As Figure 3-8 indicates, Peak III appears only under the two conditions: (1) at a high $LiClO_4$ salt concentration (25 wt% or higher), and (2) in the ternary blends $LiClO_4$/PEO/PCL having a fixed $LiClO_4$ concentration and various compositions of PEO/PCL = 60/40, 40/60 or 20/80. Nevertheless, Peak III does not appear in binary blends of $LiClO_4$/PEO and $LiClO_4$/PCL.

Figure 3-9 shows the ^{7}Li MAS NMR spectra of LiClO$_4$/PEO/PCL ternary blends recorded at a constant PEO/PCL ratio (40/60), but with varying LiClO$_4$ content. Peaks I-III appear simultaneously when the concentration of LiClO$_4$ is 25 wt% or higher because the excess of LiClO$_4$ interacts simultaneously with both PCL and PEO. The relative intensities of Peak I and III increase as the LiClO$_4$ content increases. This phenomenon suggests a relative decrease in PEO content in these ternary blends such that eventually no PEO is left and available to interact with PCL; in this situation, PCL can interact only with the LiClO$_4$, resulting in the increased intensity of Peak I. Discussing Figure 3-9 on the molar basis, the salt aggregation is formed whenever Li/O is greater than 1/4 regardless of PCL content due to stronger interaction between Li$^+$ and PEO than that between Li$^+$ and PCL. An excess content of LiClO$_4$ tends to self-aggregate, which is consistent with the DSC studies.

Three pairs of interactions are present in these ternary LiClO$_4$/PEO/PCL blends: between LiClO$_4$ and PEO, LiClO$_4$ and PCL, and PEO and PCL. The combination of these mutually competitive interactions dictates the final miscibility of these ternary blends and also the mobility of the Li$^+$ cation within the polymer chains. From the solid-state NMR spectra, we conclude that an excess content of LiClO$_4$ tends to result in aggregation and increase the mobility of the polymer chains due to the dilution effect.

3-3-4 Ionic Conductivity

Figure 3-10 presents plots of the Arrhenius ionic conductivity as a function of temperature for LiClO$_4$/PEO/PCL ternary blend-based electrolyte systems containing a constant LiClO$_4$ salt concentration (25 wt%). From DSC data, we know that the T_gs of PEO and PCL are similar (ca. -60 °C), but the ionic conductivity of LiClO$_4$/PCL is ca. 1-2 orders lower than that of LiClO$_4$/PEO. In addition to the chain mobility of the

polymer matrix, we must also consider the ability of the Li^+ cation to coordinate to the polar groups present in the polymer matrix. According to the information we obtained from the solid-state ^7Li NMR spectra, the Li^+ cation has a much greater preference for coordination with PEO rather than with PCL. Therefore, the $LiClO_4$/PEO system has a higher ionic conductivity than that of the $LiClO_4$/PCL system. Figure 3-10 indicates, however, that the maximum ionic conductivity occurs for the ternary blend $LiClO_4$/PEO/PCL = 25/60/15. The addition of PCL into the $LiClO_4$/PEO or PEO into the $LiClO_4$/PCL binary blend increases their ionic conductivities at lower temperature of 20 °C. The FTIR spectra clearly reveal that the crystalline phases of PEO and PCL still exist in both the $LiClO_4$/PEO and $LiClO_4$/PCL binary blends, respectively. The addition of the third component (PCL or PEO) to these binary blends tends to retard or destroy the crystalline phase and results in higher ionic conductivity as a result of the strong miscibility between PEO and PCL. In addition, the crystalline phase can be reduced or inhibited and higher conductivity occurs upon raising the temperature, as is expected. If we consider, for example, a composition of 25/75/0, we observe that its ionic conductivity increases drastically when the temperature is raised from 40 to 60 °C. Nevertheless, further addition of the third component results in a decrease in ionic conductivity because phase separation (immiscibility) occurs, which causes $LiClO_4$ to aggregate in these ternary blends. As a result, the maximum ionic conductivity occurs at the composition at which phase separation begins. The addition of PCL tends to retard or inhibit PEO crystallization, while the excess content of PCL tends to be excluded. In fact, a slight PCL phase separation promotes the ionic conductivity.

3-4 CONCLUSIONS

We have investigated the miscibility behavior, interaction mechanism, and ionic conductivity of LiClO$_4$/PEO/PCL ternary blend-based electrolyte systems by the use of DSC, FTIR, solid-state ^{7}Li NMR spectroscopy, and ac impedance measurements. Although each of the three individual binary pairs is fully miscible, a closed-loop immiscibility region exists in the ternary blend's phase diagram. Lithium cation more preferably coordinates with the ether oxygen atom of PEO rather than with the carbonyl group of PCL. When LiClO$_4$ is added to the PEO/PCL binary blend, the PCL component tends to be excluded, which causes phase separation of these ternary blends. The presence of a small PCL content in the PEO phase is able to retard or inhibit crystallization because PEO and PCL are fully miscible at all compositions. This factor is responsible for the observed increase in ionic conductivity of the LiClO$_4$/PEO/PCL blend. The maximum ionic conductivity (6.3×10^{-7} Scm^{-1}) of the ternary blend at room temperature occurs at the LiClO$_4$/PEO/PCL composition of 25/60/15.

3-5 REFERENCES

1. Cheradame, H.; Le Nest, J. F. In *Polymer Electrolyte Reviews*; MacCallum, J. R., Vincent, C. A., Eds.; Elsevier: Amsterdam, 1987/1989; Vols. 1 and 2.

2. Scrosati, B.; In *Applications of Electroactive Polymers*; Scrosati, B., Ed.; Chapman & Hall: New York; 1993.

3. Armand, M. B. *Solid State Ionics* **1983**, *9-10*, 745.

4. Murata, K.; Izuchi, S.; Yoshihisa, Y. *Electrochim. Acta.* **2000**, *45*, 1501.

5. Lee, I. J.; Song, G. S.; Lee, W. S.; Suh, D. H. *J. Power Sources* **1994**, *89*, 47.

6. Chen, H. W.; Chiu, C. Y.; Wu, H. D.; Shen, I. W.; Chang, F. C. *Polymer* **2002**, *43*, 5011.

7. Xia, D. W.; Smid, J. *J. Polym. Sci., Polym. Lett.* **1984**, *22*, 617.

8. Li, J.; Khan, I. M. *Macromolecules* **1993**, *26*, 4544.

9. Kuo, S. W.; Lin, C. L.; Chang, F. C. *Macromolecules* **2002**, *35*, 278.

10. Berthier, C.; Forecki, W.; Minier, M.; Armand, M. B.; Chabagno, J. M.; Rigaud, P. *Solid State Ionics* **1983**, *11*, 91.

11. Wright, P. V. *Br. Polym. J.* **1975**, *7*, 39.

12. MacDonald, J. R. *J. Chem. Phys.* **1974**, *61*, 3977.

13. Watanabe, M.; Ohashi, S.; Sanui, K.; Ogata, N.; Kobayashi, T.; Ohtaki, Z. *Macromolecules* **1985**, *18*, 1945.

14. Li, J.; Khan, I. M. *Macromol. Chem.* **1991**, *192*, 3043.

15. Chen, H.W.; Chiu, C. Y.; Chang, F. C. *J. Polym. Sci., Polym. Phys. Ed.* **2002**, *40*, 1342.

16. Kim, J. H.; Min, B. R.; Won, J.; Kang, Y. S. *J. Phys. Chem. B* **2003**, *107*, 5901.

17. Chintapalli, S.; Frech, R. *Macromolecules* **1996**, *29*, 3499.

18. Fu, R.; Ma, Z.; Zheng, J. P.; Au, G.; Plichta, E. J.; Ye, C. *J. Phys. Chem. B* **2003**, *107*, 9730.

19. Wang, H. L.; Kao, H. M.; Wen, T. C. *Macromolecules* **2000**, *33*, 6910.

20. Dai, Y.; Wang, Y.; Greenbaum, S. G.; Bajue, S. A.; Golodnitsky, D.; Ardel, G.; Strauss, E.; Peled, E. *Electrochim. Acta.* **1998**, *43*, 1557.

21. Liang, W. J.; Kuo, P. L. *Macromolecules* **2004**, *37*, 840.
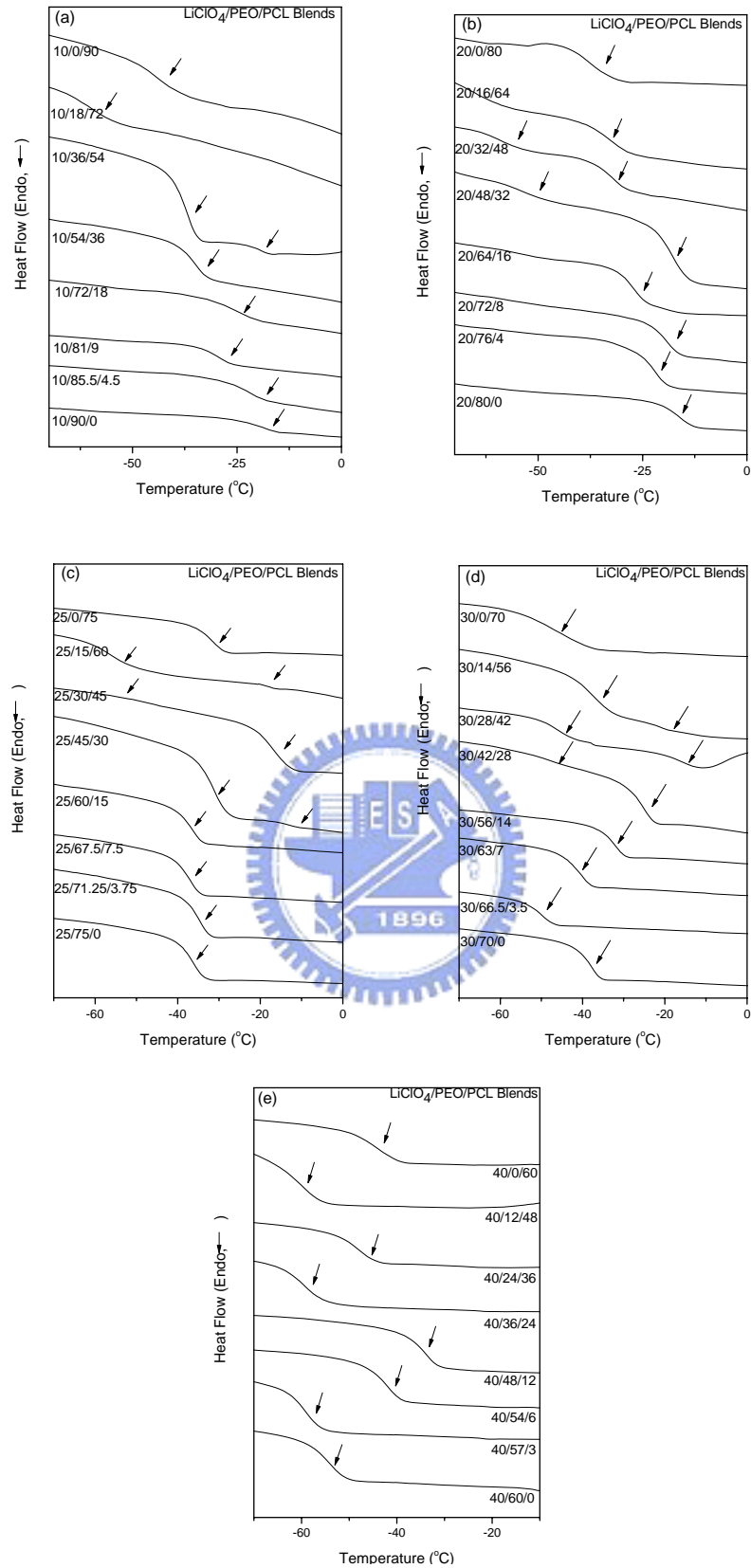
Figure 3-1. DSC thermograms of ternary blends of $LiClO_4$/PEO/PCL containing a constant composition of $LiClO_4$. (a) 10 wt%, (b) 20 wt%, (c) 25 wt%, (d) 30 wt%, (e) 40 wt%.
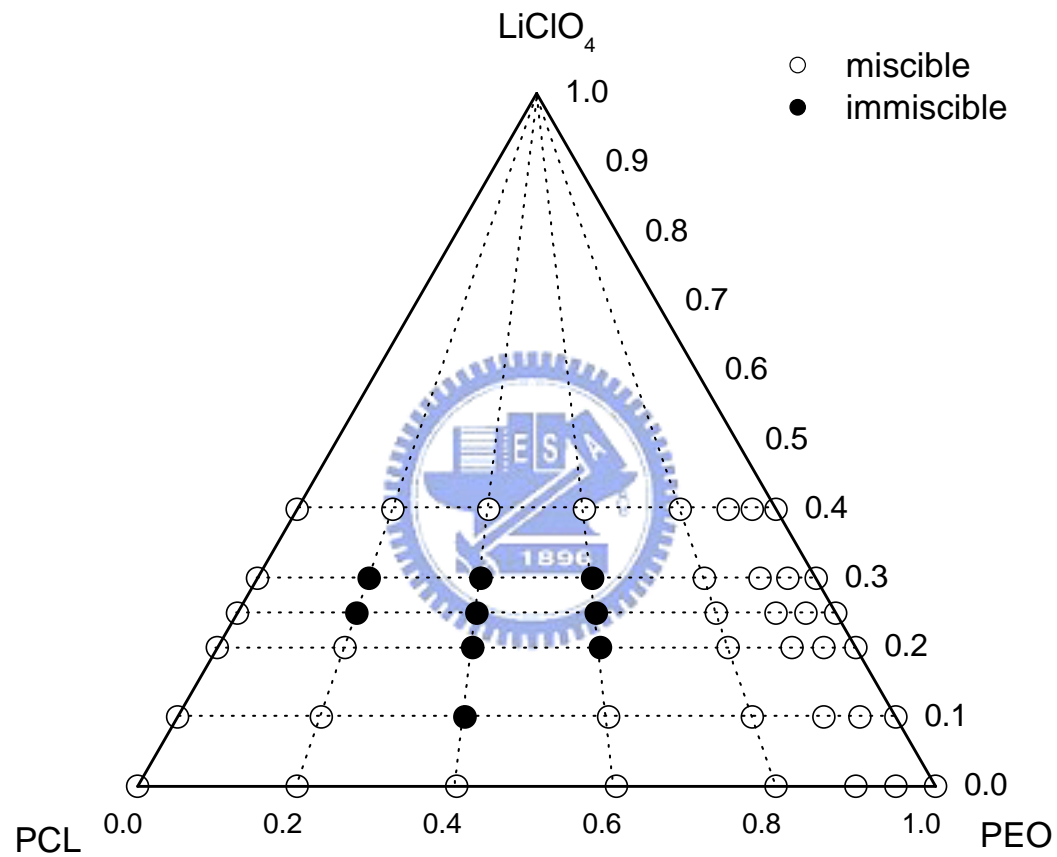
Figure 3-2. Ternary phase diagram of the LiClO$_4$/PEO/PCL system. The open circles represent a miscible ternary blend, and the full circles represent an immiscible ternary blend.
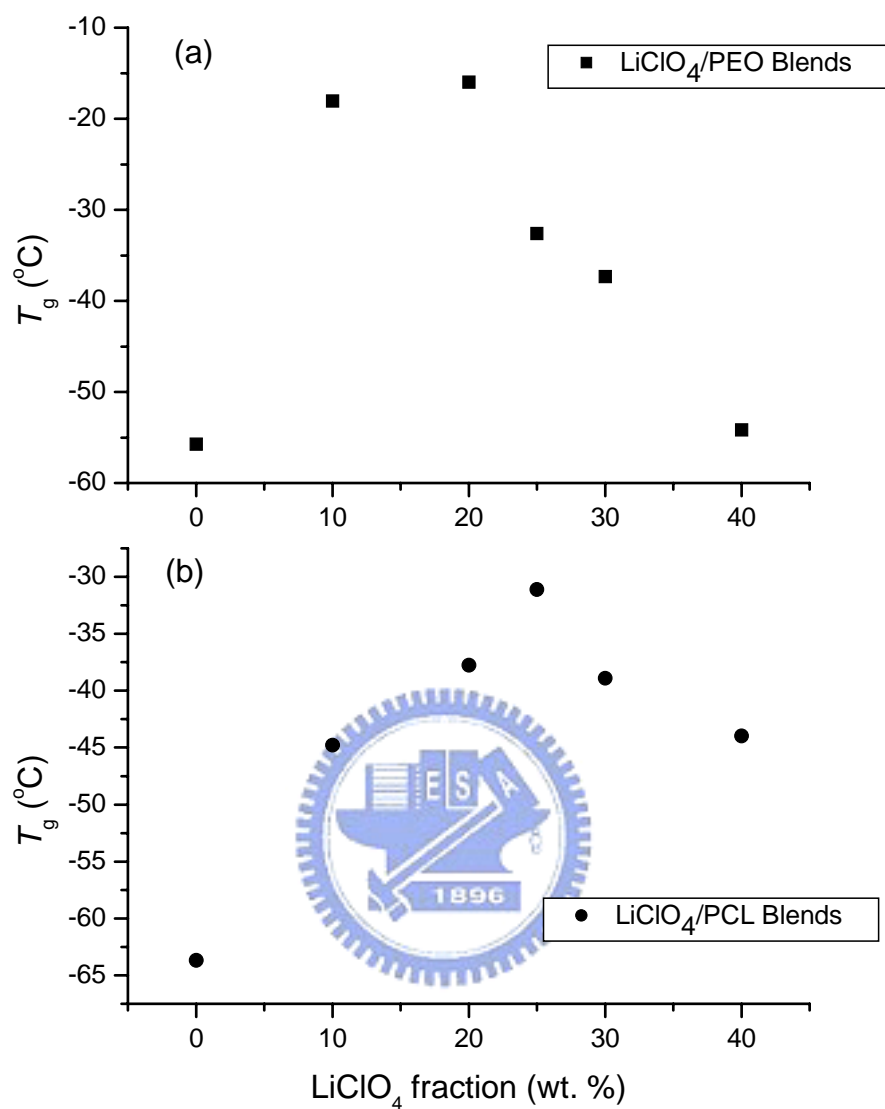
Figure 3-3. Effect of $LiClO_4$ content on the glass transition temperatures of (a) $LiClO_4$/PEO and (b) $LiClO_4$/PCL.
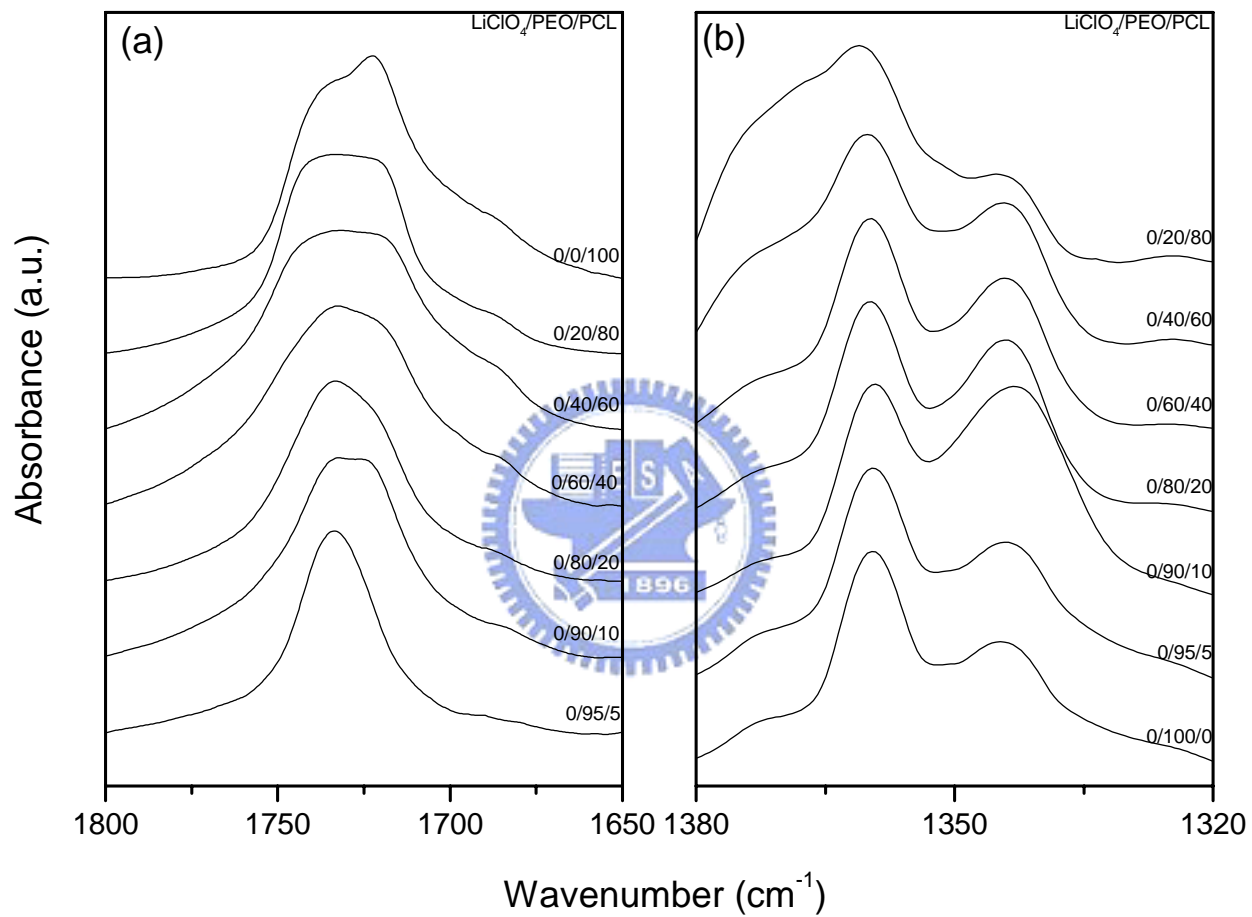
Figure 3-4. Infrared spectra of binary blends of PEO/PCL, recorded at room temperature, displaying (a) the carbonyl stretching, and (b) CH_2 wagging regions.
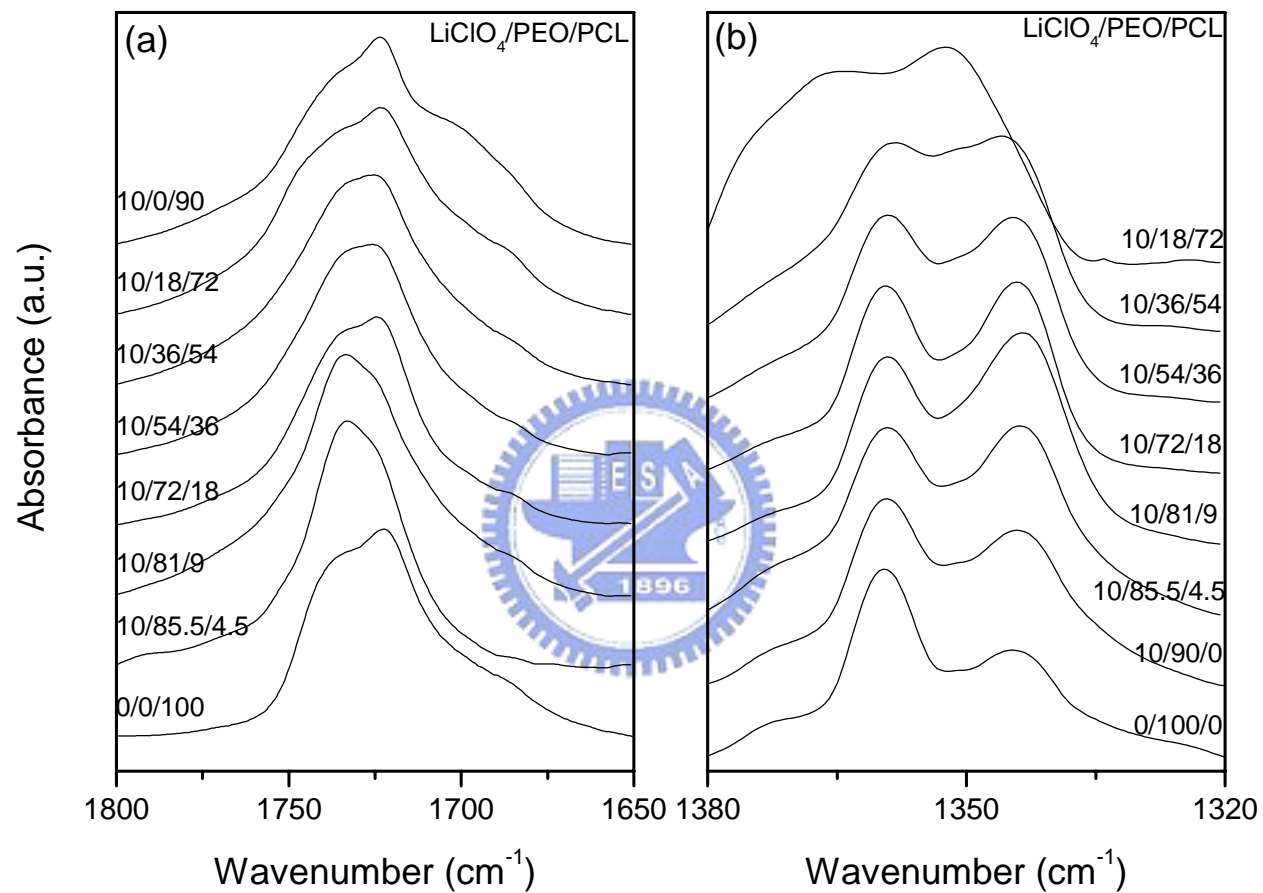
Figure 3-5. Infrared spectra of ternary blend of LiClO$_4$/PEO/PCL containing a constant composition (10 wt%) of LiClO$_4$, recorded at room temperature, displaying (a) the carbonyl stretching, and (b) CH$_2$ wagging regions.
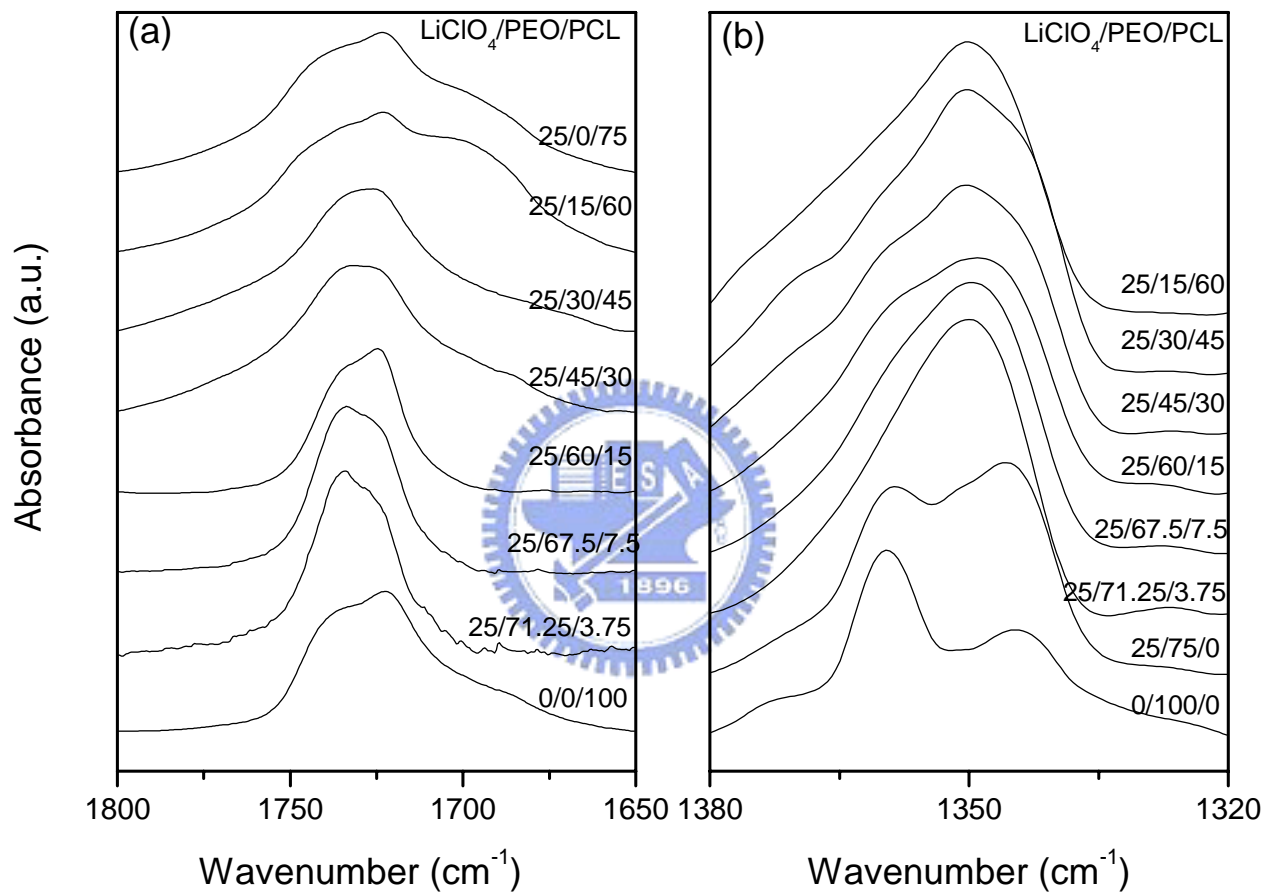
Figure 3-6. Infrared spectra of ternary blend of LiClO$_4$/PEO/PCL containing a constant composition (25 wt%) of LiClO$_4$, recorded at room temperature, displaying (a) the carbonyl stretching, and (b) CH$_2$ wagging regions.
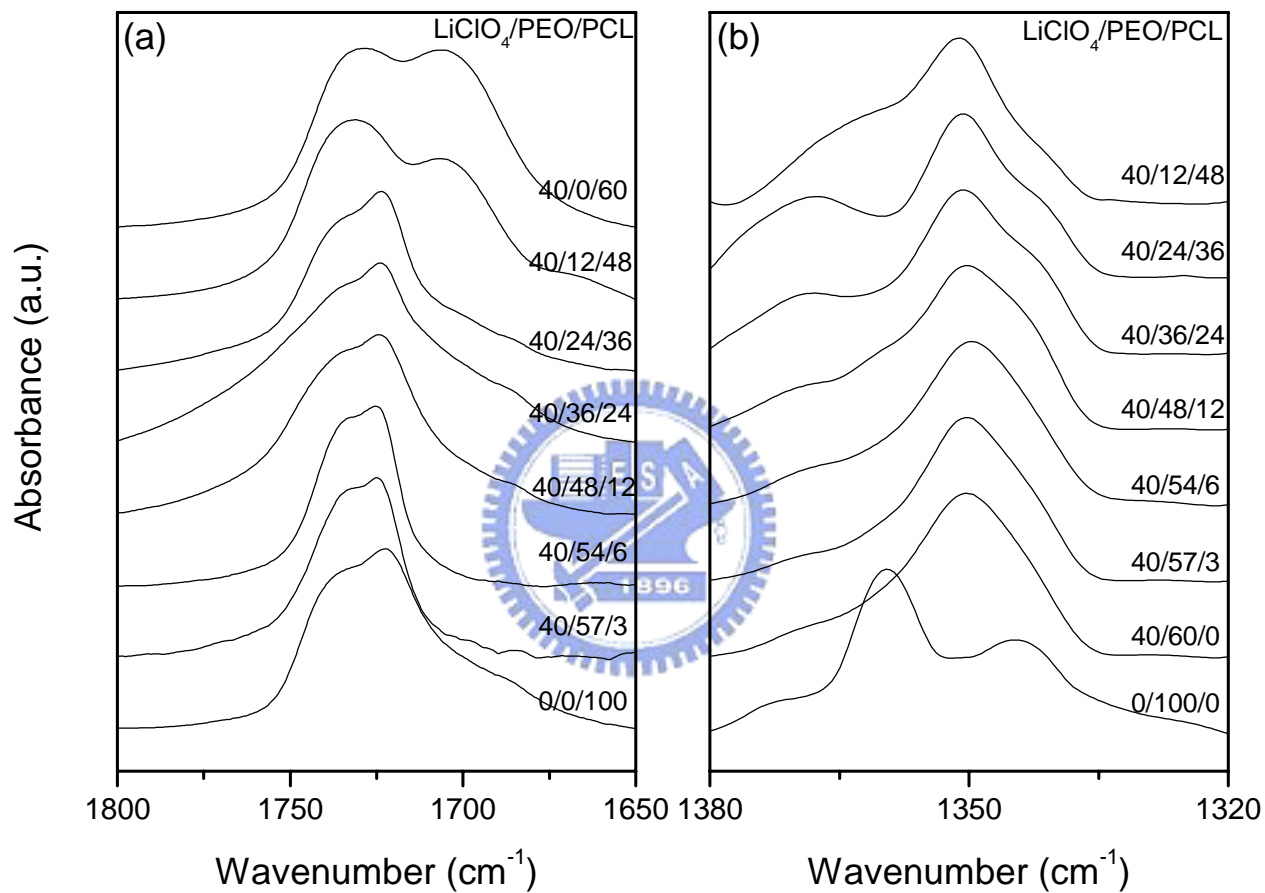
Figure 3-7. Infrared spectra of ternary blend of LiClO$_4$/PEO/PCL containing a constant composition (40 wt%) of LiClO$_4$, recorded at room temperature, displaying (a) the carbonyl stretching, and (b) CH$_2$ wagging regions.
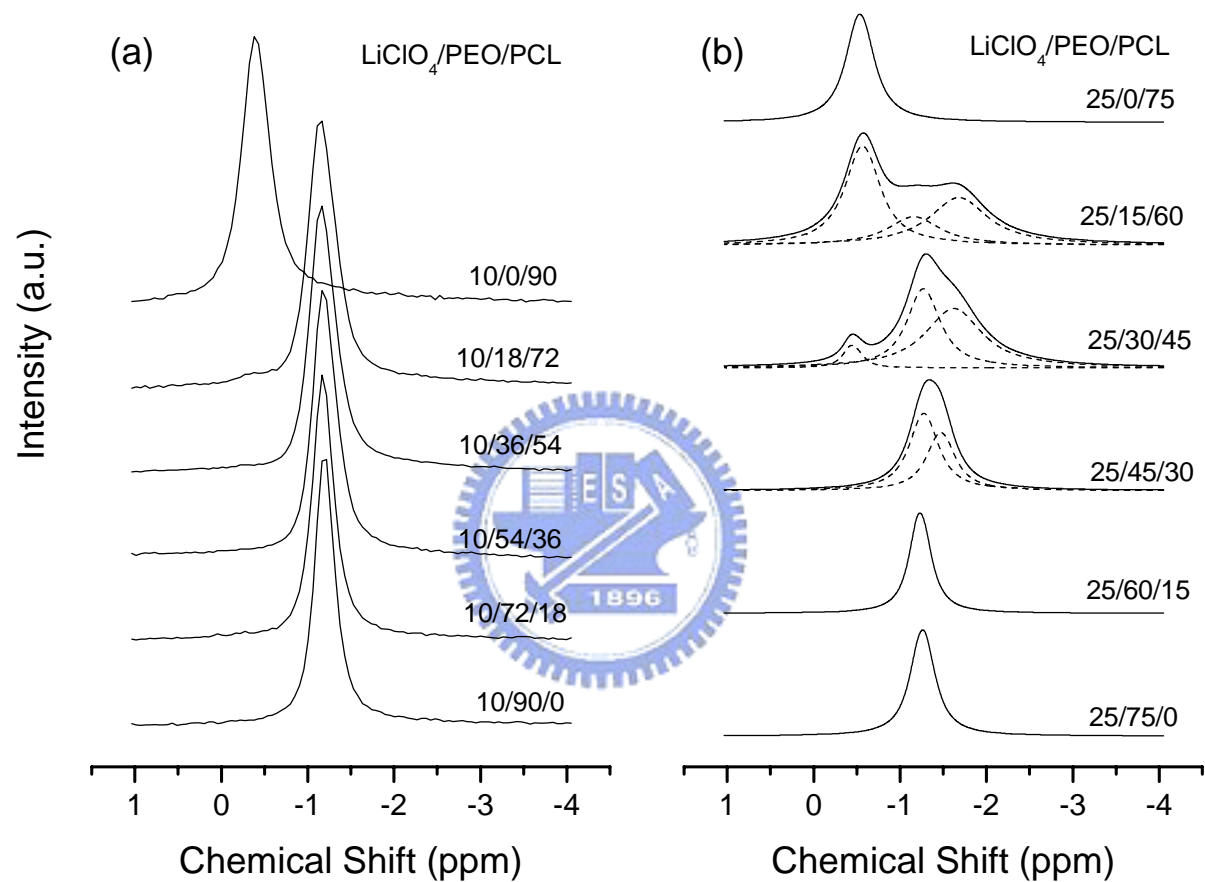
Figure 3-8. Solid-state ^7Li proton-decoupled MAS NMR spectra of ternary blends of $LiClO_4$/PEO/PCL containing constant $LiClO_4$ concentrations of (a) 10 and (b) 25 wt%.
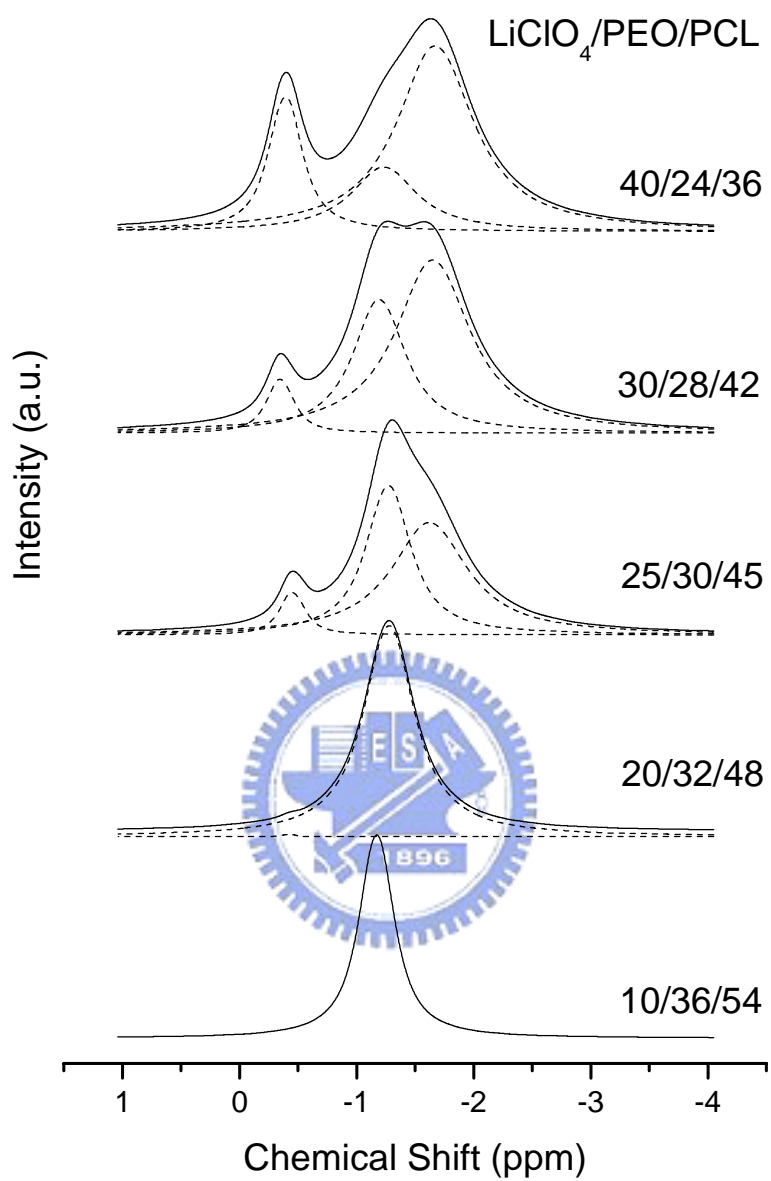
Figure 3-9. Solid-state ^{7}Li proton-decoupled MAS NMR spectra of ternary blends of $LiClO_4$/PEO/PCL having a fixed PEO/PCL ratio of 40/60.
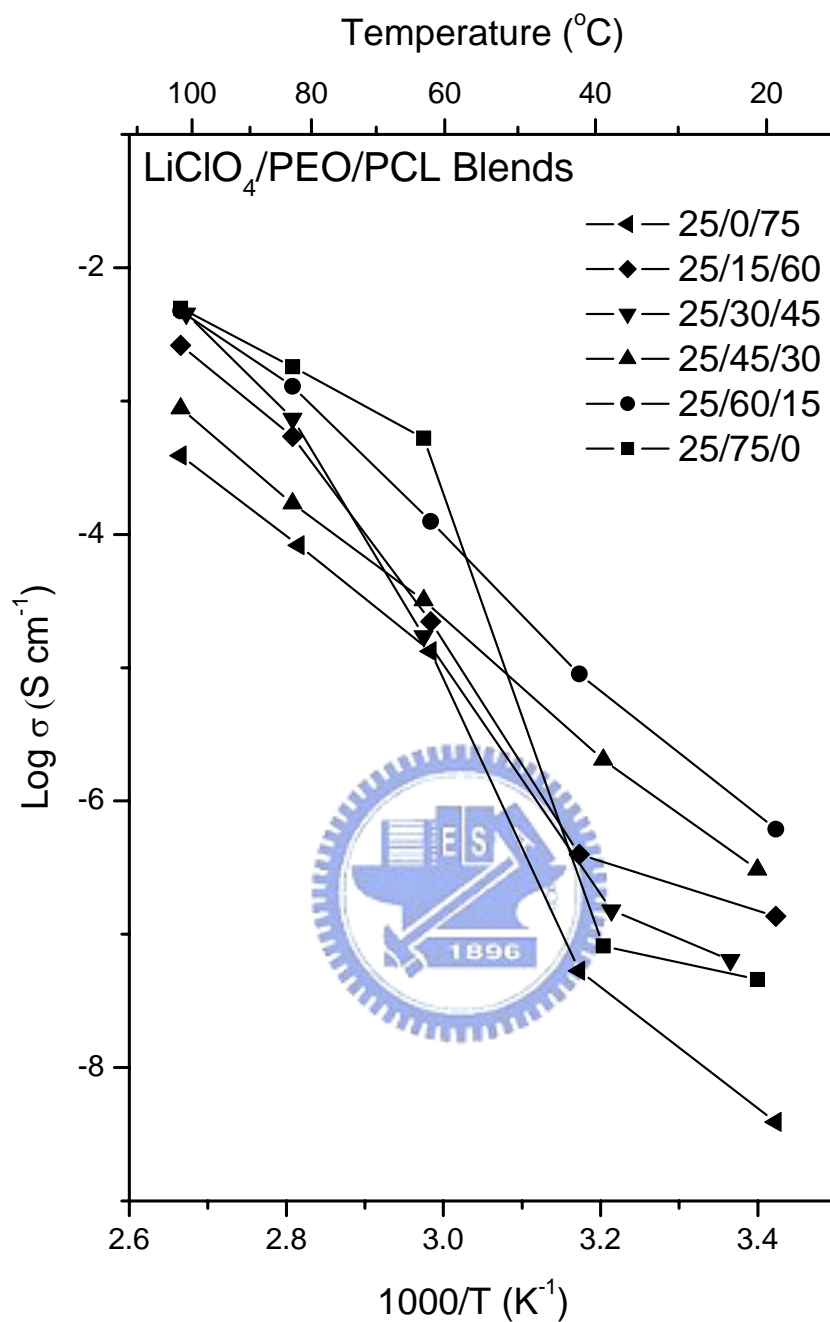
Figure 3-10. Arrhenius ionic conductivity plots as a function of temperature for LiClO₄/PEO/PCL ternary blend-based electrolyte systems containing constant LiClO₄ concentration (25 wt%).

CHAPTER 4

Miscibility Behavior and Interaction Mechanism of polymer Electrolytes Comprising LiClO$_4$ and MPEG-*block*-PCL Copolymers

ABSTRACT

We have used DSC, FTIR spectroscopy, and ac impedance techniques to investigate in detail the miscibility behavior, interaction mechanism and ionic conductivity of polymer electrolytes composed of lithium perchlorate (LiClO$_4$), and monomethoxy-poly(ethylene glycol)-*block*-poly (ε-caprolactone) (MPEG-PCL) diblock copolymer. The existence of the PCL phase in the MPEG-PCL block copolymer tends to retard the crystallinity of MPEG and results in a higher ionic conductivity for the LiClO$_4$/MPEG-PCL based polymer electrolyte. DSC analyses indicated that the phase separation occurred for some compositions of the LiClO$_4$/MPEG-PCL blends. In addition, FTIR spectroscopy studies revealed the complicated interactions that occur within the LiClO$_4$/MPEG-PCL blend system upon varying the LiClO$_4$ content and increasing the temperature. For the LiClO$_4$/MPEG-PCL blend system, the relative intensity of the 'complexed' carbonyl stretching band of PCL tended to increase when either the LiClO$_4$ concentration or the length of the PCL block increased. For some compositions of LiClO$_4$/MPEG-PCL, when the temperature increased from 120 to 180 °C, the relative intensity of the 'complexed' C=O group increased; this phenomenon is different from that observed for the LiClO$_4$/PCL homopolymer blend.

4-1 INTRODUCTION

A polymer electrolyte may be defined generally as a membrane having transport properties that are comparable with those of the common liquid ionic solutions [1-5]. These systems are of technological interest due to their applications as solid electrolytes in electrochemical devices, such as energy conversion units (batteries, fuel cells), smart windows, components in solid state sensors, and solid state transistors [6-9]. Consequently, the lithium salt-based electrolytes have been the focus of a wide variety of fundamental and application-oriented studies. However, Li^+-based polymer electrolytes exhibit several disadvantages that affect the commercialization of such cells; for example, one major drawback is the low ionic conductivity of the electrolyte at ambient temperatures [10]. Thus, it is of great importance to optimize their performance through a detailed understanding of the fundamental ionic interactions that occur within polymeric electrolytes.

Poly(ethylene oxide) (PEO) exhibits good complexation properties and high flexibility and retains good mechanical stability at temperatures up to its melting point, but its relatively high degree of crystallinity limits the ionic conductivity of these PEO-based electrolytes [1-3,11]. Extensive research efforts have been devoted toward lowering the temperature of operation of the PEO-based electrolytes into the ambient region [12-15].

Monomethoxy-poly(ethylene glycol)-*block*-poly(ε-caprolactone) (MPEG-PCL) diblock copolymer is a desirable polymer electrolyte because the existence of strong interaction between the PEO and PCL units tends to suppress the crystallization of PEO [16]. In a previous study [17], we reported that the addition of PCL into an electrolyte system based on $LiClO_4$/PEO tends to retard or inhibit the crystallization of PEO and subsequently increases the ionic conductivity. Thus, we became interested in studying polymer electrolytes composed of $LiClO_4$ and the MPEG-PCL

diblock copolymer. It seemed reasonable to us to expect that MPEG-PCL may be more miscible than the PEO/PCL binary blend when considering our previous studies in which we compared the miscibility between block copolymers and blends [18]. Therefore, we expected that this salt/block copolymer blend system, LiClO$_4$/MPEG-PCL, would possess higher ionic conductivity than those of previously reported electrolyte systems based on LiClO$_4$/PEO binary blends.

Previous reports have described blend systems of PEO-containing block copolymers doped with a range of inorganic salts [19,20]. These studies, however, involved the use of amphiphilic block copolymers, such as poly(ethylene oxide)-*block*-polyisoprene (PEO-PI), and concentrated mainly on the morphologies, phase behavior, and thermal and mechanical properties of these block copolymer/salt mixtures. To the best of our knowledge, there have been no studies on the influences that the miscibility behavior and interaction mechanism have on the variation of ionic conductivity in polymer electrolytes comprising LiClO$_4$ and block copolymers possessing two LiClO$_4$-miscible blocks. In this study, we employed differential scanning calorimetry (DSC), Fourier transform infrared (FTIR) spectroscopy, and alternating current (ac) impedance to investigate the miscibility and related conductivity behavior of LiClO$_4$/MPEG-PCL blend systems.

4-2 EXPERIMENTAL

4-2-1 Materials

Monomethoxy-poly(ethylene glycol) having a molecular weight of 5,000 (MPEG-5k) was obtained from Aldrich and dried by an azeotropic distillation with dry toluene. ε-Caprolactone (ε-CL, from Acros) was purified by vacuum distillation over CaH_2. The fraction collected at room temperature (5 mmHg) was used for polymerization. Tin(II) 2-ethylhexanoate [stannous octoate, $Sn(Oct)_2$] and acetonitrile, both from Aldrich, were used as received. Lithium perchlorate ($LiClO_4$; Aldrich) was dried in a vacuum oven at 80 °C for 24 h and stored in desiccator prior to use.

4-2-2 Synthesis of Monomethoxy-poly(ethylene glycol)-block-poly(ε-caprolactone) *(MPEG-PCL)* [21]

Block copolymers are readily prepared through the ring-opening polymerization of CL and MPEG in the presence of stannous octoate as a catalyst (Scheme 4-1). The reaction mixture was prepared by introducing, under a nitrogen atmosphere, a known volume of ε-caprolactone monomer into a silanised flask containing a pre-weighted amount of MPEG. One drop of $Sn(Oct)_2$ was added into the mixture. The flask was connected to a vacuum line, evacuated, sealed off and heated at 130 °C. After 24 h, the resulting block copolymer was dissolved in methylene chloride, precipitated in an excess of cold hexane, and dried at 40 °C under vacuum. Diblock copolymers having different degrees of polymerization (DP) of PCL were obtained upon adjusting the feed ratio of CL to MPEG. The results of these polymerizations are summarized in Table 4-1.

4-2-3 Characterizations

The molecular weights and polydispersities of the copolymers were determined by gel permeation chromatography (GPC) using N,N-dimethylformamide (DMF) as an eluent at 50 °C and poly(ethylene oxide) standards were employed for column calibration.

^{1}H NMR spectra of the copolymers were recorded in deuterated chloroform (CDCl$_3$) solutions at 25 °C using a Varian UNITY INOVA-400 NMR spectrometer. The molecular weights and MPEG/PCL ratios of the various types of copolymers that were evaluated from these ^{1}H NMR spectra and compared with the corresponding values obtained by GPC.

4-2-4 Sample Preparations

Polymer electrolytes of LiClO$_4$/MPEG-PCL in various blend compositions were prepared by solution casting. The desired amounts of MPEG-PCL and LiClO$_4$ salt were dissolved in acetonitrile and stirred continuously for 24 h at 60 °C. The solution was cast onto a Teflon dish and maintained at 50 °C for an additional 24 h to remove the solvent; then the dish was further dried under vacuum at 80 °C for 2 days. To prevent its contact with air or moisture, the polymer electrolyte film was transferred to a glove box under a nitrogen atmosphere.

4-2-5 Differential Scanning Calorimetry (DSC)

Thermal analyses were performed using a DSC instrument (DuPont TA 2010). The sample was heated from -110 to 150 °C under an atmosphere of dry N$_2$. The glass transition temperature (T_g) was obtained as the inflection point of the heat capacity jump recorded at a scan rate of 20 °C /min.

4-2-6 Fourier Transform Infrared Spectroscopy (FTIR)

The conventional potassium bromide (KBr) disk method was employed to measure the infrared spectra of the blend films. All polymer films were prepared under a N_2 atmosphere. The acetonitrile solution was cast onto a KBr disk, from which the solvent was evaporated under vacuum at 70 °C for 48 h. All IR spectra were obtained within the range 4000-400 cm^{-1} using a Nicolet AVATAR 320 FTIR spectrometer (Nicolet Instruments, Madison, WI) operating at a resolution of 1 cm^{-1}.

4-2-7 Conductivity Measurements

Ionic conductivity measurements with alternation current were conducted on an AUTOLAB designed by Eco Chemie within a frequency range from 10 MHz to 10 Hz. The electrolyte film was sandwiched between stainless-steel blocking electrodes (diameter: 1 cm). The specimen thickness varied from 0.08 to 0.12 mm; the impedance response was gauged over the range from 20 to 100 °C. The conductivity was calculated from the bulk resistance according to the equation [22,23]

$$\sigma = L / A \times R_b$$

where σ is the conductivity, L is the thickness of the electrolyte film, A is the section area of the stainless-steel electrode, and R_b is the bulk resistance.

4-3 RESULTS AND DISCUSSION

4-3-1 Synthesis of MPEG-PCL

The ring-opening polymerization of ε-caprolactone was initiated with MPEG in the presence of stannous octoate as catalyst (Scheme 4-1). We performed the polymerization in the bulk at 130 °C for 24 h and varied the concentration of ε-caprolactone to obtain copolymers having a range of PCL block lengths. Table 4-1 summarizes the data of the polymers characterized by ^{1}H NMR spectroscopy and GPC.

4-3-2 DSC Studies

According to the results of a previous study [24], ionic aggregation may have a dramatic effect on the miscibility and thermal properties of a polymer/salt blend. First of all, we carried out thermal analyses to determine whether the properties of these systems are affected by the addition of the lithium salt. Figure 4-1 shows the typical second-run DSC analyses of various LiClO$_4$/MPEG-PCL blends. The composition of each system (Figures 4-1 (a) ~ (d)) varies with the content of the lithium salt; either single T_g or two T_gs are identified in all blends. A single T_g strongly suggests that these blends are fully miscible and exist as a homogeneous amorphous phase. Meanwhile, a blend having two T_gs is considered to be immiscible or partially miscible in the amorphous phase. Kuo et al. have reported [16] that the binary blends of poly(ethylene oxide) (PEO) and PCL at various ratios are miscible in their amorphous phase. Thus, the MPEG-PCL diblock copolymer, regardless of the length of its PCL block, is expected to be miscible in the amorphous phase. However, blending MPEG-PCL block copolymers with LiClO$_4$ salt results in phase separation. Figures 4-1 (a), (b), and (c) display two T_gs at lower LiClO$_4$ contents. Moreover, Figure 4-1 (d) suggests that no phase separation appears

at any composition of the $LiClO_4/EO_{114}\text{-}CL_{516}$ blend system. These results can be interpreted as arising from a complicated set of interactions occurring between $LiClO_4$ and both the blocks of MPEG and PCL. Our previous study indicated that the interaction between $LiClO_4$ and PEO is stronger than that between $LiClO_4$ and PCL [17]. Figures 4-1 (a), (b), (c) and (d) show DSC thermograms of $LiClO_4/MPEG\text{-}PCL$ blends containing varying lengths of the PCL block in the block copolymer (i.e., different molecular weight ratios of MPEG and PCL). For the $LiClO_4/EO_{114}\text{-}CL_{42}$ blend system, which contains a shorter-length of PCL block, the observed phase separation (non-homogeneity) is caused by the exclusion of the PCL block. This phase separation disappears upon increasing the molecule weight of the PCL block. The higher PCL content is allowed to interact simultaneously with both the MPEG block and $LiClO_4$, which, thus, results in single phase in their amorphous phase. In addition, increasing the concentration of the $LiClO_4$ salt also tends to increase miscibility.

Interestingly, the glass transition temperature (Figures 4-1 (b), (c), and (d)), increases continuously upon increasing the content of $LiClO_4$, even when the salt content is as high as 40 wt%. In contrast, the value of T_g of $LiClO_4/PEO$ blend system tends to achieve its maximum at a $LiClO_4$ content of 20 wt% [17]; the excess $LiClO_4$ tends to self-aggregate and causes the T_g of $LiClO_4/PEO$ to decrease owing to the dilution effect [25,26]. As a result, the MPEG-PCL block copolymer is able to accommodate higher $LiClO_4$ salt content in the $LiClO_4/MPEG\text{-}PCL$ blend system than can the PEO matrix in $LiClO_4/PEO$ blend systems. It is understandable that because blends of PEO and PCL are miscible in the amorphous region, the incorporation of PCL block into the PEO domain tends to retard PEO crystallization. As a result, the greater fraction of the amorphous PEO is able to coordinate with $LiClO_4$ salt. Figure 4-1 (d) presents that T_g of the $LiClO_4/MPEG\text{-}PCL$ blend system

tends to decrease by increasing the $LiClO_4$ content up to 50 wt%..

Figure 4-2 shows the variations of melting temperature (T_m) and melting enthalpy (ΔH_m) obtained form DSC analyses of $LiClO_4/EO_{114}$-CL_{516} blends with various $LiClO_4$ contents. It is well known that the value of ΔH_m correlates to the degree of crystallization. In the $LiClO_4/EO_{114}$-CL_{516} blend system, the addition of $LiClO_4$ reduces the degree of crystallization. Eventually, the melting peak disappears when the $LiClO_4$ content salt is increased to 25 wt%. However, two melting peaks appear at 35 °C and 93 °C when the salt content is at 50 wt%. The lower-temperature peak is assigned as the melting peak of the diblock copolymer EO_{114}-CL_{516}, while the higher-temperature peak corresponds to that of the $LiClO_4$ salt. Excess $LiClO_4$ tends to aggregate and causes the crystallization of both the EO_{114}-CL_{516} diblock copolymer and the $LiClO_4$ salt. The results of thermal properties of the blends obtained from DSC measures are listed in Table 4-2; similar trend is observed for each system. When comparing all of the MPEG-PCL blends which contain $LiClO_4$ content fixed at 50 wt%, T_m and ΔH_m of the $LiClO_4$ salt increase with increasing the length of PCL block; this situation arises because the longer PCL chain is more miscible with the MPEG block, and thus, lower amount of free MPEG is available to dissociate the lithium perchlorate ion pair [17]. As a result, $LiClO_4$ salt tends to crystallize at a relatively lower MPEG content.

4-3-3 FT-IR Spectroscopy

Figure 4-3 presents infrared spectra recorded at room temperature, displaying the bands representing the carbonyl stretching (a) and CH_2 wagging (b) of a series of MPEG-PCL block copolymers. As observed in Figure 4-3 (a), the carbonyl stretching for the PCL block is split into two bands: absorptions of the amorphous and the crystalline conformations at 1734 and 1724 cm^{-1}, respectively [27,28]. The

relative intensity of the crystalline conformation of PCL block (1724 cm^{-1}) is lowest for EO$_{114}$-CL$_{111}$ block copolymer; the relative intensity of the crystalline conformation of the PCL block increases when the length of the PCL block is increased, i.e., for EO$_{114}$-CL$_{247}$ and EO$_{114}$-CL$_{516}$. Furthermore, Figure 4-3 (b) shows IR spectra of the CH$_2$ wagging vibration, in the region 1380-1320 cm^{-1}, of the pure MPEG-5k and various MPEG-PCL block copolymer. The pure MPEG-5k exhibits two bands, at 1360 and 1343 cm^{-1}, that represent its crystalline phase [16]. The crystallinity of MPEG is gradually destroyed when the length of the PCL block is increased. Therefore, we confirm that the interaction between MPEG and PCL tends to decrease the fraction of the crystalline phases of both MPEG and PCL.

Since the carbonyl group (C=O) is an electron donor within the PCL-based polymer electrolyte, the Li$^+$ ion tends to coordinated with oxygen atom of the carbonyl group. Infrared spectroscopy is a powerful tool to monitor such ionic interaction. Thus, we focus on the change of the carbonyl group within the PCL-block of the MPEG-PCL diblock copolymer and determine the strengths of the ionic interactions between Li$^+$ and the EO and CL blocks of MPEG-PCL. Figure 4-4 presents the infrared spectra (carbonyl stretching region) recorded at room temperature of the MPEG-PCL diblock copolymers having different EO/CL ratios and blended with 20 wt% LiClO$_4$. When the LiClO$_4$ salt is added, a shoulder at ca. 1704 cm^{-1} appears in Figure 4-4, corresponding to the interaction between the C=O group and Li$^+$. It is clearly observed in Figure 4-4 that the relative intensity of the shoulder at ca. 1704 cm^{-1} increases upon increasing the length of PCL block at a fixed LiClO$_4$ concentration. From Figure 4-3 we conclude that the crystalline conformation of MPEG in EO$_{114}$-CL$_{247}$ tends to be destroyed, due to the strong miscibility between MPEG and PCL. No free MPEG block is available to coordinate with Li$^+$ ion while the length of the PCL block is increased, thus, more Li$^+$ ion is

able to coordinate with the PCL.

4-3-3-1 Effect of LiClO₄ Salt Content

Figure 4-5 illustrates the carbonyl stretching region (1800 ~ 1650 cm^{-1}) of IR spectra recorded at 120 °C for various LiClO$_4$/MPEG-PCL blends containing a range of LiClO$_4$ contents. The PCL crystalline phase tends to be destroyed at 120 °C, thus the IR spectrum shows a single peak at ca. 1734 cm^{-1} corresponding to the amorphous PCL. The addition of LiClO$_4$ salt causes the appearance of an absorption band at 1704 cm^{-1}, assigned as the interaction between Li$^+$ and carbonyl group, i.e., 'complexed' C=O. In Figure 4-5 (a), the absorption band of the 'complexed' carbonyl group only appears when the composition of LiClO$_4$/EO$_{114}$-CL$_{42}$ is at 50/50. Nevertheless, upon increasing the length of PCL block, as shown in Figures 4-5 (b) ~ (d), the 'complexed' C=O band at 1704 cm^{-1} clearly appears at a relatively lower content of the LiClO$_4$. In order to further clarify the effect of LiClO$_4$ content on the charge environment surrounding the carbonyl group of PCL block in MPEG-PCL block copolymer, relative fractions of 'free' and 'complexed' C=O sites have been quantified by decomposing the C=O stretching band into two Gaussian peaks [29-31], and summarized in Table 4-3. At a lower concentration of PCL in the MPEG-PCL copolymer, the absorption band of 'complexed' C=O appears until the LiClO$_4$ content is increased to 40 ~ 50 wt%. Besides, no 'complexed' C=O appears for any composition of MPEG-PCL block copolymer system at lower LiClO$_4$ content (10 wt%). These results suggest that MPEG is preferred to interact with Li$^+$ cation than PCL does. The coordination between Li$^+$ ion and the carbonyl group of PCL in LiClO$_4$/MPEG-PCL blend system will occur at a higher concentration of LiClO$_4$ salt or when PCL is present at a relatively higher content relative to MPEG.

4-3-3-2 Effect of Temperature

Figure 4-6 (a) indicates the carbonyl group vibration region of FTIR spectra recorded at different temperatures by blending 25 wt% $LiClO_4$ with PCL homopolymer. As mentioned above, the 'complexed' C=O band is located at 1704 cm^{-1}, while the 'free' C=O band is located at 1734 cm^{-1}. The relative intensity of the 'free' carbonyl vibration band increases at the expense of the 'complexed' C=O band with the increase of temperature, implying that the fraction of the 'complexed' carbonyl group decreases accordingly. The 'complexed' C=O band arises from the interaction between Li^+ ion and carbonyl group; it is well known that the strength of such ionic interaction tends to decrease upon raising the temperature [32]. Figure 4-6 (b) presents the absorption peaks of the ether groups (C-O-C) recorded at different temperatures by blending 25 wt% $LiClO_4$ with PEO homopolymer. The band centered at around 1103 cm^{-1} is attributed to the stretching of the 'free' ether group, while the band at about 1080 cm^{-1} is assigned to the coordination between Li^+ with ether groups, i.e., 'complexed' ether group [33-34]. The relative intensity of the 'free' ether group vibration band increases with increasing the temperature. These changes indicate that the ionic interaction between Li^+ cation and the ether group on PEO weakens as the temperature is increased [35], which is similar to the trend observed in Figure 4-6 (a). The IR spectra with different temperatures of $LiClO_4/EO_{114}-CL_{42}$ (30/70) recorded in both regions of carbonyl group stretching and ether group stretching was shown in Figures 4-7 (a) and (b), respectively. Form Figure 4-5 (a) and Table 4-3, no 'complexed' carbonyl band is observed for $LiClO_4/EO_{114}-CL_{42}$ (30/70) in the IR spectra recorded at 120 °C. Figure 4-7 (a) shows, however, that the relative intensity of the 'complexed' C=O band increases gradually when the temperature is raised from 120 to 180 °C. In addition, Figure 4-7 (b) displays that the relative intensity of the 'free' ether stretching band at ca. 1103

cm^{-1} increases with the increase of the temperature. It is interesting to notice that the ion-dipole interaction between Li$^+$ ion and the carbonyl group increases but the interaction between Li$^+$ ion and the ether group decreases upon increasing the temperature of the LiClO$_4$/EO$_{114}$-CL$_{42}$ (30/70) blend system. Furthermore, the LiClO$_4$/EO$_{114}$-CL$_{111}$ (30/70) blend system also exhibits the same behavior in its IR spectra by varying the temperature from 120 to 180 °C (Figure 4-8). The relative intensity of 'complexed' ether stretching band decays but that of 'complexed' carbonyl stretching band increases when the temperature is increased. Since Li$^+$ cation is capable of coordinating with both the ether group of the MPEG block and carbonyl group of the PCL block in the LiClO$_4$/MPEG-PCL blend system, it is reasonable to assume that there exist two different ion-dipole interactions, representing two interaction parameters, k_E (between Li$^+$ and ether group) and k_C (between Li$^+$ and carbonyl group), as depicted in Scheme 4-2. Both of these interaction parameters, k_E and k_C, are dependent on the temperature, and their values decrease with increasing the temperature. Making a summary form Figures 4-6 ~ 4-8, k_E decreases more rapidly than k_C at the temperature range from 120 to 180 °C [36]. The Li$^+$ cation prefers to coordinate with PEO rather than PCL, hence, at the beginning of the addition of lithium perchlorate, LiClO$_4$ is preferable to enter the MPEG phase at lower temperature. The ion-dipole interaction between Li$^+$ and the ether group weakens upon increasing the temperature and the dissociated Li$^+$ cation turns to coordinate with the carbonyl group (Figures 4-7 (a) and 4-8 (a)). As a result, the relative intensity of the 'complexed' C=O stretching band increases by raising the temperature. However, there are two factors as below controlling the variation of the relative intensity of the 'complexed' C=O stretching band upon increasing the emperature: (1) the ion-dipole interaction weakens as the temperature increases and (2) the dissociated Li$^+$ cation from MPEG turns to interact with carbonyl group,

causing the absorption of the 'complexed' C=O group to increase. Therefore, the trend of the relative intensity of the 'complexed' C=O stretching band is somewhat unexpectable. Figure 4-9 indicates the carbonyl (a) and ether (b) group stretching regions of the IR spectra of $LiClO_4/EO_{114}-CL_{111}$ (40/60) recorded at temperatures from 120 to 180 °C. The variation of the intensity of the 'complexed' C=O stretching band has no order while the temperature increases (Figure 4-9 (a)) because of factors mentioned above. Nevertheless, the relative intensity of 'complexed' ether stretching band always decreases (Figure 4-9 (b)) due to the weakening of the ion-dipole interaction at elevated temperature.

4-3-4 Ionic Conductivity

Figure 4-10 presents the Arrhenius ionic conductivities ploted as a function of temperature for $LiClO_4$/MPEG-PCL blend-based electrolyte systems containing a constant $LiClO_4$ salt concentration (25 wt%). From the DSC data, we know that the crystallinity of PEO decreases upon increasing the length of PCL block. Furthermore, previous studies have stated that the $LiClO_4$/PEO system has a higher ionic conductivity than that of the $LiClO_4$/PCL system, owing to the fact that the Li^+ cation has a much greater preference for coordination with PEO rather than it does with PCL. This factor is responsible for the observed increase in ionic conductivity of the $LiClO_4$/MPEG-PCL blend. Although the $LiClO_4/EO_{114}-CL_{247}$ (25/75) and $LiClO_4/EO_{114}-CL_{512}$ (25/75) blends have lower crystallinity than does $LiClO_4/EO_{114}-CL_{111}$ (25/75), Figure 4-10 indicates that the maximum ionic conductivity at room temperature occurs for the $LiClO_4/EO_{114}-CL_{111}$ at a fixed $LiClO_4$ content of 25 wt%.

4-4 CONCLUSIONS

This paper describes the miscibility behavior, interaction mechanism, and ionic conductivity of $LiClO_4$/MPEG-PCL blend-based electrolyte systems using DSC, FTIR spectroscopy, and ac impedance measurements. The presence of PCL in the MPEG-PCL block copolymer tends to suppress the crystallinity of MPEG as a consequence of the miscibility between MPEG and PCL. Thus, the ionic conductivity of $LiClO_4$/MPEG-PCL blend system at room temperature is higher than that of $LiClO_4$/MPEG-based polymer electrolyte. Lithium cation coordinates more preferably with the ether oxygen atom of PEO rather than with the carbonyl group of PCL. Although the MPEG-PCL diblock copolymers are miscible over their entire range of compositions, the addition of $LiClO_4$ salt in a blend with MPEG-PCL results in a distinct phase separation, which causes the maximum ionic conductivity of $LiClO_4$/MPEG-PCL blend system occurring at $LiClO_4$/EO_{114}-CL_{111}(25/75). Besides, raising the concentration of $LiClO_4$ salt or increasing the length of the PCL block in the $LiClO_4$/MPEG-PCL blend increases the relative intensity of stretching band for the 'complexed' carbonyl group in IR spectra. However, the relative intensities of the 'complexed' carbonyl and 'complexed' ether stretching groups tend to be changed in different directions for some compositions of the $LiClO_4$/MPEG-PCL blend system when the temperature is increased.

4-5 REFERENCES

1. Cheradame, H.; Le Nest, J. F. In *Polymer Electrolyte Reviews*; MacCallum, J. R.; Vincent, C. A., Eds.; Elsevier: Amsterdam, 1987/1989; Vols. 1 and 2.

2. Scrosati, B. In *Applications of Electroactive Polymers*; Scrosati, B., Ed.; Chapman and Hall: London, 1993.

3. Ratner, M. A.; Shriver, D. F. *Chem. Rev.* **1988**, *88*, 109.

4. Wright, P. V. *Br. Polym. J.* **1975**, *7*, 319.

5. Armand, M. B. *Solid State Ionics* **1983**, *9-10*, 745.

6. Mani, T.; Stevens, J. R. *Polymer* **1992**, *33*, 834.

7. Madou, M.; Otagawa, T. *Solid State Ionics* **1988**, *28-30*, 1653.

8. Farnier, F.; Horowitz, G.; Peng, X.; Fichou, D. *Adv. Mater.* **1990**, *2*, 592.

9. Chao, S.; Wrighton, M. S. *J. Am. Chem. Soc.* **1987**, *109*, 2197.

10. Armand, M. B.; Sanchez, J. Y.; Gauthier, M.; Choquette, Y. In *The Electrochemistry of Novel Materials*; Liplowski, J.; Ross, P. N., Eds.; VCH: New York, 1994.

11. Berthier, C.; Gorecki, W.; Minier, M.; Armand, M. B.; Chabagno, J. M.; Rigaud, P. *Solid State Ionics* **1983**, *11*, 91.

12. Wieczorek, W.; Such, K.; Zalewska, A.; Raducha, D.; Florjanczyk, Z.; Stevens, J. R. *J. Phys. Chem. B* **1998**, *102*, 352.

13. Croce, F.; Curini, R.; Martinelli, A.; Persi, L.; Ronci, F.; Scrosati, B.; Caminiti, R. *J. Phys. Chem. B* **1999**, *103*, 10632.

14. Chen, H. W.; Chiu, C. Y.; Wu, H. D.; Shen, I. W.; Chang, F. C. *Polymer* **2002**, *43*, 5011.

15. Li, J.; Khan, I. M. *Macromolecules* **1993**, *26*, 4544.

16. Kuo, S. W.; Lin, C. L.; Chang, F. C. *Macromolecules* **2002**, *35*, 278.

17. Chiu, C. Y.; Chen, H. W.; Kuo, S. W.; Huang, C. F.; Chang, F. C.

Macromolecules **2004**, *37*, 8424.

18. Kuo, S. W.; Huang, C. F.; Tung, P. H.; Huang, W. J.; Huang, J. M.; Chang, F. C. *Macromolecules* **2005**, submitted.

19. Epps, T. H.; Bailey, T. S.; Waletzko, R.; Bates, F. S. *Macromolecules* **2003**, *36*, 2873.

20. Robitaille, C.; Prud'homme, J. *Macromolecules* **1983**, *16*, 665.

21. Yuan, M.; Wang, Y.; Li, X.; Xiong, C.; Deng, X. *Macromolecules* **2000**, *33*, 1613.

22. Watanabe, M.; Ohashi, S.; Sanui, K.; Ogata, N.; Kobayashi, T.; Ohtaki, Z. *Macromolecules* **1985**, *18*, 1945.

23. Li, J.; Khan, I. M. *Macromol*. *Chem*. **1991**, *192*, 3043.

24. Eisenberg, A.; Rinaudo, M. *Polym*. *Bull*. **1990**, *24*, 671.

25. Chen, H. W.; Chiu, C. Y.; Chang, F. C. *J*. *Polym*. *Sci*., *Polym*. *Phys*. *Ed*. **2002**, *40*, 1342.

26. Kim, J. H.; Min, B. R.; Won, J.; Kang, Y. S. *J*. *Phys*. *Chem*. *B* **2003**, *107*, 5901.

27. Coleman, M. M.; Zarian, J. J. *J*. *Polym*. *Sci*., *Polym*. *Phys*. *Ed*. **1979**, *17*, 837.

28. Sanchis, A.; Prolongo, M. G.; Salom, C.; Masegosa, R. M. *J*. *Polym*. *Sci*., *Phys*. *Ed*. **1998**, *36*, 95.

29. Chen, H. W.; Lin, T. P.; Chang, F. C. *Polymer* **2002**, *43*, 5281.

30. Zhu, B.; He, Y.; Yoshie, N.; Asakawa, N.; Inoue, Y. *Macromolecules* **2004**, *37*, 3257.

31. Li, J.; He, Y.; Inoue, Y. *J*. *Polym*. *Sci*., *Phys*. *Ed*. **2001**, *39*, 2108.

32. He, Y.; Asakawa, N.; Inoue, Y. *Macromol*. *Chem*. *Phys*. **2001**, *202*, 1035.

33. Hong, L.; Shi, L.; Tang, X. *Macromolecules* **2003**, *36*, 4989.

34. Ferry, A.; Jacobsson, P.; van Heumen, J. D.; Stevens, J. R. *Polymer* **1996**, *37*, 737.

35. Arun, N.; Vasudevan, S.; Ramanathan, K. V. *J. Chem. Phys.* **2003**, *119*, 2840.

36. Coleman, M. M.; Narvett, L. A.; Painter, P. C. *Polymer* **1998**, *39*, 5867.

Scheme 4-1. Synthesis of Monomethoxy-poly(ethylene glycol)-*block*-poly(ε-caprolactone) (MPEG-PCL).
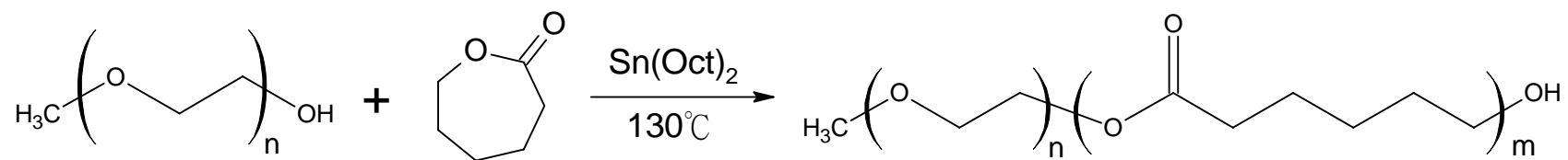
Scheme 4-2. Ionic Interactions of Li^+ Cation with Ether and Carbonyl Groups.
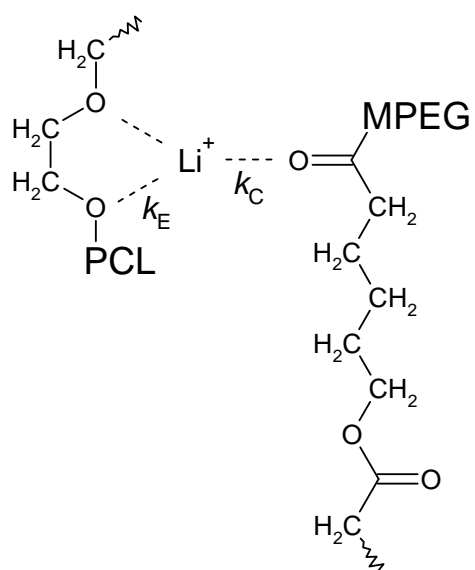
Table 4-1. Compositions and Molecular Weights of MPEG-PCL Block Copolymers.

copolymer MPEG-PCL	EO/CL in feed	EO/CL^a in product	$\overline{DP}_{MPEG}$ ^{b}	$\overline{DP}_{PCL}$ ^{a}	M_n ^{a}	M_n ^{c}	M_n/M_w ^{c}	MPEG/PCL wt %
EO$_{114}$-CL$_{42}$	2.85	2.71	114	42	9800	8900	1.22	51/49
EO$_{114}$-CL$_{111}$	1.14	1.03	114	111	17650	13400	1.29	28/72
EO$_{114}$-CL$_{247}$	0.49	0.46	114	247	33200	29800	1.38	15/85
EO$_{114}$-CL$_{516}$	0.23	0.22	114	516	63900	57000	1.43	8/92

[a] Calculated by using the integration ratio of resonances due to MPEG blocks at 3.60 ppm (-O-CH$_2$-CH$_2$-) and to PCL blocks at 4.01 ppm [(-CO)-O-CH$_2$-] in the ^{1}H NMR spectra. [b] Degree of polymerization of MPEG = 5000/44 = 114. [c] Obtained from GPC.

Table 4-2. DSC Results of LiClO$_4$/MPEG-PCL Blends.

copolymer MPEG-PCL	LiClO$_4$ content (wt%)	T_g (°C)	T_m (°C)	ΔH_m (J/g)
MPEG-5k[a]	0	-58.5	60.2	185.6
EO$_{114}$-CL$_{42}$	0	-56.9	56.8	120.6
	10	-39.1	58.5	64.0
	20	-58.5 -32.0	59.3	37.2
	25	-61.7 -10.8	59.4	32.6
	30	-49.7 -36.3	--	--
	40	-36.7	--	--
	50	-38.5	42.2 80.2[b]	11.2 24.0
EO$_{114}$-CL$_{111}$	0	-59.2	54.1	104.2
	10	-54.6 -21.2	58.4	51.4
	20	-54.8 -6.8	55.1	36.0
	25	-40.8	48.2	5.8
	30	-28.6	--	--
	40	-20.4	--	--
	50	-35.9	28.9 88.4	2.0 40.8
EO$_{114}$-CL$_{247}$	0	-57.5	59.2	91.5
	10	-55.7 -13.1	57.2	65.2
	20	-28.3	53.9	37.1
	25	-32.3	--	--
	30	-31.5	--	--
	40	-5.9	--	--
	50	-38.7	42.1 89.8	20.5 56.4
EO$_{114}$-CL$_{516}$	0	-57.2	59.1	89.4
	10	-43.5	54.9	45.6
	20	-35.2	46.4	9.7
	25	-24.5	--	--
	30	-23.7	--	--
	40	-2.3	--	--
	50	-38.2	34.7 93.0	12.5 58.4

[a] The macro-initiator of ring-opening of ε-caprolactone in the synthesis of MPEG-PCL.

[b] The melting point of pure LiClO$_4$ is at ca. 95 °C.

Table 4-3. Curve-Fitting Results of Infrared Spectra of C=O Group Stretching Region Recorded at 120 °C for the LiClO$_4$/MPEG-PCL Blends with Various LiClO$_4$ Salt Content.

Copolymer MPEG-PCL	LiClO$_4$ content (wt%)	Free C=O		Complexed C=O	
		ν_f (cm^{-1})	A_f (%)	ν_c (cm^{-1})	A_c (%)
EO$_{114}$-CL$_{42}$	0	1734.9			
	10	1734.3			
	20	1734.4			
	25	1733.5			
	30	1733.9			
	40	1734.1			
	50	1733.4	53.59	1705.3	46.41
EO$_{114}$-CL$_{111}$	0	1734.7			
	10	1734.6			
	20	1734.2			
	25	1734.5			
	30	1734.4			
	40	1732.7	40.90	1704.7	59.10
	50	1731.8	28.04	1704.7	71.96
EO$_{114}$-CL$_{247}$	0	1735.0			
	10	1734.8			
	20	1734.8	81.96	1702.0	18.04
	25	1734.1	73.36	1703.5	26.64
	30	1734.4	58.12	1705.1	41.88
	40	1732.4	32.46	1704.4	67.54
	50	1732.8	25.12	1704.7	74.88
EO$_{114}$-CL$_{516}$	0	1734.4			
	10	1734.6			
	20	1734.7	65.81	1704.0	34.19
	25	1733.7	59.34	1704.7	40.66
	30	1734.1	45.44	1703.5	54.56
	40	1732.7	32.66	1705.0	67.34
	50	1731.9	21.28	1704.8	78.72
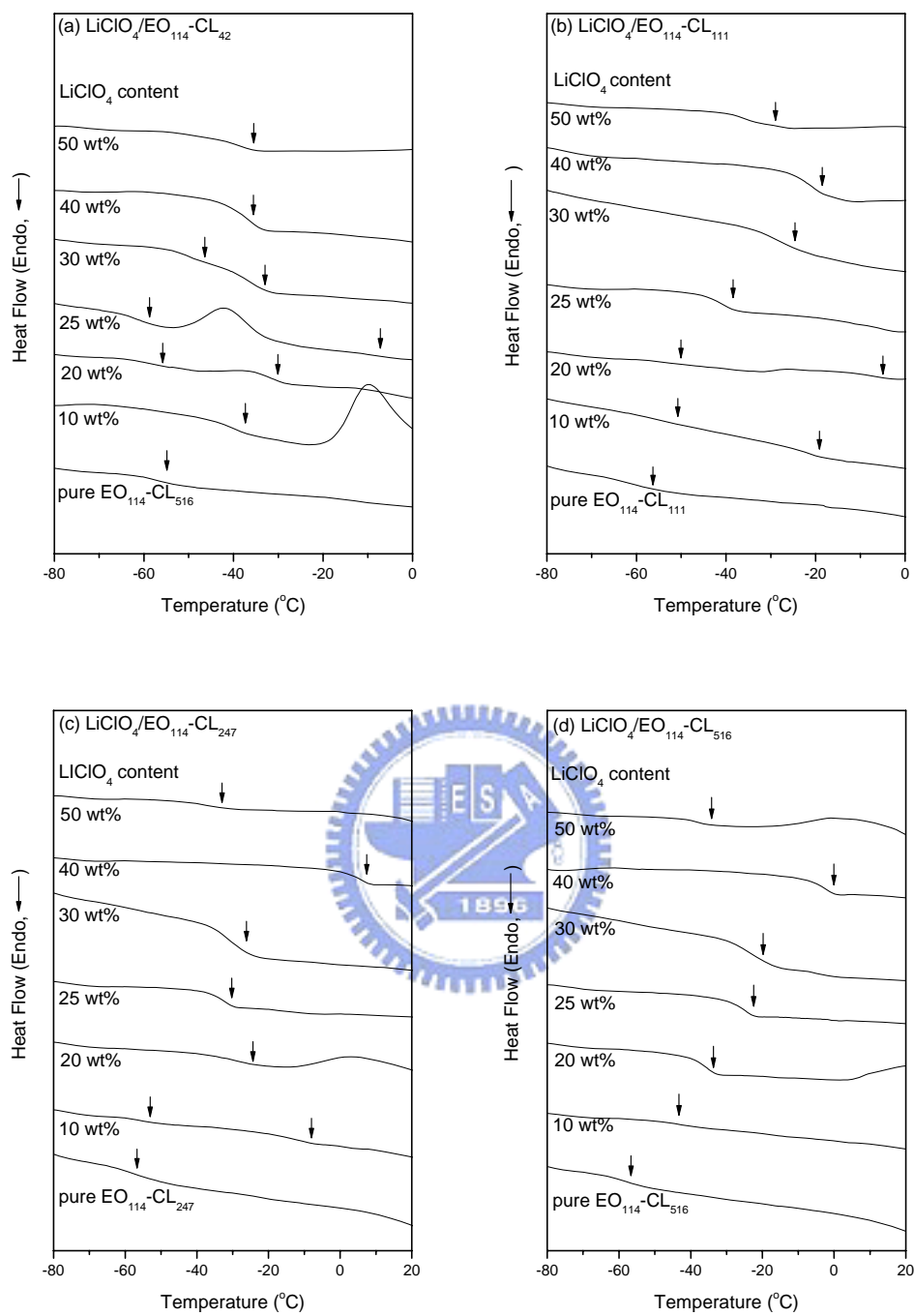
Figure 4-1. DSC thermograms of LiClO$_4$/MPEG-PCL blend with various LiClO$_4$ salt content: (a) EO$_{114}$-CL$_{42}$, (b) EO$_{114}$-CL$_{111}$, (c) EO$_{114}$-CL$_{247}$, (d) EO$_{114}$-CL$_{516}$.
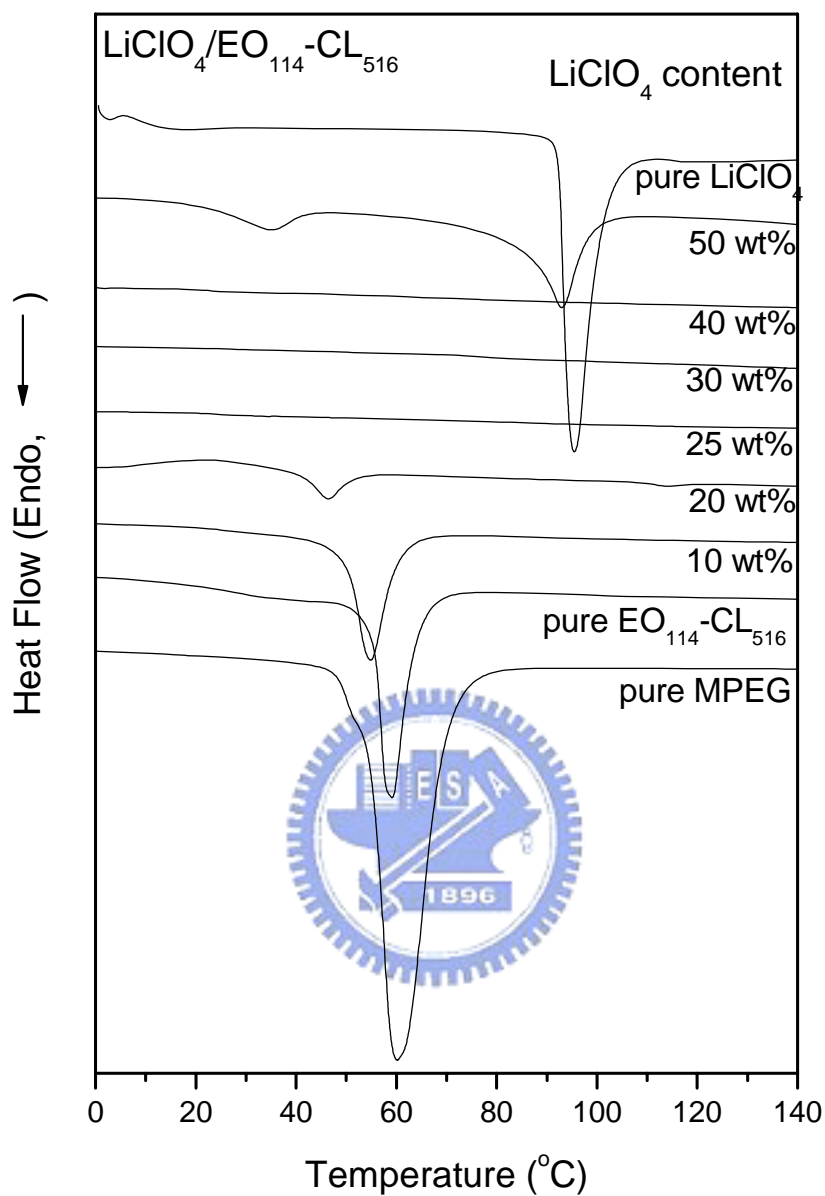
Figure 4-2. Variations of melting temperature (T_m) and melting enthalpy (ΔH_m) of LiClO$_4$/EO$_{114}$-CL$_{516}$ blends with various LiClO$_4$ content.
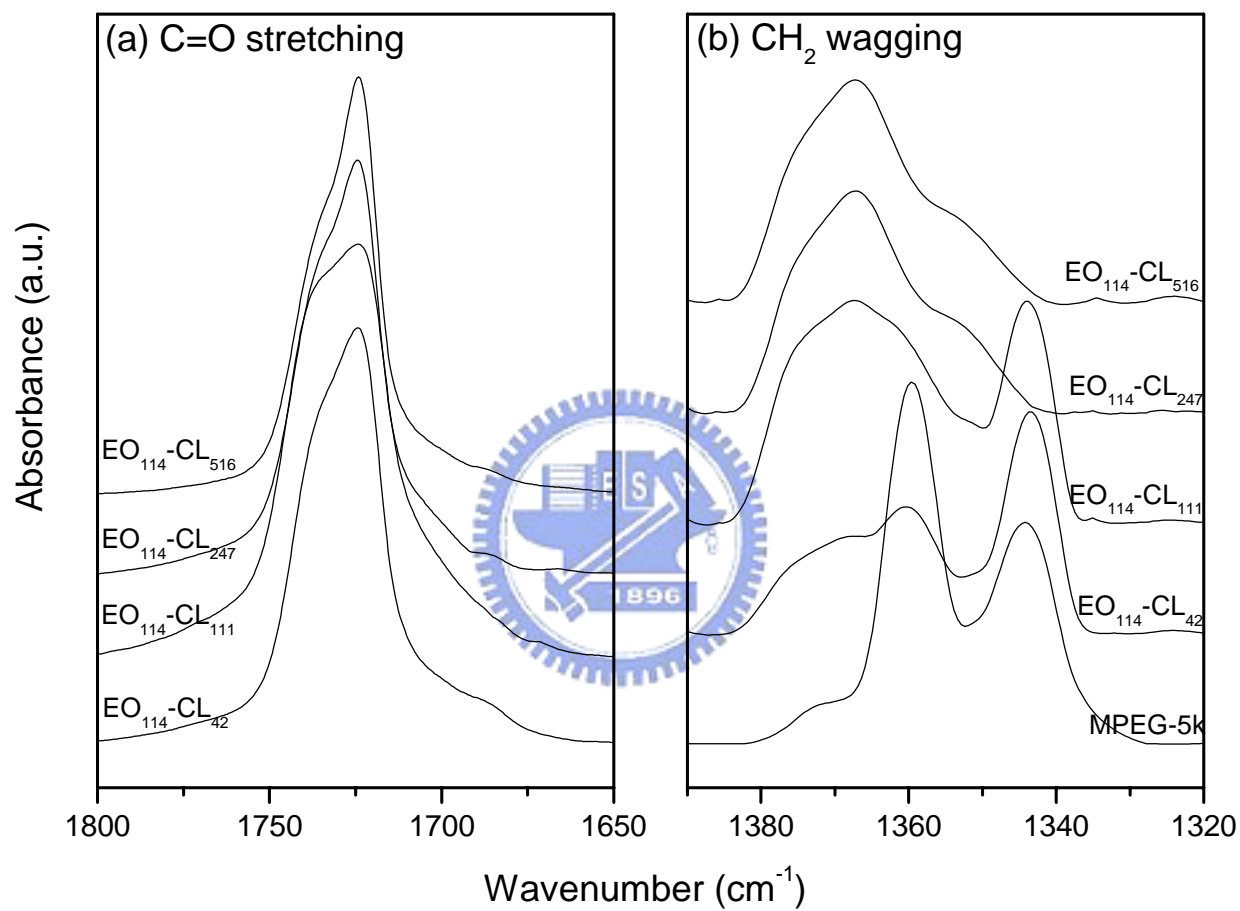
Figure 4-3. Infrared spectra of MPEG-PCL block copolymers with various EO/CL ratios, recorded at room temperature, displaying (a) the carbonyl stretching and (b) CH$_2$ wagging regions.
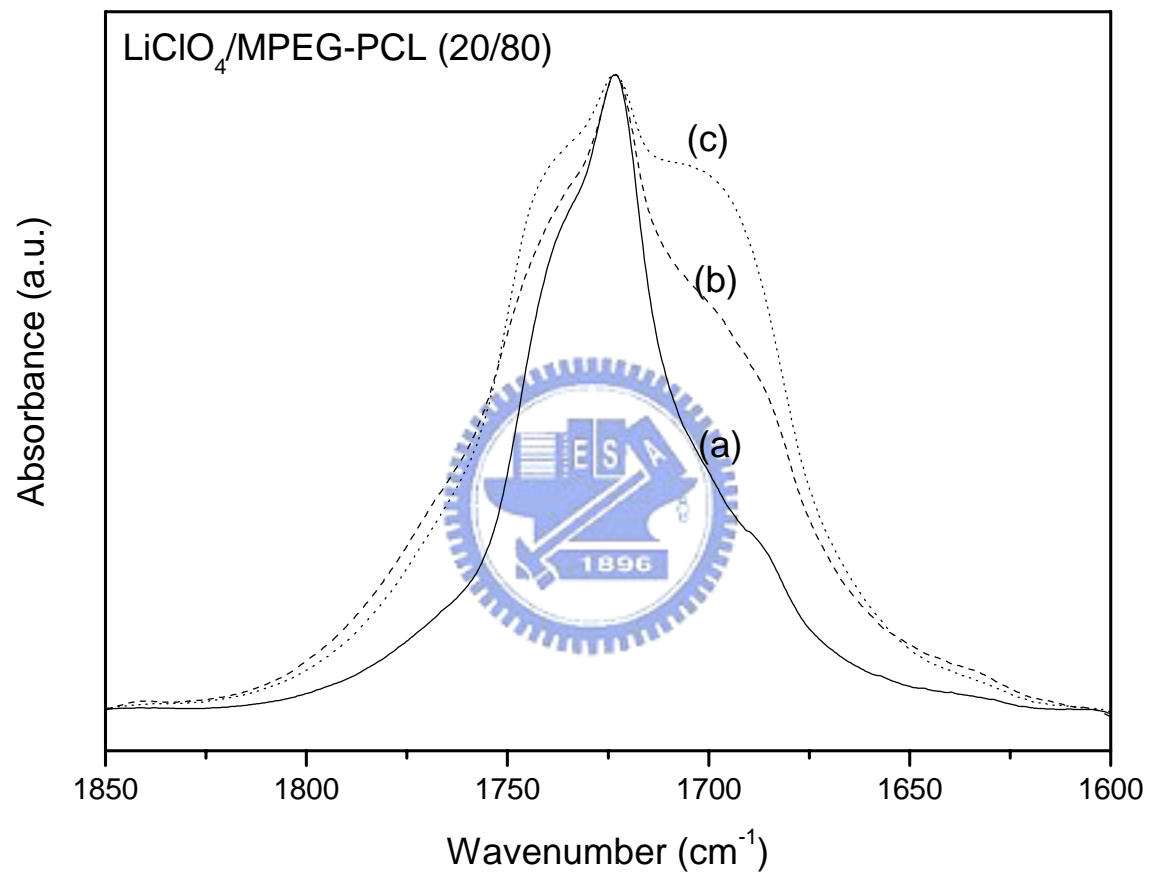
Figure 4-4. Carbonyl group stretching region of IR spectra recorded at room temperature for MPEG-PCL block copolymers having different EO/CL ratios after blending with 20 wt% $LiClO_4$: (a) EO_{114}-CL_{111}, (b) EO_{114}-CL_{247}, (c) EO_{114}-CL_{516}.
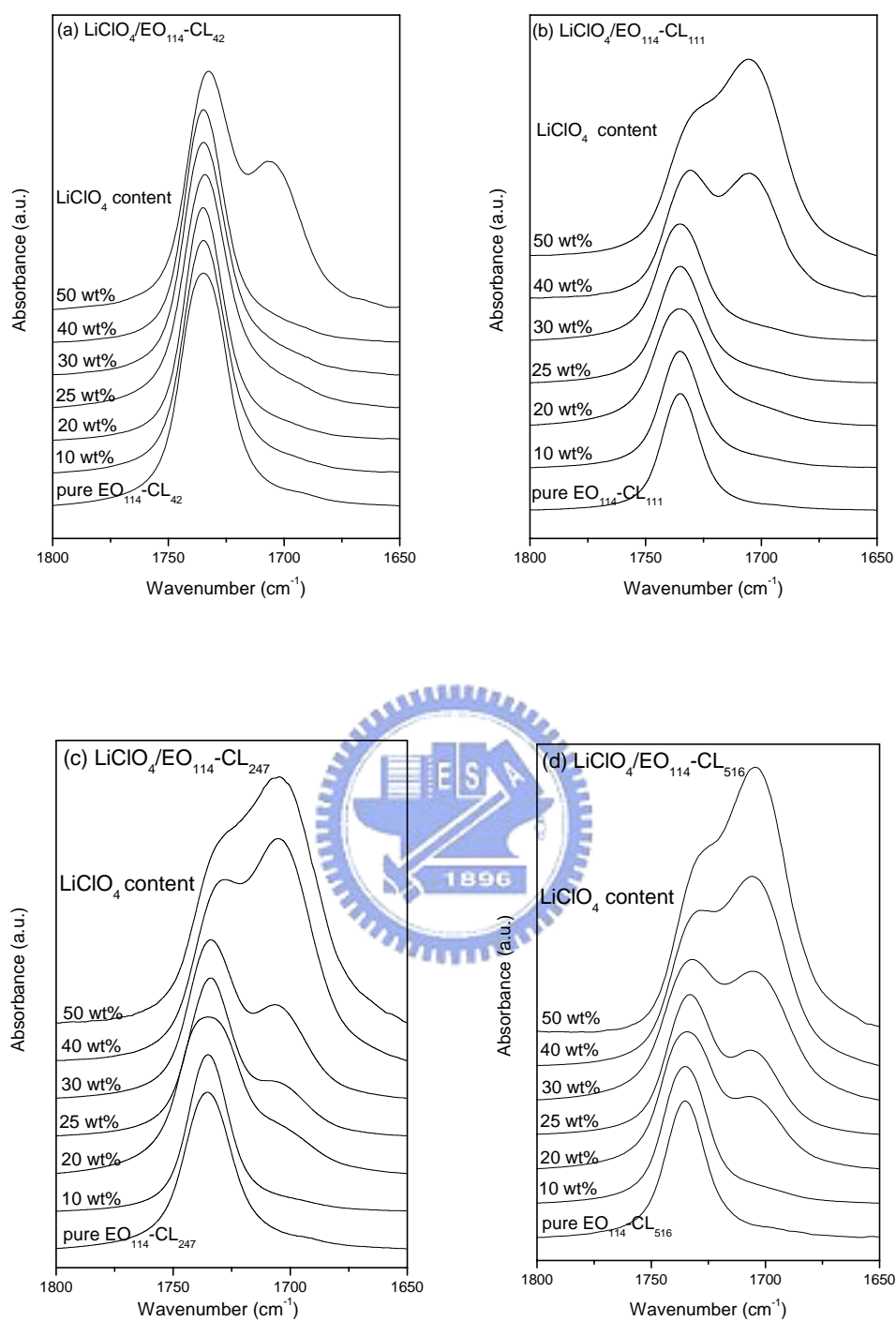
Figure 4-5. Carbonyl group stretching region of the IR spectra recorded at 120 °C for LiClO$_4$/MPEG-PCL blends having different LiClO$_4$ contents: (a) EO$_{114}$-CL$_{42}$, (b) EO$_{114}$-CL$_{111}$, (c) EO$_{114}$-CL$_{247}$, (d) EO$_{114}$-CL$_{516}$.

110
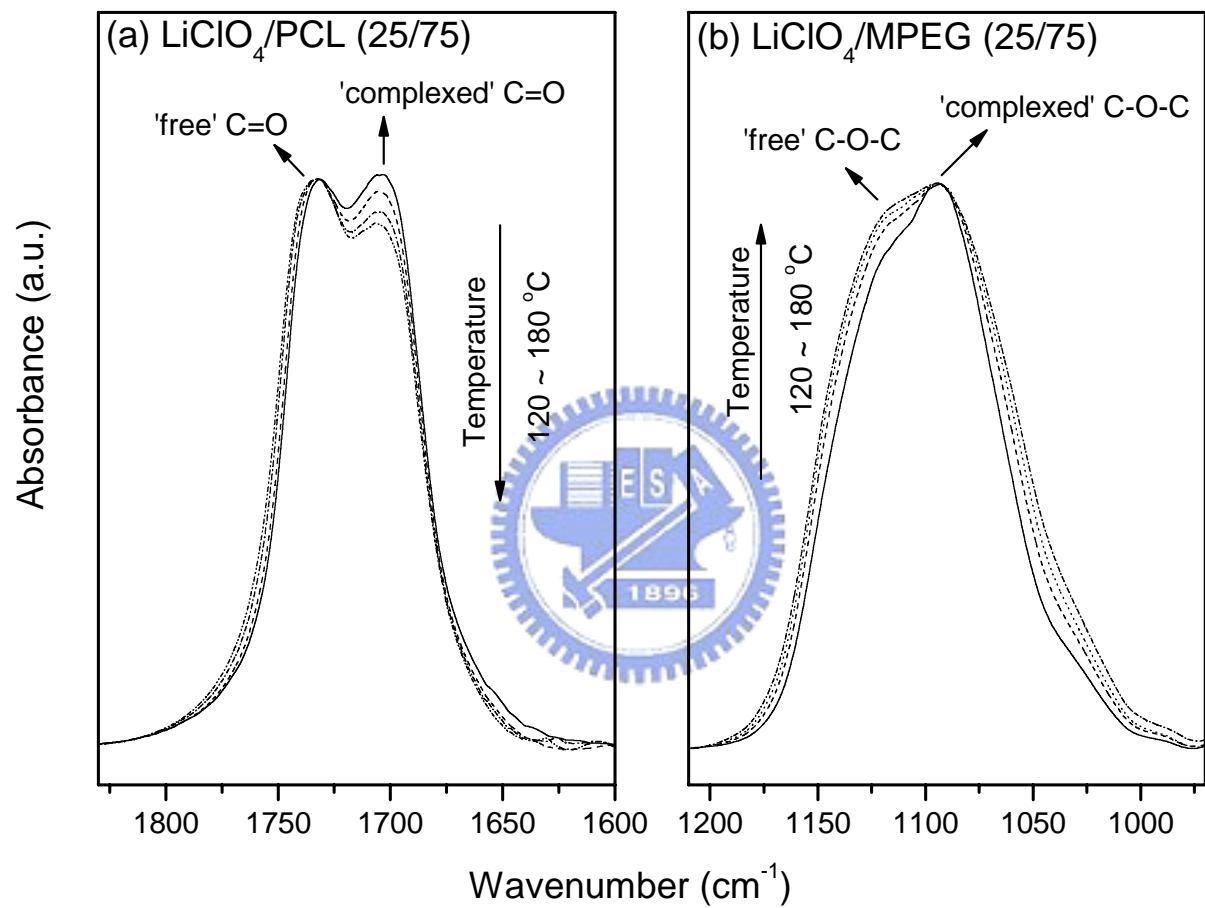
Figure 4-6. FTIR spectra recorded at temperatures from 120 to180 °C of blends of (a) LiClO4/PCL homopolymer (25/75), displaying the carbonyl group vibration region, and (b) LiClO4/MPEG-5k homopolymer (25/75), displaying the ether group stretching region.
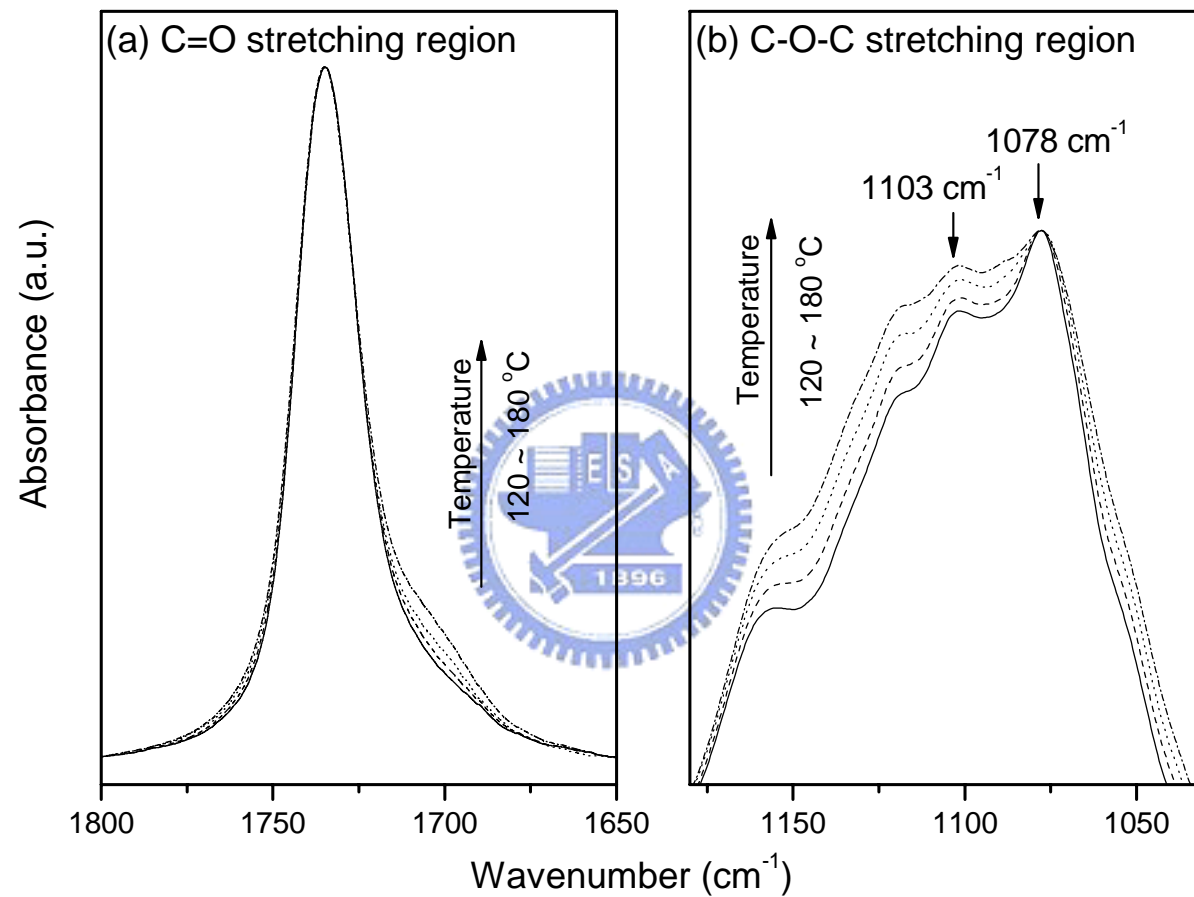
Figure 4-7. FTIR spectra of $LiClO_4/EO_{114}\text{-}CL_{42}$ (30/70) recorded at temperatures from 120 to 180 °C displaying both the (a) carbonyl group stretching and (b) ether group stretching regions.
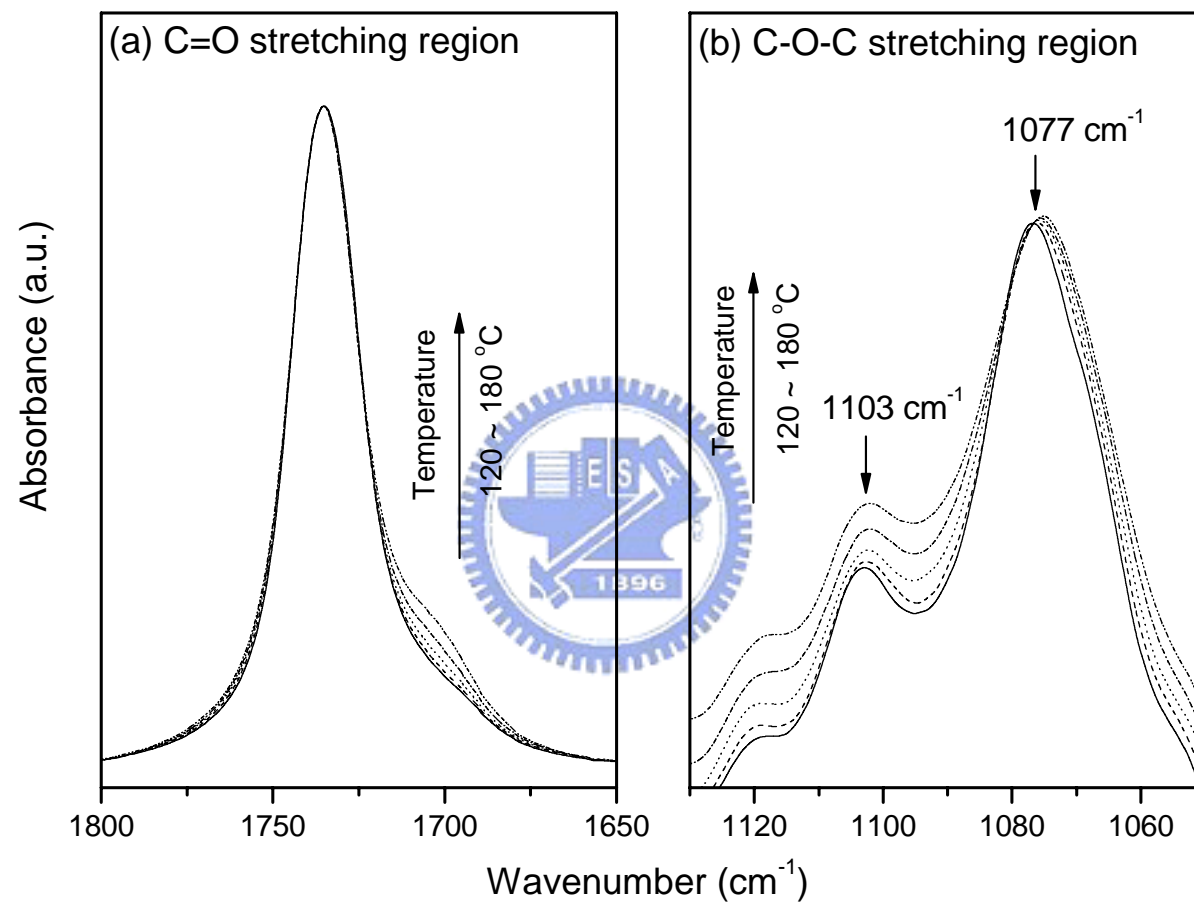
Figure 4-8. FTIR spectra of $LiClO_4/EO_{114}$-CL_{111} (30/70) recorded at temperatures from 120 to 180 °C displaying both the (a) carbonyl group stretching and (b) ether group stretching regions.
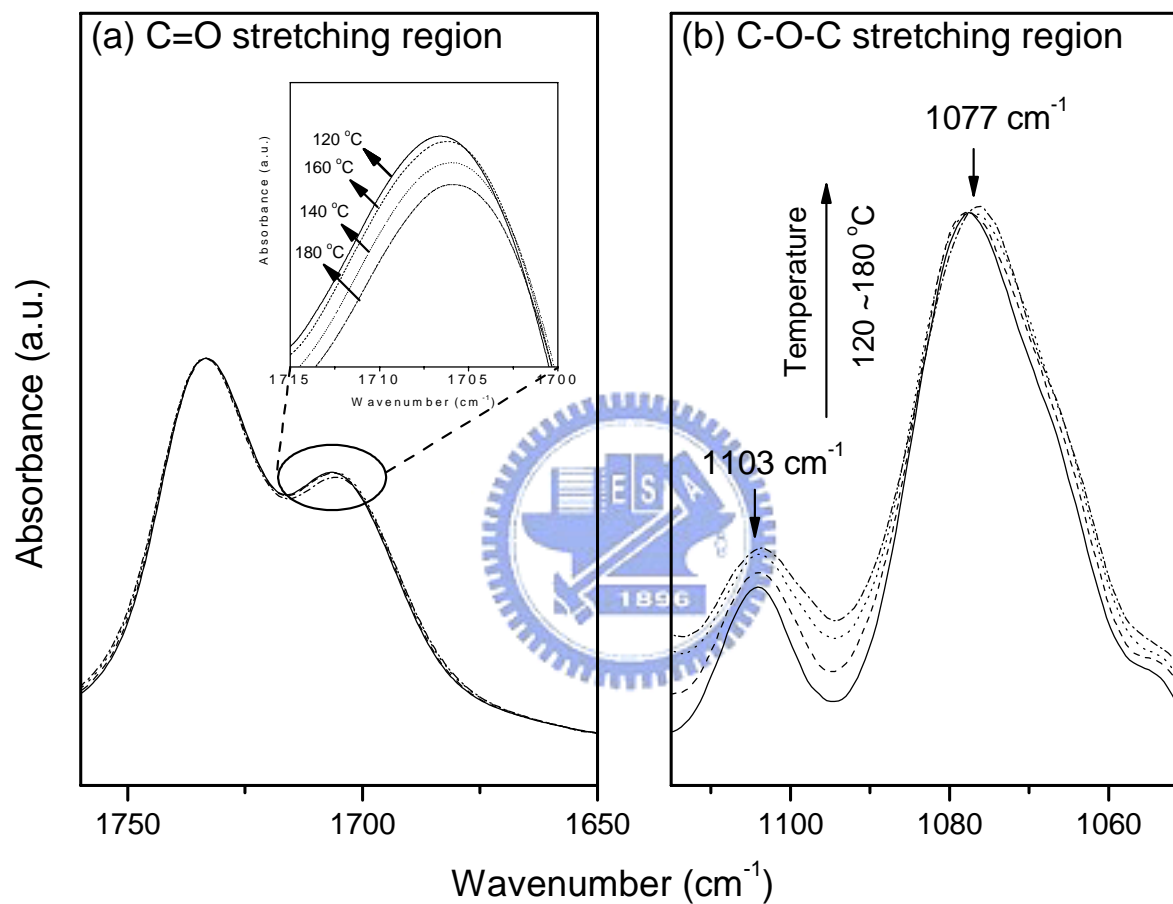
Figure 4-9. FTIR spectra of LiClO$_4$/EO$_{114}$-CL$_{111}$ (40/60) recorded at temperatures from 120 to 180 °C displaying both the (a) carbonyl group stretching and (b) ether group stretching regions.
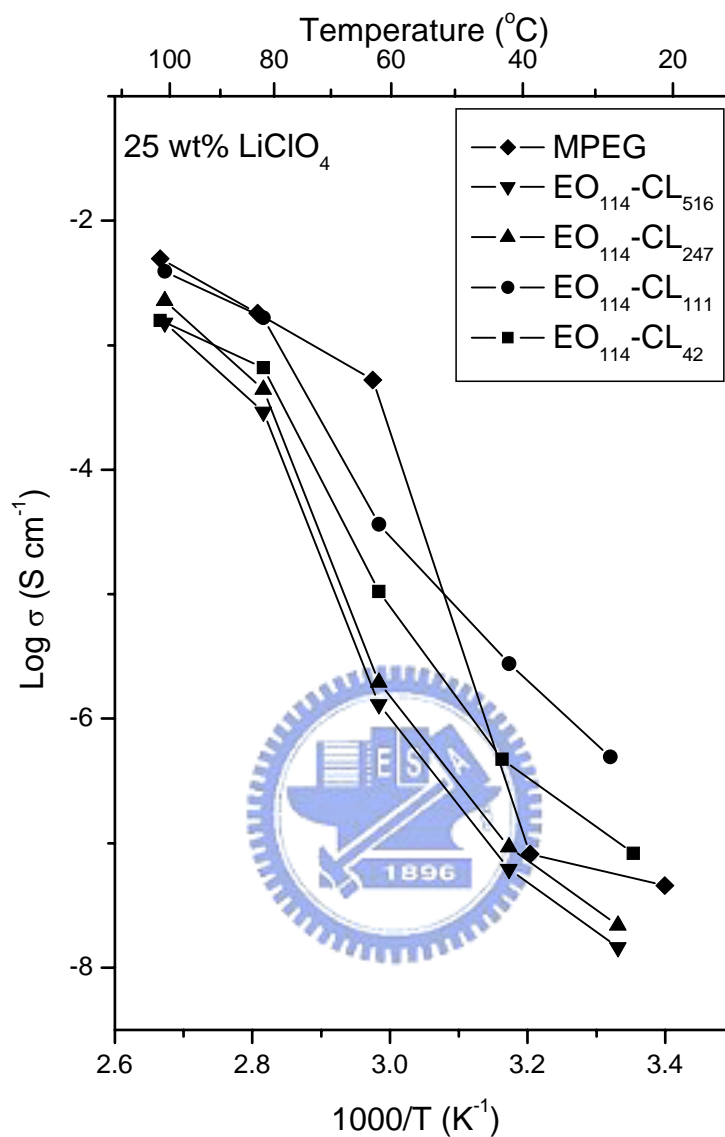
Figure 4-10. Arrhenius ionic conductivities plotted as a function of temperature for LiClO$_4$/MPEG-PCL blend-based electrolyte systems containing a constant LiClO$_4$ concentration (25 wt%).

CHAPTER 5

Studying the Effect of Complicated Interaction on the Phase Behavior and Ionic Conductivity of PVP-*co*-PMMA-Based Polymer Electrolytes

ABSTRACT

The phase behavior, complicated interaction and ionic conductivity of poly(vinyl pyrrolidone-*co*-methyl methacrylate) (PVP-*co*-PMMA) with lithium perchlorate (LiClO$_4$) have been investigated in detail by means of DSC, FTIR spectroscopy, and ac impedance technique. The presence of MMA moiety in the PVP-*co*-PMMA random copolymer acts as an inert diluent role to reduce the self-association of the PVP molecules and causes the negative deviation of the glass transition temperature (T_g). For the binary blend of LiClO$_4$/PVP, the addition of low LiClO$_4$ content tends to reduce the strong dipole-dipole interaction within PVP and leads to lower T_g of PVP; further addition of LiClO$_4$ promotes higher T_g of PVP increasing due to the ion-dipole interaction between LiClO$_4$ and PVP. In the LiClO$_4$/PVP-*co*-PMMA blend systems, all these three individual systems, PVP-*co*-PMMA copolymer, LiClO$_4$/PVP blend and LiClO$_4$/PMMA are miscible at all compositional ratios, immiscibility loop exists with certain compositions due to the complicated interactions among LiClO$_4$, PVP and PMMA. The PMMA-rich component in the PVP-*co*-PMMA copolymer tends to be excluded and results in phase separation. Finally, we found that a maximum value of ionic conductivity is present at the composition of LiClO$_4$/VP57 (57 mol% VP unit in PVP-co-PMMA copolymer) at fixed 20 wt% LiClO$_4$ salt.

5-1 INTRODUCTION

Polymer electrolytes are compounds formed by the dissolution of salts in polar and high molar mass macromolecules which form strong interaction with cations. The proposed use of solvent-free polymer electrolytes for high energy density batteries and other solid-state electrochemical devices [1-5] has spurred considerable interest in the ion-transport properties of these materials. For most potential applications, it is desirable that the solid polymer electrolytes display a reasonable conductivity ($\sim 10^{-4}$ S cm^{-1}), dimensional stability, processability and flexibility in ambient conditions. Great progress has been made over the last 20 years in increasing the level of ionic conductivity exhibited by polymer electrolytes [6]. However, in recent years, despite innovative designs of flexible polymers and the synthesis of salts containing asymmetric anions capable of suppressing crystallinity, levels of ionic conductivity are persistently limited to a ceiling of around 10^{-4} cm^{-1} at room temperature. Such a level is insufficient for many lithium battery applications [7,8]. It is important now to change our thinking concerning how to optimize and further increase the ionic conductivity. It is of vital importance to promote their performance upon understanding the fundamental interaction behavior of polymer electrolytes in order to better understand the ion transport mechanism.

The poly(vinyl pyrrolidone) (PVP) is amorphous and exhibits high T_g due to the presence of the rigid pyrrolidone group, in which a tertiary amide group provides a more marked Lewis-base character to the carbonyl group. This character arises from its strong polar character, which is known to form various complexes with many inorganic salts [9]. However, its high T_g tends to limit the mobility of the ions based on Li-PVP polymer electrolyte and results in the poor ionic conductors.

On other hand, gel-type polymer electrolyte based on poly(methyl methacrylate) (PMMA) [10,11] has been proposed for lithium battery mainly due to its beneficial

effects on the stabilization of the lithium-electrode interface [12]. However, a reasonable conductivity achieved of such plasticizer film is offset by its relatively poorer mechanical properties at a high concentration of the plasticizer. Furthermore, the interaction between Li^+ cation and PMMA is significantly weaker than that of other polymer matrix such as poly(ethylene oxide) and PVP, therefore, the PMMA is less helpful to dissociate the lithium salt and to further facilitate the cations transporting. Li-PMMA polymer electrolyte in all solid state also presents low ionic conductivity.

Since PVP and PMMA both possess their own advantages to act as polymer electrolytes, we are interested in studying the polymer electrolyte by incorporating lithium perchlorate with both PVP and PMMA. However, the blends of PVP and PMMA are immiscible, therefore, we chose the PVP-*co*-PMMA random copolymer as replacement which was synthesized by free radical polymerization. It seems reasonable to expect that the gel-type polymer electrolyte based on PVP-*co*-PMMA may not only sustain the mechanical properties of PMMA-based gel polymer electrolyte but also increase the dissolubility of the lithium salt due to the strong withdrawing group within PVP [9]. To our knowledge, no previous study has been reported on the influence of the miscibility behavior and interaction mechanism on the ionic conductivity in polymer electrolyte comprising $LiClO_4$ and random copolymers. In this work, we employed differential scanning calorimetry (DSC), Fourier transform infrared (FTIR) spectroscopy, and alternating current (ac) impedance to investigate the interaction behavior and related conductivities of all solid state polymer electrolytes of the $LiClO_4$/PVP-*co*-PMMA blend system.

5-2 EXPERIMENTAL

5-2-1 Materials

Benzene, pyridine, azobisisobutyronitrile (AIBN), N-vinyl-2-pyrrolidone (VP), methyl methacrylate (MMA) and lithium perchlorate (LiClO₄) were purchased from Aldrich Chemical Co. The AIBN was purified by recrystallization from ethanol. Benzene and pyridine were fractionally distilled after addition of CaH₂. Both monomers, MMA and VP, were purified by vacuum distillation over CaH₂ and the fractions collected at room temperature and 50 °C, respectively. LiClO₄ was dried in a vacuum oven at 80 °C for 24 h and stored in desiccator prior to use.

5-2-2 Syntheses of Poly(N-vinyl-2-pyrrolidone-co-methyl methacrylate) (PVP-co-PMMA) Random copolymers

Solution copolymerization of N-vinyl-2-pyrrolidone with methyl methacrylate was carried out in benzene at 80 °C under a nitrogen atmosphere in a glass reaction flask equipped with a condenser (Scheme 1). AIBN (3 wt% with respect monomers) was employed as an initiator for free radical polymerization. To determine reactivity ratios, the sample of the copolymer was taken from the reaction flask in the early stage of copolymerization when the degree of conversion was low (between 4 and 9 %) [13]. The mixture was stirred for about 24 h, and then purified into excess ethyl ether with vigorous agitation to precipitate the product. The filtered polymer product was dried until reaching a constant weight.

5-2-3 Characterizations

Molecular weights and polydispersities of these synthesized copolymers were determined by gel permeation chromatography (GPC) using N,N-dimethylformamide (DMF) as an eluent at 50 °C and polystyrene standards were employed for molecular

weight calibration. The composition of the copolymer was further ascertained by means of ^{1}H NMR spectroscopy and elementary analysis (EA).

The ^{1}H NMR spectrum of the copolymer was recorded in deuterated chloroform (CDCl$_3$) solution at 25 °C using a Varian UNITY INOVA-400 NMR Spectrometer. EA was carried out in an oxidative atmosphere at 1021 °C using a Heraeus CHN-O Rapid Elementary Analyzer. The copolymer compositions of VP and MMA correspond to the repeating unit of C$_6$H$_9$NO and C$_5$H$_8$O$_2$, respectively. The VP content (mol%) was determined using the Eq. (1) and based on the content of C and N atoms [14].

$$VP(mol\%) = \frac{30N}{7C - 6N} \times 100 \tag{5-1}$$

5-2-4 Sample Preparations

Polymer electrolytes of LiClO$_4$/PVP-*co*-PMMA in various blend compositions were prepared by solution casting. The desired amounts of PVP-*co*-PMMA and LiClO$_4$ salt were dissolved in pyridine and stirred continuously for 24 h at 60 °C. The solution was cast onto a Teflon dish and maintained at 50 °C for an additional 24 h to remove the solvent; then the dish was further dried under vacuum at 80 °C for 2 days. To prevent its contact with air or moisture, the polymer electrolyte film was transferred to a glovebox under a nitrogen atmosphere.

5-2-5 Differential Scanning Calorimetry (DSC)

Thermal analysis was carried out using a DSC instrument (DuPont TA 2010). The instrument was calibrated with indium standards and conducted under a nitrogen flow rate of ca. 40 mL/min. The sample was sequentially heated from 30 to 200 °C for the first scan, maintained at 200 °C for 10 min, cooled rapidly to 0 °C, and then

reheated to 300 °C. The glass transition temperature (T_g) was obtained as the inflection point of the heat capacity jump recorded at a scan rate of 20 °C/min.

5-2-6 Fourier Transform Infrared Spectroscopy (FTIR)

The infrared spectrum of the polymer film was determined using the conventional KBr disk method at 120 °C. All polymer films were prepared under a N_2 atmosphere. The pyridine solution was cast onto KBr disk, from which the solvent was evaporated under vacuum at 80 °C for 48 h. All films used in this study are sufficiently thin to obey the Beer-Lambert law. FTIR measures were recorded in the range of 4000-400 cm^{-1} using a Nicolet AVATAR 320 FTIR Spectrophotometer (Nicolet Instruments, Madison, WI) and 32 scans were collected with a spectral resolution of 1 cm^{-1}.
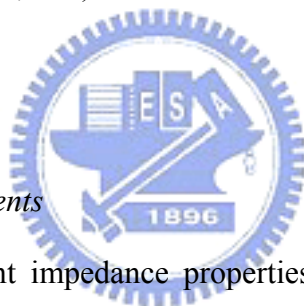
5-2-7 Conductivity Measurements

The frequency-dependent impedance properties of the polymer complex was measured by using an Autolab designed by Eco Chemie (10 MHz to 10 Hz). The sample was pressed into disks for conductivity measurements with the thickness of the pellets varying from 0.50 to 0.15 mm. The disks were loaded into a sealed conductivity cell between stainless steel blocking electrodes, and the impedance response was measured from 30 to 100 °C.

5-3 RESULTS AND DISCUSSION

5-3-1 PVP-co-PMMA Copolymer Characterization

Copolymerization of N-vinyl-2-pyrrolidone with methyl methacrylate was carried out at 80 °C by using AIBN as initiator (Scheme 5-1). A series of copolymers were prepared containing various VP and MMA monomer concentrations. The VP content (mol%) in the copolymer was determined by ^{1}H NMR and EA, results are summarized in Table 5-1. Since trace of water presence in PVP-*co*-PMMA copolymers may overestimate the integration of PVP signals for ^{1}H NMR and result in slightly higher PVP content in the products than feeds, EA was performed. Quantilies of N and C atoms are used for the calculation of VP content using Eq. (5-1). As shown in Eq. (5-1), H atoms from the moisture, even from the polymers, are not taken into account for the calculation of VP content by EA. Comparing results obtained from EA and ^{1}H NMR data, EA results are quite reproducible regardless of the moisture. Actually, the results of VP content from ^{1}H NMR are usually 5-10 % greater than those determined by EA. Thus, EA analysis turned out to be more suitable for quantification of the VP content in PVP-*co*-PMMA copolymers. Therefore, the sample codes of PVP-*co*-PMMA copolymers in the following discussion will be based on the VP content obtained by EA.

Table 5-1 lists the monomer feed ratios and resultant copolymer compositions from which reactivity ratios (r_1 and r_2) were calculated using the methodology of Kelen and Tüdös [15-17]. All polymerizations were performed in benzene under the same conditions described in the Experimental Section and terminated below 10 % monomer conversion to minimize errors due to changes in the feed ratios. The values of r_1 and r_2 represent the ratios of homo-propagation and cross-propagation rate constants for each monomer (i.e., $r_1 = k_{11}/k_{12}$ and $r_2 = k_{22}/k_{21}$, where k is the rate constant). The Kelen-Tüdös equation is given by Eq. (5-2)

$$\eta = \left(r_1 + \frac{r_2}{\alpha} \right) \xi - \frac{r_2}{\alpha} \tag{5-2}$$

where

$$\eta = \frac{G}{\alpha + F} \qquad \text{and} \qquad \xi = \frac{F}{\alpha + F}$$

F and G can be obtained by the quantities of x and y, where $x = M_1/M_2$ is the ratio of molar concentration of monomers 1 and 2, and $y = dM_1/dM_2$ is the mole ratio of these monomers in the copolymer, $F = x^2/y$ and $G = x(y\text{-}1)/y$. The value of α, chosen as $\alpha = (F_m F_M)^{1/2}$, where F_m and F_M are the lowest and highest F values from the experimental data. By plotting of η versus ξ, we can obtain r_2 and r_1 from the intercept and slope. The results are shown in Figure 5-1 from which values of $r_{PVP} = 0.97$ and $r_{PMMA} = 0.94$ are calculated. Previous literature [18] has proposed that a copolymerization behavior is termed ideal when the product of the two reactivity ratios is unity ($r_1 r_2 = 1$). Moreover, when $r_1 = r_2 = 1$, these two monomers show equal reactivities toward both propagating species. The copolymer composition is the same as the comonomer feed with a random distribution of these two monomers along the copolymer chain. Such behavior is referred to as random or Bernoullian. In this study, these PVP-co-PMMA copolymers synthesized by free radical polymerization are essentially in random fashion with a slight tendency toward ideal copolymer (the product of r_{PVP} and r_{PMMA} is 0.91).

The values of T_g of above samples are shown in Table 5-1. Several empirical or semi-empirical equations have been suggested for predicting the dependence of T_g on the composition of copolymers. In this study, a more suitable equation for a weakly interacting system is the Gordon-Taylor equation [19,20]:

$$T_g = \frac{w_1 T_{g1} + k w_2 T_{g2}}{w_1 + k w_2} \tag{5-3}$$

where w_1 and w_2 are weight fractions of the components, T_{g1} and T_{g2} represent the corresponding glass transition temperatures and k is the fitting constant. Figure 5-2

displays T_g versus PVP weight fraction of the PVP-*co*-PMMA copolymers. A value of $k = 0.45$ is obtained by a nonlinear least squares "best fit" analysis. This low value of k implies that the interaction between VP and MMA units in this copolymer is not strong [21]. The presence of even distributed MMA moiety actually plays an inert diluent role to hinder the self-association interaction of PVP moiety. Moreover, at a relatively lower PVP content (20 mol%), the diluent role plays the dominant role and thus results in lower T_g. On the contrary, the dipole-dipole interactions of PVP units play a dominant role at a higher PVP content and result in higher T_g. Fox and Gordon-Taylor equations are generally recognized to hold for miscible blends or copolymers where only weak intermolecular interactions occur. It is highly cognitively to employ them for the analysis of the composition behavior of PVP-*co*-PMMA copolymer taking into account that negative deviation from the Fox equation as in this study has been observed for copolymers where one of the components have a strong tendency to self-associate (e.g., form dimmers or multimers) [22,23]. As a result, the T_g behavior at higher PVP content shows relatively smaller deviation predicted by both equations than that at lower PVP content [21,24,25].

Figure 5-3 shows the scale expanded infrared spectra recorded in the region from 1800 to 1630 cm^{-1} for neat PVP, neat PMMA and a series of PVP-*co*-PMMA copolymers at 120 °C. The absorption peaks at ca. 1680 and ca. 1730 cm^{-1} are assigned to the carbonyl vibration bands of PVP and PMMA, respectively. Interestingly, it is found that the maximum of the carbonyl vibration band of PVP slightly shifts toward higher frequency when the MMA moiety is incorporated into the PVP. It implies that the dipole-dipole interaction of the PVP molecules tends to be eliminated due to the inert diluent role of the MMA moiety [26]. Therefore, this behavior observed from IR spectra is consistent with the DSC results (Figure 5-2). This factor is responsible for the observed decrease in T_g of the PVP-*co*-PMMA

copolymers.

5-3-2 LiClO$_4$/PVP and LiClO$_4$/PMMA Binary Blends

It has been reported that the properties of a polymer/salt mixture can be changed dramatically as a result of ionic aggregation [27-29]. To begin with, we carried out thermal analyses to determine whether properties of LiClO$_4$/PVP and LiClO$_4$/PMMA blends are affected by the addition of the lithium perchlorate salt. Figure 5-4 shows DSC thermographs of LiClO$_4$/PMMA and LiClO$_4$/PVP blends containing various LiClO$_4$ salt contents. Figure 5-4 (a) indicates that the maximum enhancement of the T_g is ca. 145 °C for PMMA containing 20 wt% LiClO$_4$. The ionic interaction or ionic cluster formation in the amorphous region of the ionomer usually resembles physical cross-linking. The mobility of polymer chain is restrained by such physical cross-linking and, thus leads to higher glass transition temperature relative to that of the mother polymer. Generally, the value of T_g increases gradually upon the addition of the salt because of increased ion-polymer and ion-ion interactions, and a maximum glass transition temperature is achieved at a certain content of LiClO$_4$ salt. Excess LiClO$_4$ tends to self-aggregate and causes the T_g of LiClO$_4$/PMMA blends even lower owing to the dilution effect [30,31]. It has been clearly demonstrated that most studies based on polymer/salt blends, such as poly(ethylene oxide) (PEO)/lithium salt [32], poly(2-ethyl-2-oxazoline) (PEtOx)/silver salt [33], and poly(4-vinylpyridine) (P4VP)/zinc salt [28], result in similar trend as the above-mentioned phenomenon obtained from DSC analyses.

However, the LiClO$_4$/PVP blend, as shown in Figure 5-4 (b), presents the novel behavior of the variation of the glass transition temperature with increasing LiClO$_4$ salt content. The addition of low LiClO$_4$ salt (5 wt%) causes the decrease in T_g of PVP. This is an unusual phenomenon comparing with prior results based on polymer/salt

blends. Relative to the PMMA, PVP is a water-soluble polymer in which the tertiary amide group provides a more marked Lewis-base character toward the carbonyl group. This character arises from its strong polar nature, with a dipole moment of ca. 4 Debye [34,35]. Therefore, it seems reasonable to expect that the PVP may possess a higher T_g at 181 °C due to its strong intermolecular dipole-dipole interaction. Many factors may contribute the high T_g of the PVP, however, the dipole-dipole interaction is still an important contributor. Initially, the presence of $LiClO_4$ moiety at a relative smaller content actually reduces the self-association interaction of PVP molecules and results in lower T_g [25], because the electron donor group of PVP is able to interact, through the formation of ion-dipole interaction, with electron acceptor species (i.e., Li^+ cation). As a result, there exist two interactions for competition, the self-association of PVP through dipole-dipole interaction and the ion-dipole interaction between Li^+ cation and the carbonyl group of PVP. The mobility of polymer chain tends to be restrained by the addition of $LiClO_4$, and results in higher T_g. On the other hand, the presence of $LiClO_4$ also tends to reduce the dipole-dipole interaction of PVP molecules simultaneously and results in lower T_g. These factors are responsible for the observed variation in the glass transition temperature of the $LiClO_4$/PVP complex system. As shown in Figure 5-4 (b), when the $LiClO_4$ content is increased from 0 to 30 wt%, the T_g increases from 181 to 191 °C. The increment of T_g (ΔT_g) is ca. 10 °C which is less than that of $LiClO_4$/PEO ($\Delta T_g \sim 35$ °C) or $ZnClO_4$/P4VP ($\Delta T_g \sim 140$ °C) blend system in our previous studies [28,32]. Further addition of $LiClO_4$ content from 30 to 40 wt%, T_g of $LiClO_4$/PVP blend system increases dramatically and tends to achieve its maximum at 233 °C. When the $LiClO_4$ content is increased to 50 wt%, however, the value of T_g decreases. According to the above observation, the optimal ion-dipole interaction condition between $LiClO_4$ and PVP in terms of T_g enhancement is at 40/60. Excess $LiClO_4$ content above 40 wt%

126

results in salt-aggregation and thus lower T_g because of increasing interchain distance above the optimized lithium salt content [33].

In order to further understand the T_g variation mechanism in the LiClO$_4$/PMMA and LiClO$_4$/PVP blend systems, FTIR characterization was performed. The most frequently employed method for quantifying the relative fractions of free and bonded carbonyl sites within a PMMA or PVP polymer chain by monitoring the carbonyl stretching bands as a function of the blend composition. Figure 5-5 presents the expanded IR spectra of the carbonyl stretching absorption, ranging from 1800 to 1550 cm^{-1}, of the LiClO$_4$/PVP blends containing various LiClO$_4$ contents recorded at 120 °C. The stretching band of the "free" carbonyl of the uncomplexed PVP appears at 1680 cm^{-1}. The pure PVP shows that this "free" carbonyl is asymmetric and significantly broader than the other non-complexed carbonyl bands [35-37]. Moreover, Painter and co-workers [38,39] have demonstrated that the real "free" or "unperturbed" carbonyl stretching band sited at ca. 1708 cm^{-1} is able to be obtained from IR spectra of the model compound ethyl pyrrolidone (EPr). The carbonyl stretching band of the PVP obviously broadens and shifts to a lower frequency at ca. 1680 cm^{-1} due to the strong self-association of PVP molecules (i.e., the dipole-dipole interaction between pyrrolidone groups of PVP). Hence, the "free" carbonyl in the PVP is expected to be minor, and the carbonyl band observed in PVP actually consists of bands from large associated species (multimers).

Returning to Figure 5-5, the carbonyl band broadens gradually as the LiClO$_4$ content is increased and a new band at ca. 1652 cm^{-1} appears. This newborn band corresponds to the coordination between the Li$^+$ cation and the oxygen atom on the carbonyl group of PVP. A third band clearly appears at lower frequency at ca. 1630 cm^{-1}, when the LiClO$_4$ content is increased over 20 wt%. This band sited at lower frequency, implying that an even stronger interaction is involved with the carbonyl group of the

PVP. In addition, the relative intensity of this band increases with the increase of the LiClO$_4$ content. Thus, this carbonyl absorption band at ca. 1630 cm^{-1} can be considered as the carbonyl group interacting simultaneously with several Li$^+$ cations when more Li$^+$ cations are present. To further elucidate the effect of LiClO$_4$ content of the charge environment surrounding the carbonyl group of PVP, Figure 5-6 shows relative fractions of "un-complexed" and "complexed" C=O sites by decomposing the C=O stretching band into two or three Gaussian peaks [38,40] and results are summarized in Table 5-2. Correspondingly, the above-mentioned carbonyl stretching bands sited at 1680, 1650 and 1630 cm^{-1} can be assigned to the "un-complexed", "complexed I" and "complexed II" C=O bands, respectively. The relative intensity of the "un-complexed" C=O band decreases upon increasing the LiClO$_4$ content. Moreover, the initial addition of 5 wt% LiClO$_4$ content causes the peak position of the "un-complexed" C=O bands shifting slightly to higher frequency (from 1680 to 1682 cm^{-1}). The dipole-dipole interaction of PVP molecules tends to be reduced with the addition of LiClO$_4$. On the other hand, Figure 5-7 summarizes the fractional area versus LiClO$_4$ content of the "un-complexed" and two "complexed" C=O bands for comparison. Both relative fractions of "complexed I" and "complexed II" C=O bands increase with the increase of LiClO$_4$ content up to 40 wt%. After that, the relative fraction of the "complexed I" C=O band begins to decrease while that of the "complexed II" C=O band continuously increases. Apparently, the formation of the complex I shifts gradually into the complex II when the concentration of LiClO$_4$ salt is increased. It evidences that the complex II is favorable at higher LiClO$_4$ concentration. Furthermore, it is clearly shown that not all the added Li$^+$ cations are able to associate with the carbonyl groups by forming the polymer-salt complex; some "un-complexed" C=O groups are still present, even with excessively high LiClO$_4$ concentration. This result indicates that the Li$^+$ cation is involved in equilibrium with

both ClO_4^- (counter ion) and C=O simultaneously in the blend. Accordingly, these results coincide with the phenomenon observed from the DSC analyses.

In order to further clarify this complicated interaction mechanism in the blend of $LiClO_4$/PVP system, Figure 5-8 depicts three types of proposed association schemes. Type A describes the dipole-dipole interaction between the carbonyl groups of neat PVP. This interaction tends to be disturbed or reduced and the ion-dipole interaction between Li^+ and carbonyl group of PVP as replacement when low content of $LiClO_4$ is added; however, the ion-dipole interaction between Li^+ and the carbonyl group of PVP tends to be the replacement, as depicted in type B. While further increasing the $LiClO_4$ content, an excessive of $LiClO_4$ salt causes the salt-aggregation.

Figure 5-9 shows the expanded FTIR spectra ranging from 1800 to 1650 cm^{-1} of a series of $LiClO_4$/PMMA blends recorded at 120 °C. The stretching band of the free carbonyl group of the uncomplexed PMMA appears at 1730 cm^{-1}. When the $LiClO_4$ salt is added, a shoulder at ca. 1700 cm^{-1} appears, corresponding to the ion-dipole interaction between the C=O group and Li^+. It is clearly observed in Figure 5-9 that the relative intensity of the shoulder at ca. 1700 cm^{-1} increases upon increasing the $LiClO_4$ concentration. Table 5-2 lists the curve-fitting results of the carbonyl group stretching for $LiClO_4$/PVP and $LiClO_4$/PMMA. The PVP matrix can interact with more content of $LiClO_4$ than that with PMMA. Furthermore, the type of complex II appeared in the $LiClO_4$/PVP blend system at high $LiClO_4$ concentration is absent in the $LiClO_4$/PMMA blend system. These differences can be interpreted as the stronger dipole moment of the functional group of PVP than that of PMMA. Comparison with the DSC analyses, the $LiClO_4$ salt tends to aggregate in $LiClO_4$/PMMA blend at lower salt concentration (ca. 30 wt%), while salt-aggregation for $LiClO_4$/PVP blend occurs at a higher salt content of ca. 50 wt%.

5-3-3 Blends of LiClO$_4$ Salt and PVP-co-PMMA Copolymers

Figure 5-10 displays the deconvolution of infrared spectra ranging from 1800 to 1525 cm^{-1} of the LiClO$_4$/VP79 (PVP-*co*-PMMA with 79 mol% VP unit) blend in the region of carbonyl stretching recorded at 120 °C. We concentrated on the unperturbed bands at 1680 and 1730 cm^{-1} for PVP and PMMA, respectively. As we mentioned before, the addition of lower content of LiClO$_4$ (10 wt%) in PVP results in a new band at ca. 1655 cm^{-1}, which is assigned as the "complexed I" C=O group of PVP. When the LiClO$_4$ is increased to 30 wt%, "complexed II" C=O group of PVP occurs at ca. 1630 cm^{-1}. Furthermore, the "complexed" C=O group of PMMA is formed while the LiClO$_4$ content is further increased to 40 wt% as shown in Figure 5-9. Figure 5-10 presents that there exists a competition between carbonyl groups from PVP and PMMA for coordinating with Li$^+$ cation. At low LiClO4 content, Li$^+$ tends to selectively interact only with PVP. When the LiClO$_4$ concentration is gradually increased, the Li$^+$ interacts simultaneously with PVP and PMMA. The Li$^+$ is more preferable to interact with PVP than with PMMA. All these carbonyl stretching frequencies of LiClO$_4$/PVP-*co*-PMMA blends are clearly split into several bands, which can be fitted well to the Gaussian function. For brevity, the results of the subsequent curve fitting are summarized in Table 5-3. Table 5-3 indicates that the relative intensity of "un-complexed" C=O group decreases upon the increase of LiClO$_4$ content for both VP and MMA units; the similar trend is also observed from the both binary blends of LiClO$_4$/PVP and LiClO$_4$/PMMA. In detail, comparison between LiClO$_4$/PVP (30/70) and LiClO$_4$/VP57 (20/80), which both blends possess the same molar ratio of [Li$^+$]/[VP unit] regardless of the PMMA presence, the area fraction of "un-complexed" C=O from the VP units in LiClO$_4$/VP57 blend system is less than that in LiClO$_4$/PVP blend. Since the presence of MMA unit in the PVP-*co*-PMMA copolymer plays an inert dilute role to decrease the self-association

130

of VP unit, less LiClO$_4$ content is necessary for the LiClO$_4$/PVP-*co*-PMMA blend to attain the same coordination extent between Li$^+$ and VP unit.

The DSC analysis is one of the most convenient methods for determining the miscibility in polymer blends. T_g measurements are used in this study to identify phase. Figure 5-11 shows the conventional second-run DSC thermograms of various LiClO$_4$/PVP-*co*-PMMA blends; either single T_g or two T_gs are identified in all blends. The existence of a single T_g strongly suggests that these blends are fully miscible with a homogenous phase. Meanwhile, a blend containing two T_gs is considered to be immiscible or phase separated. The binary blend of PVP and PMMA is known to be immiscible [26,41,42], however, the PVP-*co*-PMMA random copolymers at various component ratios are miscible (a single T_g is shown in Figure 5-11). Consequently, the phase diagram of the LiClO$_4$/PVP-*co*-PMMA blend at room temperature is present in Figure 5-12. Interestingly, even though these three individual systems, PVP-*co*-PMMA copolymer, LiClO$_4$/PVP blend and LiClO$_4$/PMMA, are all miscible at all compositions, immiscibility exists with certain compositions in this LiClO$_4$/PVP-*co*-PMMA blend system. The $\Delta\chi$ effect, the discrepancy between the interaction parameters χ of the third component with polymers 1 and 2, plays an important role in the phase behavior of these blends. The $\Delta\chi$ effect results from an unequal interaction strength between different component pairs [43-45]. Zeman and Patterson [46] have demonstrated that the $\Delta\chi$ effect strongly promoted phase separation in ternary systems. An immiscibility may occur in systems with specific interaction due to an "attraction" between different covalently bonded monomers of the copolymers. From the FTIR analyses (Table 5-3), LiClO$_4$ has much greater preference for coordinating with PVP than with PMMA. Therefore, the addition of the third component, LiClO$_4$ salt, tends to exclude the PMMA component in the mixture of LiClO$_4$ and PVP-*co*-PMMA and becomes immiscible. Moreover, the immiscibility

region appears when the $LiClO_4$ content is low or/and the PVP component in the PVP-*co*-PMMA copolymer is relatively high. Nevertheless, when the $LiClO_4$ concentration is gradually increased up to 30 wt%, this blend presents fully miscibility regardless of compositions of PVP-*co*-PMMA copolymers. Enough $LiClO_4$ content is available to interact with PVP and PMMA simultaneously, thus causes the $LiClO_4$/PVP-*co*-PMMA blends to be miscible. Figure 5-12 shows that a closed immiscibility loop exists in the phase diagram of $LiClO_4$/PVP-*co*-PMMA blends as a result of the complicated interactions among $LiClO_4$, PVP and PMMA.

The T_g values of $LiClO_4$/PVP-*co*-PMMA blends containing various $LiClO_4$ contents are tabulated in Table 5-4. The lower value of T_g observed at ca. 123 °C is close to the pure PMMA that can be assigned as the T_g of the PMMA-rich domain. Subsequently, the higher value of T_g above 180 °C is attributed to the T_g of the PVP-rich domain. It implies that the PMMA phase is excluded form the mixture by adding the $LiClO_4$ salt. In addition, the T_g of PVP-rich domain in $LiClO_4$/PVP-*co*-PMMA blend is higher than that of the binary blend of $LiClO_4$ and PVP containing the same $LiClO_4$ concentration. Since the presence of MMA moiety tends to reduce the self-association of the PVP components, Li^+ cation is able to coordinate with PVP unit more directly and results in higher value of T_g. These results are consistent with the FTIR analyses. It is interesting to notice that a random copolymer, PVP-*co*-PMMA, with covalently bonded monomers tends to phase separate upon doping the $LiClO_4$ salt. As a result, Figure 5-13 illustrates the schematic drawing of phase separation in the $LiClO_4$/PVP-*co*-PMMA blend.

5-3-4 Analyses of Ionic Conductivity

Figure 5-14 shows the room temperature conductivity plot versus VP content in copolymers for $LiClO_4$/PVP-*co*-PMMA blends containing a fix $LiClO_4$ content of 20

wt%. This plot indicates that the polymer electrolyte composed of LiClO$_4$/VP39 exhibits a maximum ionic conductivity at room temperature. The conductivity (σ) behavior can be interpreted by the following equation [7,40,47]:

$$\sigma = \sum_i n_i z_i \mu_i \qquad (5\text{-}4)$$

where n_i, z_i, and μ_i refer to the concentration of the charge carrier, the ionic charge on the charge carrier, and the mobility of the charge carrier, respectively. In this study, the ionic charge (z_i) is the same for all blend systems and the resulted ionic conductivity depends on n_i and μ_i.

Since the amount of charge carriers (n_i) is expected to be related with the fraction of "free" ClO$_4^-$ anion dissociated from LiClO$_4$ salt. Figure 5-15 shows IR spectra of the ν (ClO$_4^-$) internal vibration mode ranging from 660 to 600 cm^{-1} recorded at 120 °C for LiClO$_4$/PVP-*co*-PMMA blends containing a constant LiClO$_4$ content of 20 wt%. Within this region, the absorptions at around 624 and 636 cm^{-1} correspond to the free anion and the contact ion pairs, respectively [48,49]. In order to clarify the charge environment of the ClO$_4^-$ anion, the relative fraction of the free anion has been quantified by decomposing the ν (ClO$_4^-$) internal vibration mode into two Gaussian peaks. Table 5-5 lists relative fractional areas and locations of related adsorption bands for comparison. The relative fraction of the "free" ClO$_4^-$ anion increases initially by increasing the VP molar ratio of the PVP-*co*-PMMA copolymer, but decreases when the VP molar ratio is over 60 % (VP57). It is understandable that the incorporation of the PVP moiety into PMMA tends to increase the relative fraction of the "free" ClO$_4^-$ because the dipole moment of pyrrolidone group within PVP molecule is strong enough to dissociate the LiClO$_4$ salt in to Li$^+$ and ClO$_4^-$. However, Shriver et al. [9] have demonstrated that the addition of Li$^+$ forming Li-PVP complex tends to induce the N atom within PVP to become N quasi-cation via electron

resonance. The N quasi-cation of PVP prompts the electrostatic N atom to pull the anion allowing for cation-anion interaction. Therefore, the ClO_4^- anion is able to interact not only with the Li^+ cation but also with the N quasi-cation of the PVP that is responsible for the decrease of the relative fraction of the "free" anion.

On the other hand, in the solid state electrolyte system, it is reasonable to assume that the mobility of charge carrier (μ_i) is related with the mobility of the polymer matrix (i.e., dependence on T_g). Combining these effects of n_i and μ_i on ionic conductivity, it is reasonable to explain that the maximum ionic conductivity occurs at $LiClO_4$/VP57 (20/80).

5-4 CONCLUSIONS

We have used DSC, FTIR spectroscopy, and ac impedance techniques to investigate in detail the miscibility behavior, interaction mechanism, and ionic conductivity of polymer electrolyte composed of $LiClO_4$ and PVP-*co*-PMMA random copolymer. Although PVP/PMMA blends are immiscible, a single T_g is observed for corresponding copolymers and proves these copolymers are miscible. Furthermore, the presence of MMA units in PVP plays an inert diluent role to reduce the self-association of PVP molecules and thus causes negative deviation of T_g. For the binary blend of $LiClO_4$/PVP, an unusually phenomenon was observed that the addition of low content of $LiClO_4$ salt tends to reduce to strong dipole-dipole interaction of PVP and results in the decrease of T_g; then, the further increase of $LiClO_4$ promotes T_g of PVP increasing. It is interesting to notice that the $LiClO_4$/PVP-*co*-PMMA polymer electrolyte exists an immiscible loop in the phase diagram even though these three individual systems, PVP-*co*-PMMA copolymer, $LiClO_4$/PVP blend, and $LiClO_4$/PMMA blend, are all miscible in all compositions. The PMMA-rich domain tends to be excluded from the $LiClO_4$/PVP-co-PMMA blend and leads to phase separation. Combining these effects of n_i and μ_i on ionic conductivity, eventually, the maximum conductivity was found at the composition of $LiClO_4$/VP57 (20/80).
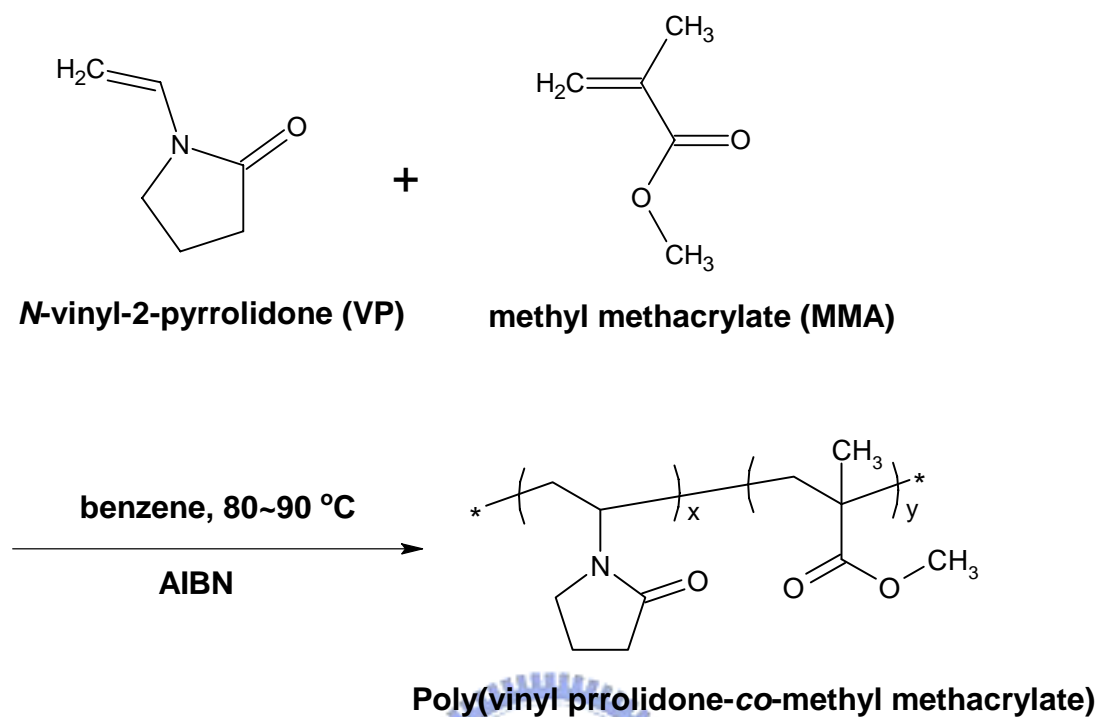
5-5 References

1. Armand, M. B.; Chabagno, J. M; Duclot, M. J. In *Fast Ion Transport in Solids*; Vashishta, P., Mundy, J. N., Shenoy, G. K., Eds.; North-Holland: New York, 1979.

2. Cheradame, H.; Le Nest, J. F. In *Polymer Electrolyte Reviews*; MacCallum, J. R., Vincent, C. A., Eds., Elsevier: New York, 1987/1989.

3. Scrosati, B. In *Applications of Electroactive Polymers*; Scrosati, B., Ed.; Chapman and Hall: London, 1993.

4. Armand, M. B. *Solid State Ionics* **1983**, *9*, *745*.

5. Chao, S.; Wrighton, M. S. *J. Am. Chem. Soc.* **1987**, *109*, 2197.

6. Bruce, P. G. *Solid State Electrochemistry*; Cambridge University: Cambridge, 1995.

7. Ratner, M. A.; Shriver, D. F. *Chem. Rev.* **1988**, *88*, 109.

8. Allcock, H. R.; Ravikiran, R.; O'Connor, S. J. M. *Macromolecules* **1997**, *30*, 3184.

9. Spindler, R.; Shriver, D. F.; *Macromolecules* **1986**, *19*, 347.

10. Rajendran, S.; Uma, T.; *Mater. Lett.* **2000**, *44*, 242.

11. Stephan, A. M.; Kumar, T. P.; Renganathan, N. G.; Pitchumani, S.; Thirunakaran, R.; Muniyandi, N. *Solid State Ionics* **2000**, *130*, 123.

12. Appetecchi, G. B.; Croce, F.; Scrosati, B. *Electrochim. Acta.* **1995**, *40*, 991.

13. Xu, Y.; Painter, P. C.; Coleman, M. M. *Polymer* **1993**, *34*, 3010.

14. Luo, L.; Ranger, M.; Lessard, D. G.; Le Garrec, D.; Gori, S.; Leroux, J.-C.; Rimmer, S.; Smith, D. *Macromolecules* **2004**, *37*, 4008.

15. Kennedy, J. P.; Kelen, T.; Tüdös, F. *J. Polym. Sci.*, *Polym. Chem. Ed.* **1975**, *13*, 2277.

16. Kelen, T.; Tüdös, F. *Macromol. Sci. Chem.* **1975**, *A9*, 1.

17. Kuo, S. W.; Chang, F. C. *Polymer* **2001**, *42*, 9843.

18. Odian, G. *Principles of Polymerization*; John Wiley & Sons: New York, 1991; Chapter 6.

19. Gordon, M.; Taylor, J. S. *J. Appl. Chem.* **1952**, *2*, 493.

20. Aubin, M.; Prud'Homme, R. E. *Macromolecules* **1988**, *21*, 2954.

21. Kuo, S. W.; Huang, W. J.; Huang, C. F.; Chan, S. C.; Chang, F. C. *Macromolecules* **2004**, *37*, 4164.

22. Feldstein, M. M. *Polymer* **2001**, *42*, 7719.

23. Painter, P. C.; Graf, J. F.; Coleman, M. M. *Macromolecules* **1991**, *24*, 5630.

24. Kuo, S. W.; Chang, F. C. *Polymer* **2003**, *44*, 3021.

25. Xu, H.; Kuo, S. W.; Lee, J. S.; Chang, F. C. *Macromolecules* **2002**, *35*, 8788.

26. Dong, J.; Fredericks, P. M.; George, G. A. *Polym. Degrad. Stab.* **1997**, *58*, 159.

27. Chiu, C. Y.; Hsu, W. H.; Yen, Y. J.; Kuo, S. W.; Chang, F. C. *Macromolecules* **2005**, *38*, 6640.

28. Kuo, S. W.; Wu, C. H.; Chang, F. C. *Macromolecules* **2004**, *37*, 192.

29. Eisenberg, A.; Rinaudo, M. *Polym. Bull.* **1990**, *24*, 671.

30. Chen, H. W.; Chiu, C. Y.; Chang, F. C. *J. Polym. Sci., Polym. Phys. Ed.* **2002**, *40*, 1342.

31. Kim, J. H.; Min, B. R.; Won, J.; Kang, Y. S. *J. Phys. Chem. B* **2003**, *107*, 5901.

32. Chiu, C. Y.; Chen, H. W.; Kuo, S. W.; Huang, C. F.; Chang, F. C. *Macromolecules* **2004**, *37*, 8424.

33. Kim, J. H.; Min, B. R.; Kim, C. K.; Won, J.; Kang, Y. S. *Macromolecules* **2002**, *35*, 5250.

34. Galin, M. *Makromol. Chem., Rapid Commun.* **1984**, *5*, 119.

35. Martinez de Ilarduya, A.; Iruin, J. J.; Fernandez-Berridi, M. J. *Macromolecules* **1995**, *28*, 3707.

36. Moskala, E. J.; Varnell, D. F.; Coleman, M. M. *Polymer* **1985**, *26*, 228.

37. Zhu, B.; He, Y.; Yoshie, N.; Asakawa, N.; Inoue, Y. *Macromolecules* **2004**, *37*, 3257.

38. Hu, Y.; Motzer, H. R.; Etxeberria, A. M.; Fernandez-Berridi, M. J.; Iruin, J. J.; Painter, P. C.; Coleman, M. M. *Macromol*. *Chem*. *Phys*. **2000**, *201*, 705.

39. Painter, P. C.; Pehlert, G. J.; Hu, Y.; Coleman, M. M. *Macromolecules* **1999**, *32*, 2055.

40. Chen, H. W.; Lin, T. P.; Chang, F. C. *Polymer* **2002**, *43*, 5281.

41. Neo, M. K.; Goh, S. H. *Polym*. *Commun*. **1991**, *32*, 200.

42. Goh, S. H.; Lee, S. Y.; Siow, K. S.; Neo, M. K. *Polymer* **1990**, *31*, 1065.

43. Zhang, H.; Bhagwagar, D. E.; Graf, J. F.; Painter, P. C.; Coleman, M. M. *Polymer* **1994**, *35*, 5379.

44. Ten Brinke, G.; Karasz, F. E.; MacKnight, W. J. *Macromolecules* **1983**, *16*, 1827.

45. Li, X. D.; Goh, S. H. *J*. *Polym*. *Sci*., *Polym*. *Phys*. *Ed*. **2002**, *40*, 1125.

46. Zeman, L.; Patterson, D. *Macromolecules* **1972**, *5*, 513.

47. Meyer, W. H. *Adv*. *Mater*. **1998**, *10*, 439.

48. Mishra, R.; Rao, K. J. *Solid State Ionics* **1998**, *106*, 113.

49. Salomon, M.; Xu, M.; Eyring, E. M.; Petrucci, S. *J*. *Phys*. *Chem*. **1994**, *98*, 8234.

Scheme 5-1. Synthesis of PVP-*co*-PMMA Random Copolymer

N-vinyl-2-pyrrolidone (VP)   **methyl methacrylate (MMA)**

benzene, 80~90 °C

AIBN

Poly(vinyl prrolidone-*co*-methyl methacrylate)

Table 5-1. PVP-*co*-PMMA Copolymer Compositional and Molecular-Weight Data[a]

| Copolymer abbreviation[b] | Monomer feed (mol%) | | Polymer composition (mol%) | | | | M_n^e | M_w/M_n^e | T_g^f (°C) |
| | | | EA[c] | | NMR[d] | | | | |
	VP	MMA	VP	MMA	VP	MMA			
PVP	100	0	100	0	100	0	18200	2.63	181
VP79	78.3	21.7	78.8	21.2	80.8	19.2	18700	2.40	161
VP57	57.5	42.5	57.0	43.0	62.6	37.4	23000	2.23	144
VP47	47.4	52.6	46.8	53.2	52.9	47.1	17000	2.29	139
VP39	37.5	65.5	38.5	61.5	40.7	59.3	20300	2.52	134
VP19	18.4	81.6	19.4	80.6	18.7	81.3	22100	2.00	123
PMMA	0	100	0	100	0	100	25700	1.76	121

[a] Polymerization conditions: initiator = AIBN; solvent = benzene; temperature = 80 °C. [b] Labeling based on VP content in the PVP-*co*-PMMA copolymers obtained from EA. [c] Calculated from the elementary analyzer using Eq. (5-1). [d] Obtained form the ^{1}H NMR spectra. [e] Determined by GPC using polystyrene standards and DMF as the eluent. [f] Characterized by DSC thermograms.
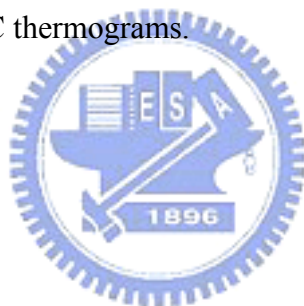
Table 5-2. Curve-Fitting Results of Infrared Spectra of C=O Group Stretching Region Recorded at 120 °C for the $LiClO_4$/PVP and $LiClO_4$/PMMA Blends with Various $LiClO_4$ Salt Content

polymer	$LiClO_4$ content, wt%	"Un-complexed" C=O			"Complexed I" C=O			"Complexed II" C=O		
		ν, cm^{-1}	$w_{1/2}$, cm^{-1}	A_f, %	ν, cm^{-1}	$w_{1/2}$, cm^{-1}	A_f, %	ν, cm^{-1}	$w_{1/2}$, cm^{-1}	A_f, %
PVP	0	1680	28	100.0						
	5	1682	34	80.9	1652	43	19.1			
	10	1679	27	78.0	1656	30	22.0			
	20	1679	31	65.0	1653	23	27.1	1630	33	7.9
	30	1678	30	55.6	1653	22	30.9	1635	33	13.5
	40	1681	30	39.5	1654	29	40.6	1632	39	19.9
	50	1673	31	40.9	1652	23	16.1	1630	43	43.0
PMMA	0	1731	22	100.0						
	10	1730	22	80.6	1704	27	19.4			
	20	1731	21	67.8	1706	32	32.2			
	30	1731	21	63.2	1707	33	36.8			
	40	1732	22	60.1	1708	34	39.9			

Table 5-3. Curve-Fitting Results of IR Spectra of C=O Group Stretching Region Recorded at 120 °C for the LiClO$_4$/PVP-*co*-PMMA Blends with Various LiClO$_4$ Content.

| | | Carbonyl group in VP unit | | | | | | | | | Carbonyl group in MMA unit | | | | | |
| | | "un-complexed" C=O | | | "complexed I" C=O | | | "complexed II" C=O | | | "un-complexed" C=O | | | "complexed" C=O | | |
Copolymesrs	LiClO$_4$ content, wt%	ν, cm^{-1}	$w_{1/2}$, cm^{-1}	A_u, %	ν, cm^{-1}	$w_{1/2}$, cm^{-1}	A_{cI}, %	ν, cm^{-1}	$w_{1/2}$, cm^{-1}	A_{cII}, %	ν, cm^{-1}	$w_{1/2}$, cm^{-1}	A_u, %	ν, cm^{-1}	$w_{1/2}$, cm^{-1}	A_c, %
VP79	0	1680	36	100.0							1729	22	100.0			
	10	1686	27	53.5	1657	30	46.5				1727	25	100.0			
	20	1685	24	42.1	1657	31	57.9				1725	25	100.0			
	30	1684	22	28.5	1658	30	61.4	1625	37	10.0	1724	26	100.0			
	40	1685	24	20.3	1656	34	59.6	1628	43	20.2	1726	24	78.5	1710	19	21.5
VP57	0	1683	28	100.0							1729	23	100.0			
	10	1684	25	58.8	1656	25	41.2				1728	25	100.0			
	20	1683	25	46.1	1656	24	44.9	1627	37	9.1	1726	24	100.0			
	30	1682	27	35.2	1656	30	52.0	1625	43	12.8	1726	26	100.0			
	40	1681	27	28.9	1655	29	52.7	1623	40	18.3	1727	23	74.8	1708	22	25.2
VP47	0	1683	24	100.0							1729	27	100.0			
	10	1685	24	53.6	1656	26	41.6	1623	37	4.7	1728	24	100.0			
	20	1682	24	45.1	1655	23	44.9	1629	33	10.0	1729	21	80.6	1705	20	19.4
	30	1682	31	41.9	1653	28	45.4	1622	40	12.7	1730	21	74.6	1706	18	25.4
	40	1682	23	20.9	1656	30	61.3	1625	41	17.8	1728	21	58.1	1709	27	41.9

VP39	0	1685	24	100.0							1729	22	100.0		
	10	1684	24	58.8	1656	22	41.2				1729	22	100.0		
	20	1682	26	45.5	1655	23	46.7	1625	36	7.7	1730	20	75.0	1707	21	25.0
	30	1683	31	42.1	1654	27	45.6	1625	39	12.3	1730	21	72.0	1705	23	28.0
	40	1683	35	33.6	1656	32	43.9	1625	41	22.5	1730	20	61.0	1705	23	39.0
VP19	0	1687	23	100.0							1730	22	100.0		
	10	1685	21	40.7	1658	24	45.8	1630	45	13.5	1730	22	95.4	1704	17	4.6
	20	1685	26	31.8	1658	26	50.9	1630	42	17.2	1731	23	72.3	1703	25	27.7
	30	1686	20	9.1	1659	29	68.0	1628	34	22.9	1731	21	68.3	1702	25	31.7
	40				1659	30	73.5	1629	38	26.5	1729	20	66.1	1702	27	33.9
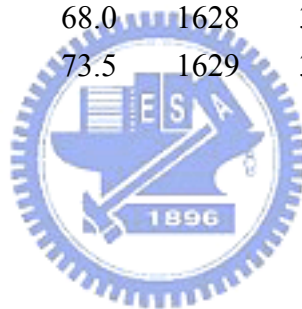
Table 5-4. T_gs of LiClO$_4$/PVP-*co*-PMMA Blends Containing Various LiClO$_4$ Content.

PVP-*co*-PMMA Copolymers	LiClO$_4$ Content, wt%	T_g, ^{o}C	PVP-*co*-PMMA Copolymers	LiClO$_4$ Content, wt%	T_g, ^{o}C
VP79	0	160	VP47	0	139
	5	126, 162		5	118, 194
	10	126, 190		10	121, 204
	15	133, 197		15	133, 209
	20	154, 205		20	150
	30	189		30	179
	40	181		40	156
	50	167	VP39	0	134
VP57	0	144		5	119, 182
	5	120, 182		10	123, 205
	10	126, 202		15	137
	15	129, 208		20	152
	20	151, 198		30	169
	30	161		40	159
	40	166	VP19	0	123
				5	125
				10	129
				15	139
				20	145
				30	159
				40	123

Table 5-5. Curve-fitting Data of Infrared Spectra at 120 °C of ν (ClO_4^-) Internal Vibration Mode of $LiClO_4$/PVP-*co*-PMMA with Various VP Content at a Fix $LiClO_4$ Concentration = 20 wt%.

Copolymers	Free anion			Contact ion pair		
	ν, cm^{-1}	$w_{1/2}$, cm$_{-1}$	A_f, %	ν, cm^{-1}	$w_{1/2}$, cm$_{-1}$	Ac, %
PMMA	626	10	76.3	637	6	23.7
VP19	625	11	80.8	636	7	19.2
VP39	624	11	84.7	636	7	15.3
VP47	624	10	84.7	636	6	15.3
VP57	624	10	84.9	636	6	15.1
VP79	626	10	79.8	637	6	20.2
PVP	627	8	71.1	636	6	28.9
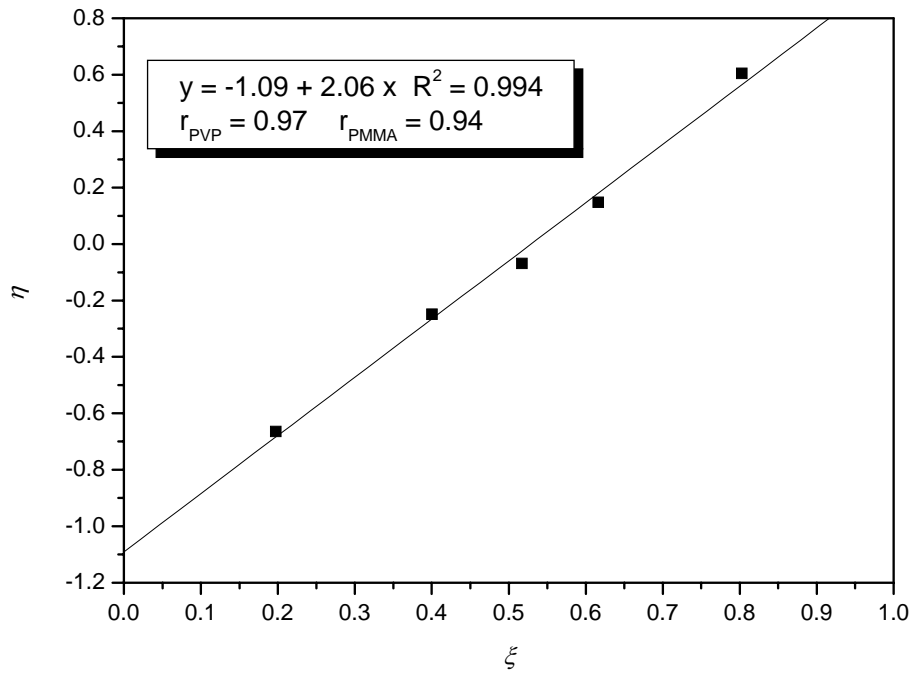
Figure 5-1. Kelen-Tudos plot for PVP-*co*-PMMA copolymers.
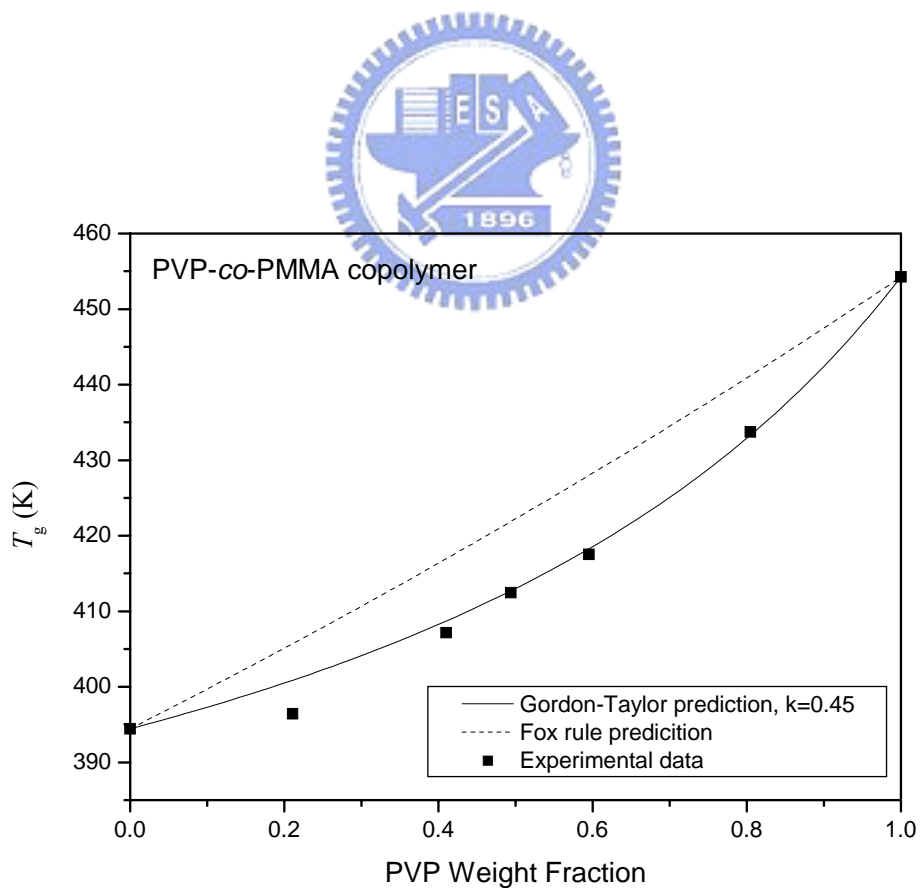
Figure 5-2. T_g versus the PVP content of PVP-*co*-PMMA copolymer.
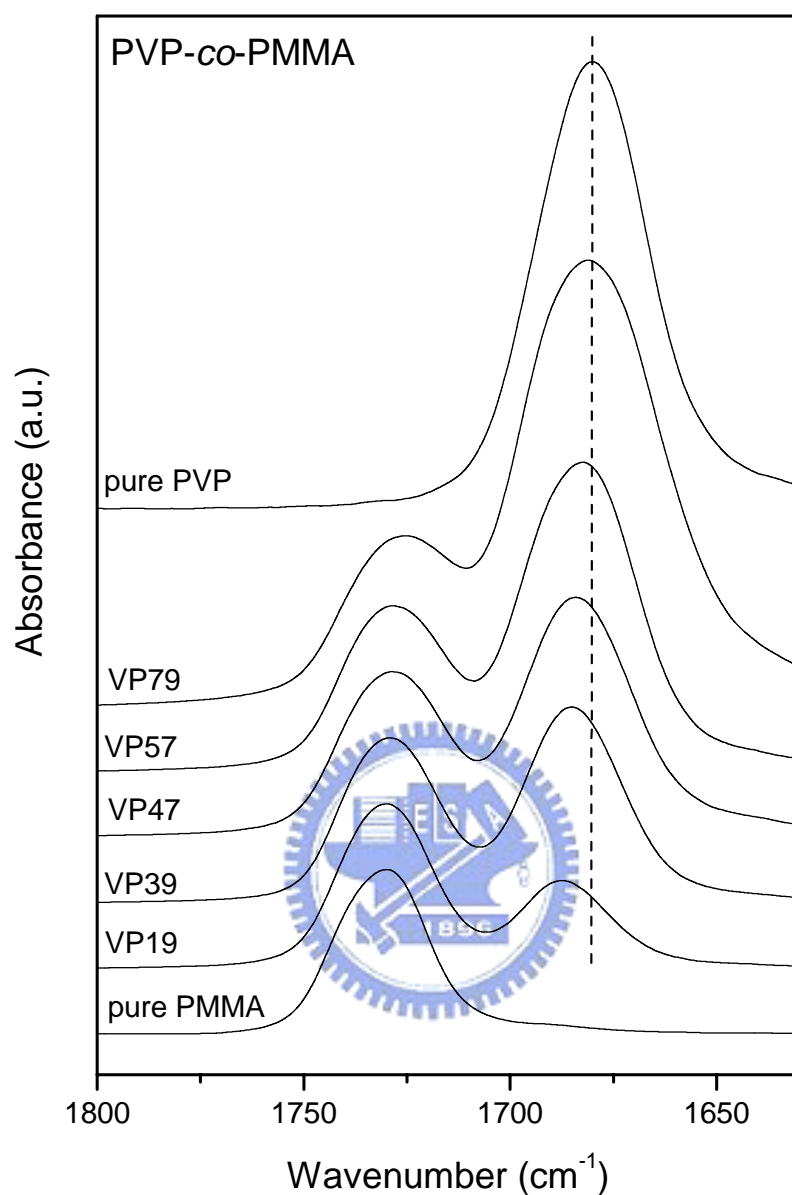
Figure 5-3. The IR spectra at 1800-1630 cm^{-1} of pure PVP, pure PMMA and PVP-*co*-PMMA copolymers with various PVP contents at 120 °C.
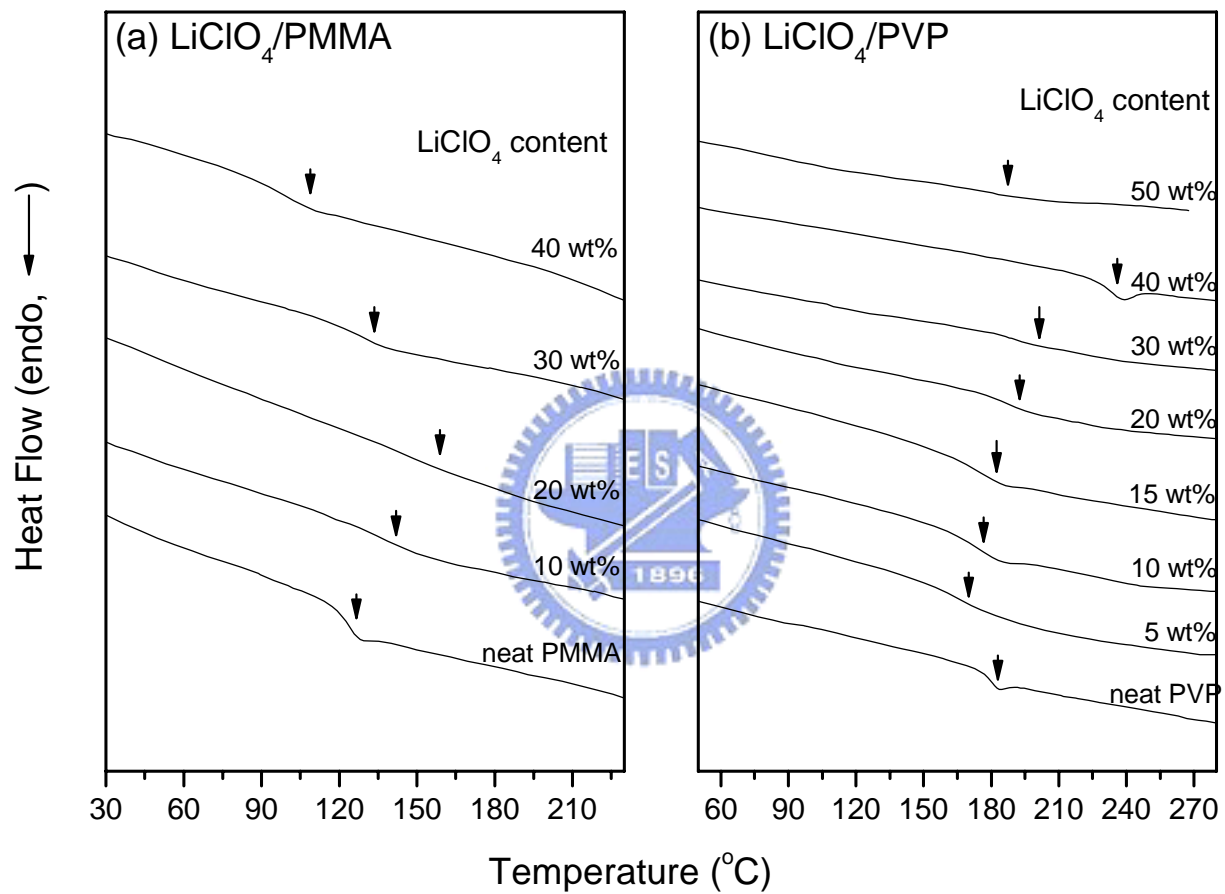
**Figure 5-4.** DSC scans for (a) LiClO₄/PVP and (b) LiClO₄/PMMA blends having varying compositions.

148
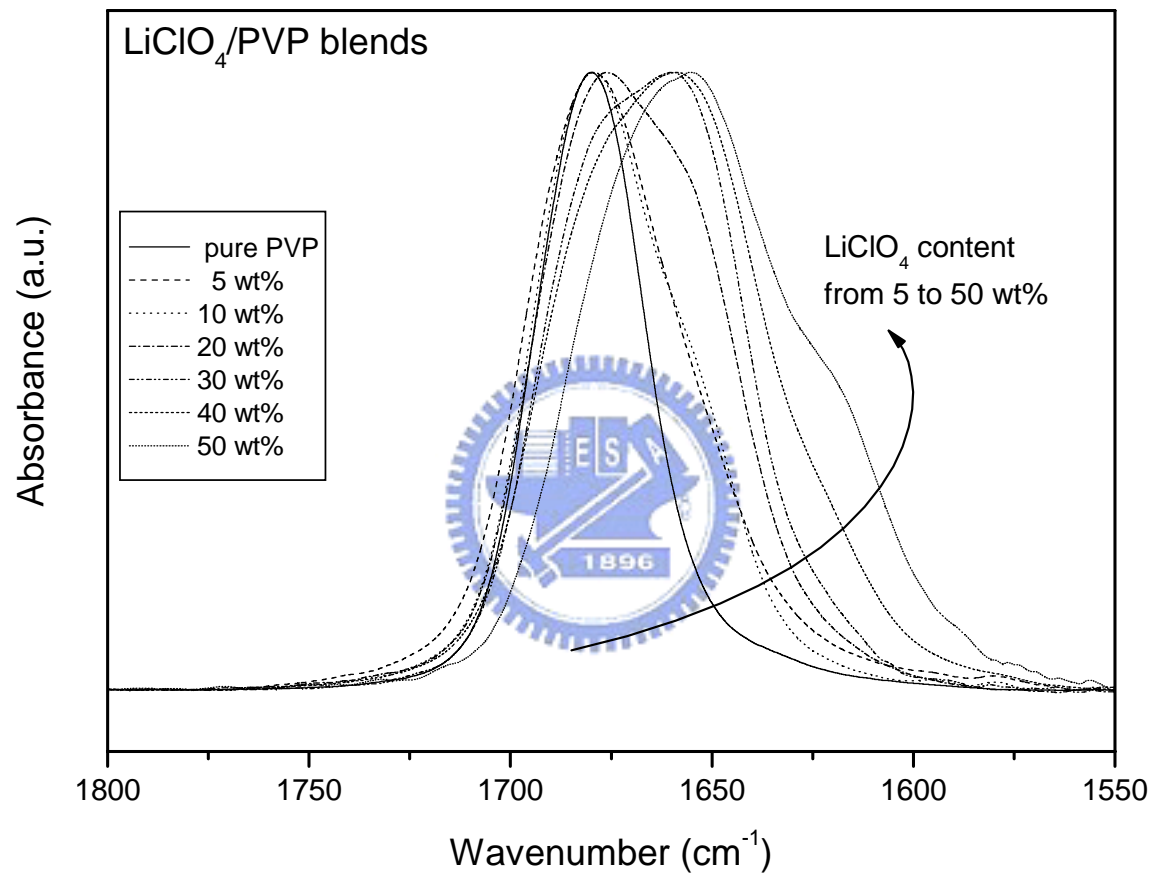
Figure 5-5. Infrared spectra of C=O stretching region of $LiClO_4$/PVP blends containing various $LiClO_4$ content at 120 °C.
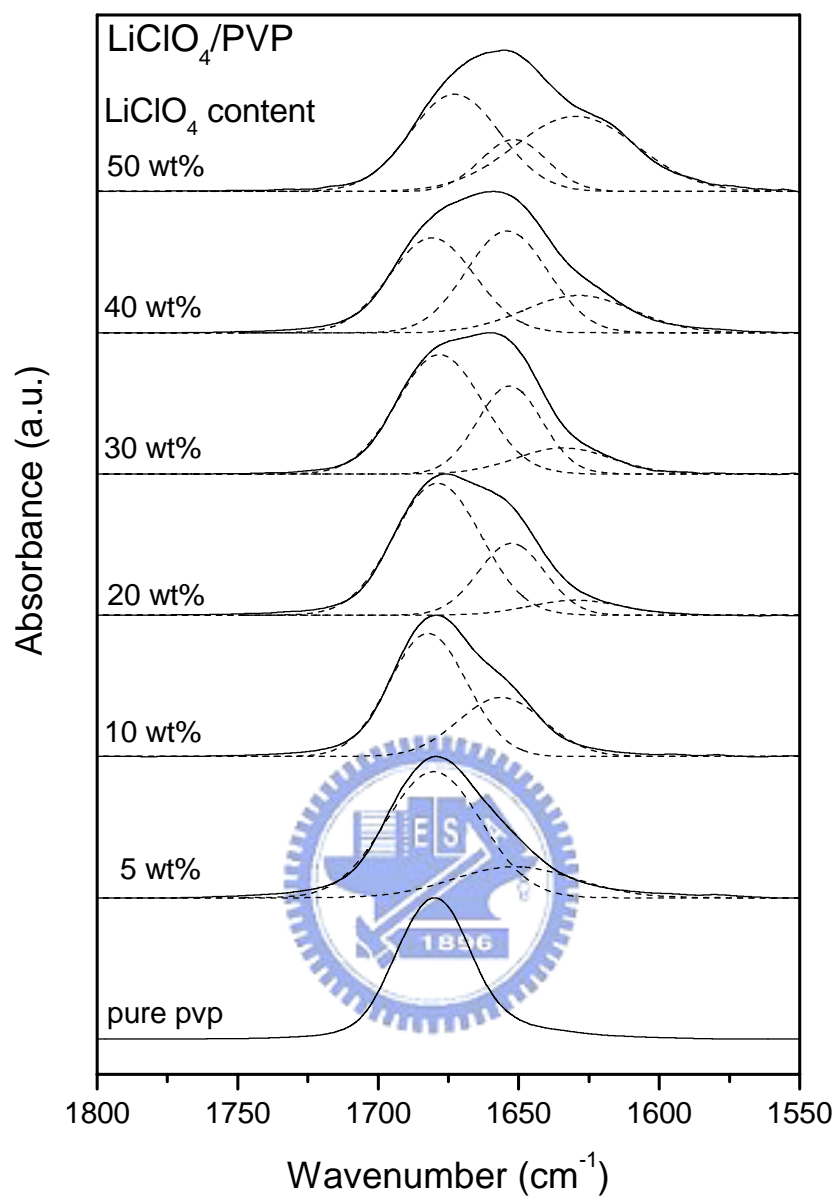
Figure 5-6. Deconvolution of infrared spectra ranging from 1800 to 1550 cm^{-1} of the LiClO$_4$/PVP blend containing various LiClO$_4$ contents in the region of carbonyl stretching recorded at 120 °C.
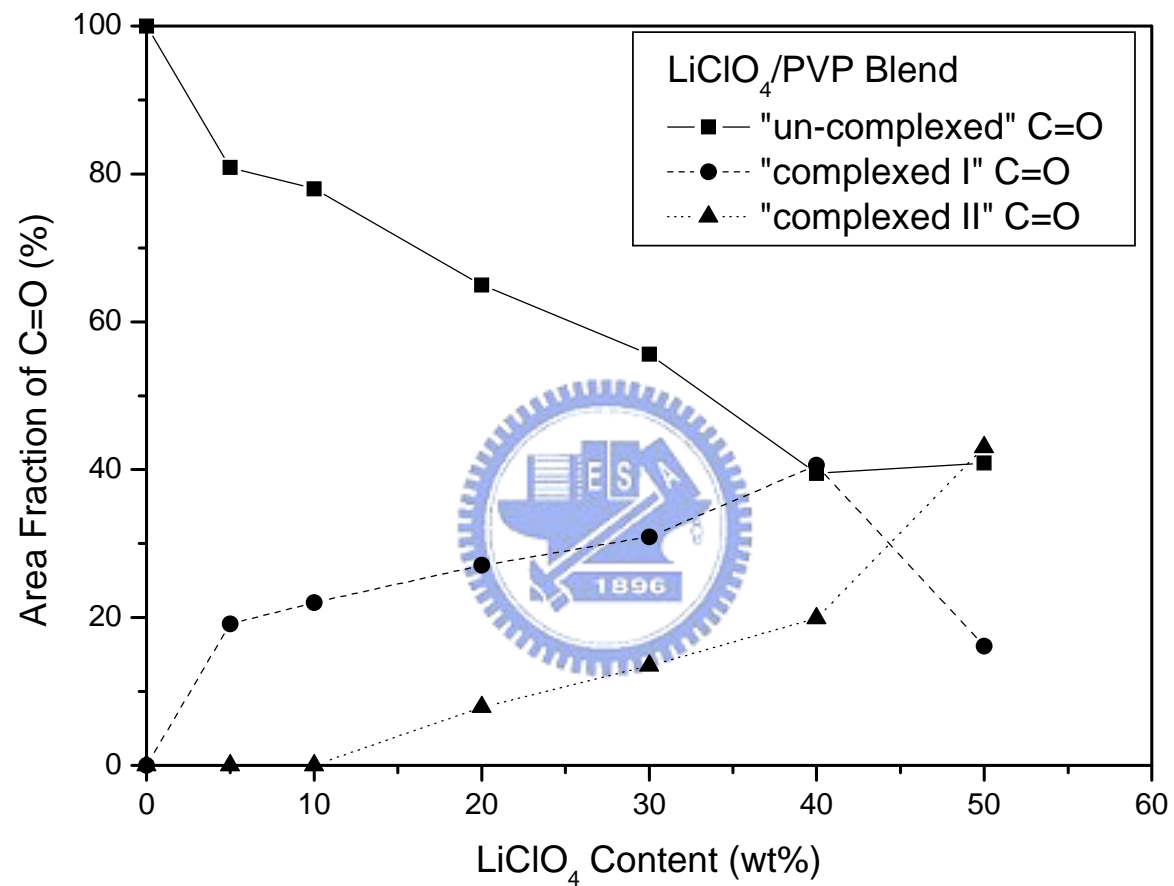
**Figure 5-7.** The dependence of "free" and "complexed" C=O band on LiClO$_4$ salt concentration.

Type A

Type B

Type C

⁙ : dipole-dipole interaction
------ : ion-dipole interaction
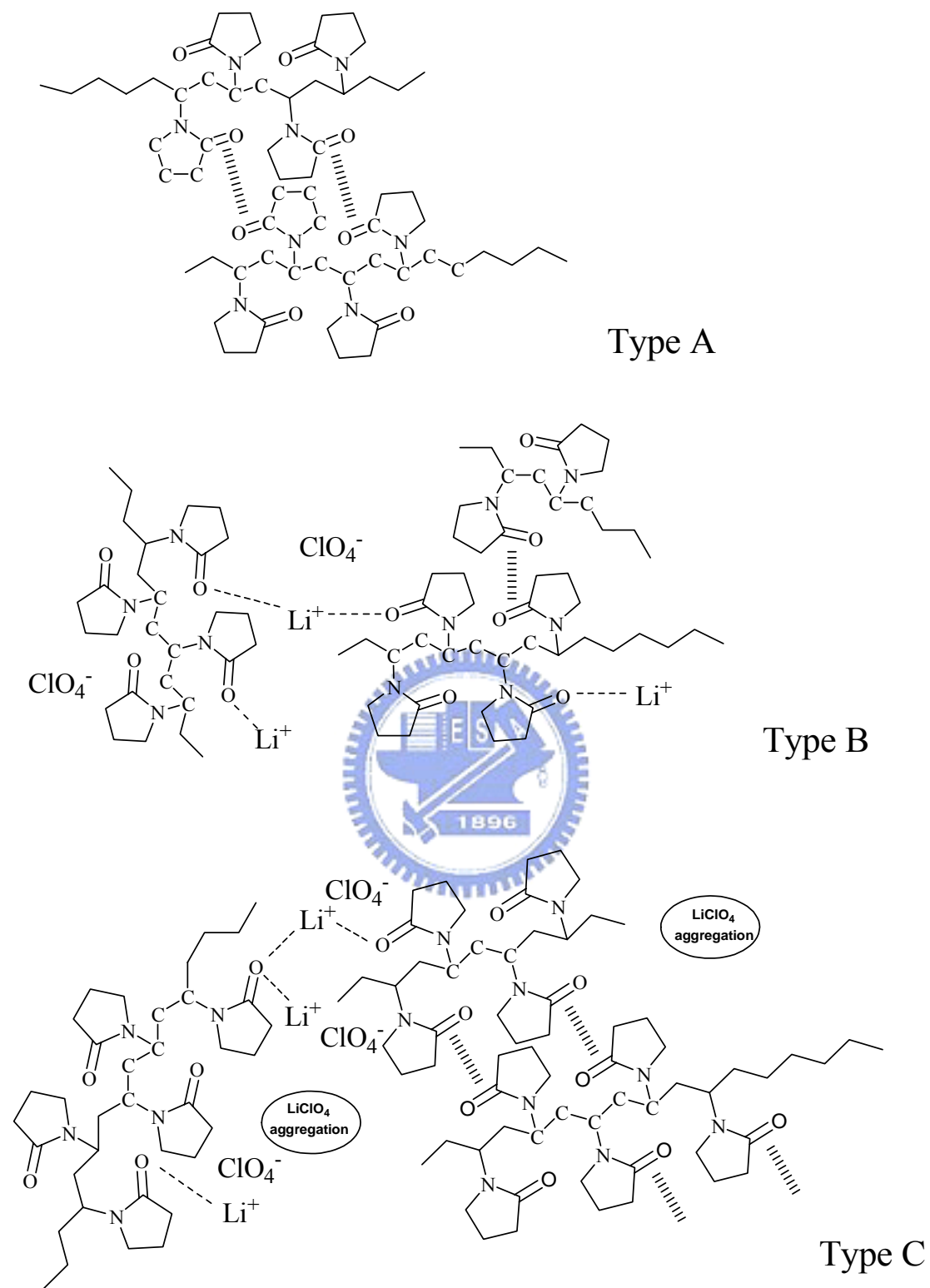
**Figure 5-8.** Proposed association schemes of polymer electrolytes based on LiClO$_4$/PVP.
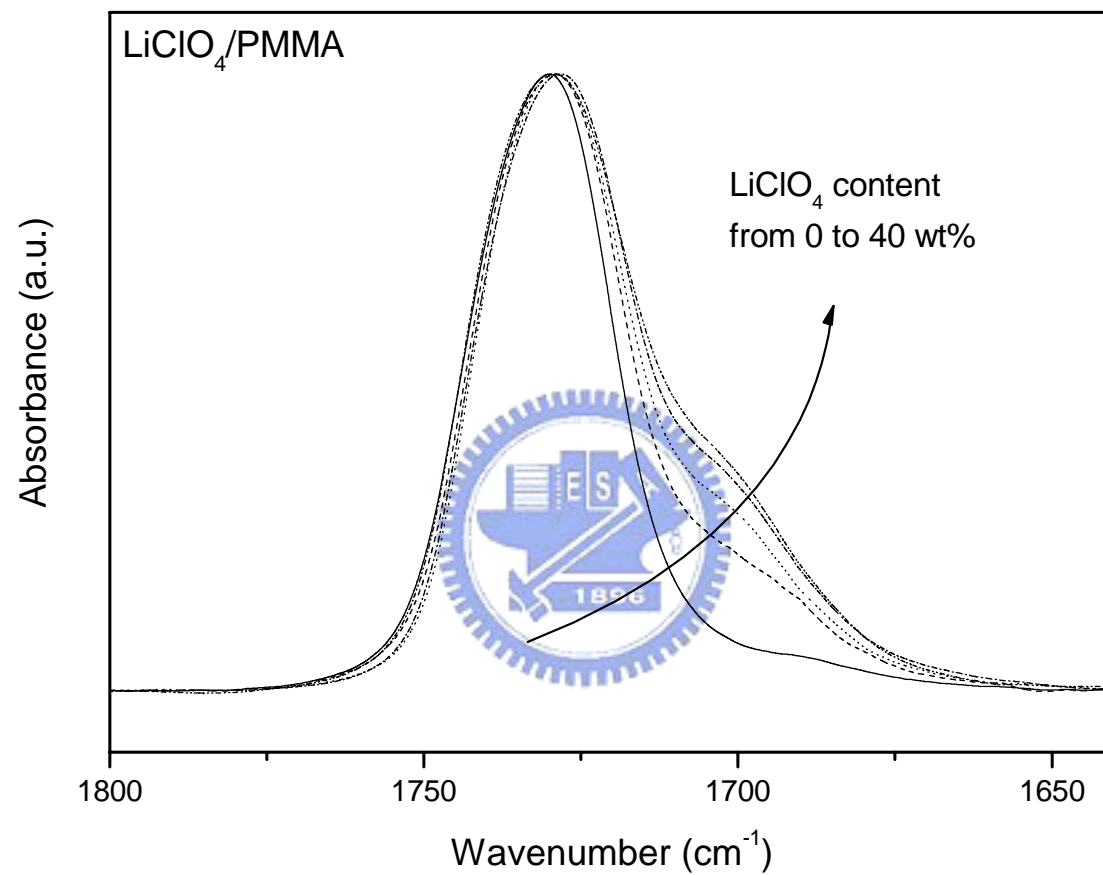
Figure 5-9. Infrared spectra of C=O stretching region of LiClO$_4$/PMMA blends containing varying LiClO$_4$ content at 120 °C.
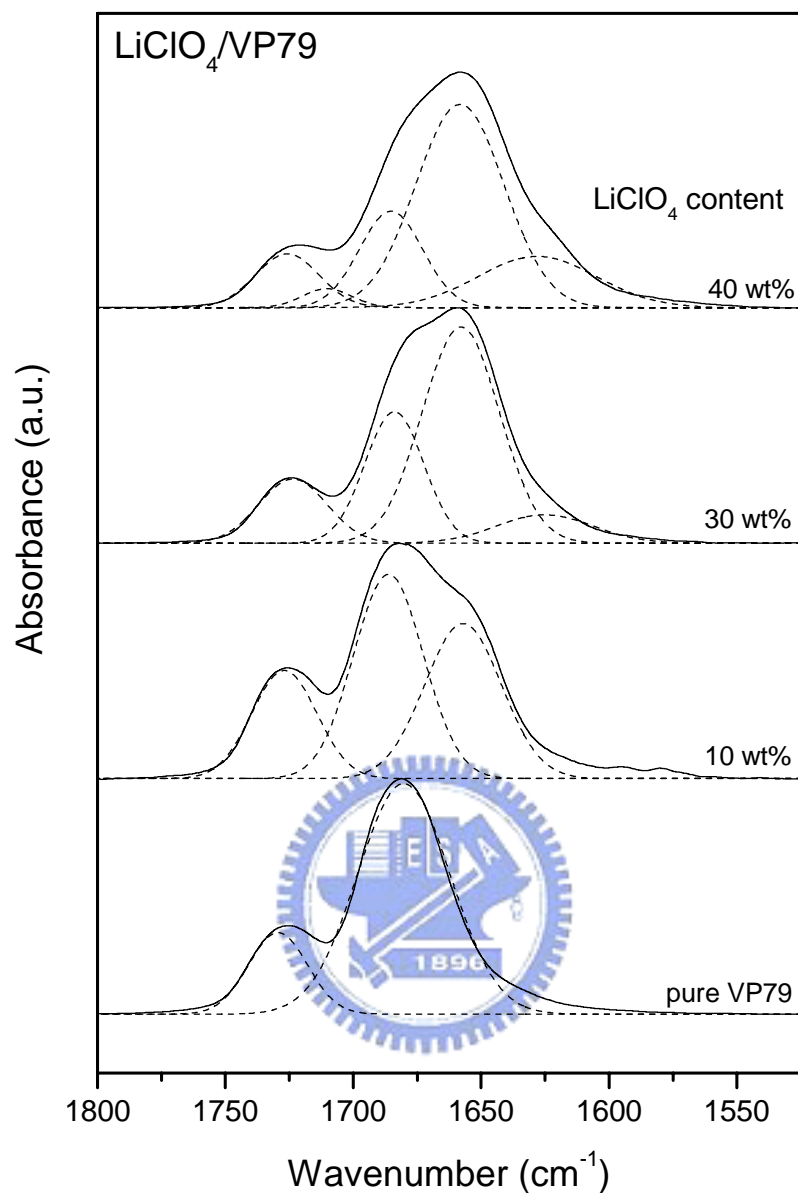
**Figure 5-10.** Deconvolution of infrared spectra ranging from 1800 to 1525 cm^{-1} of the LiClO$_4$/VP79 blend containing various LiClO$_4$ contents in the region of carbonyl stretching recorded at 120 °C.
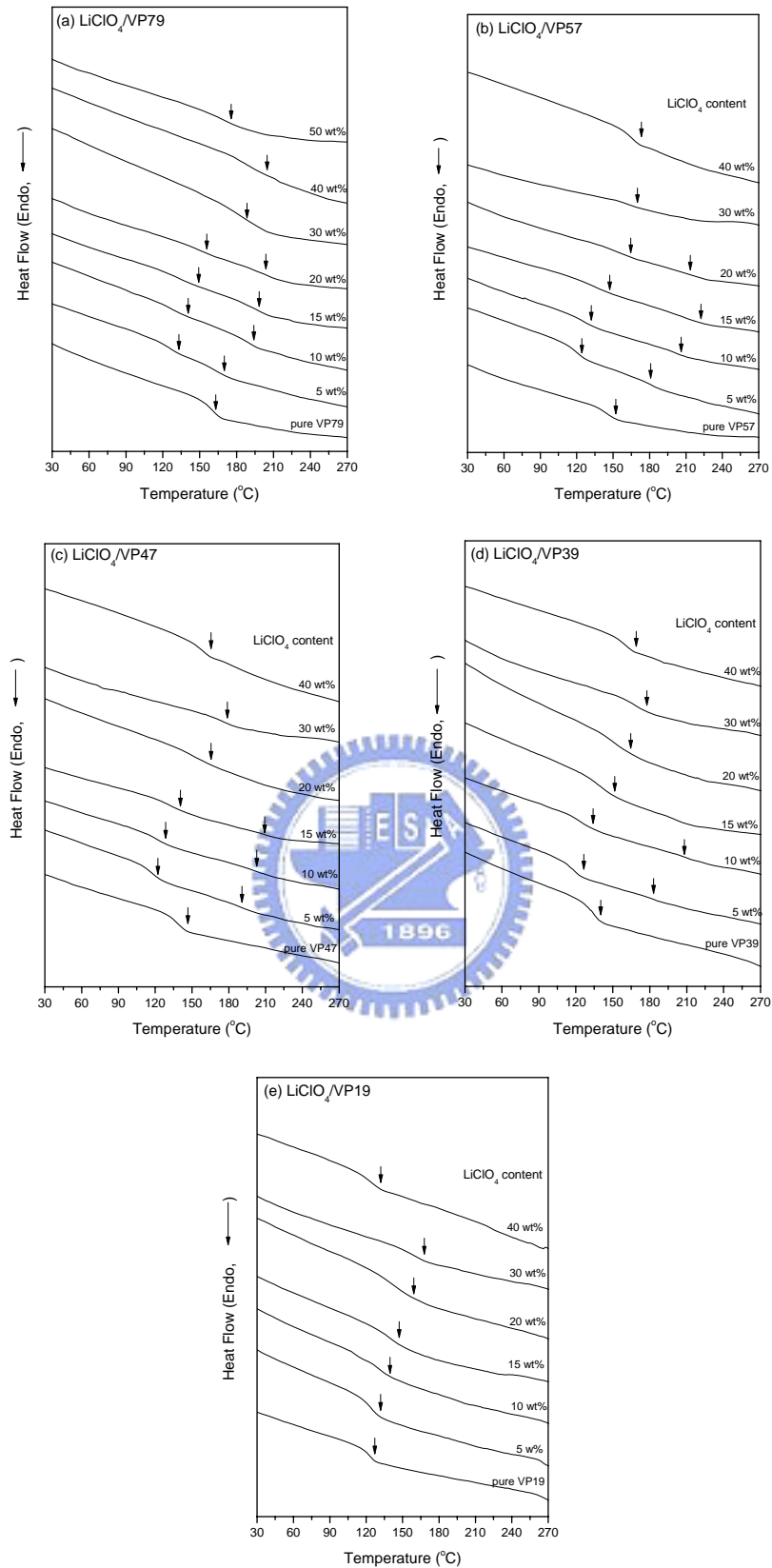
**Figure 5-11.** DSC thermograms of LiClO₄/PVP-*co*-PMMA blend containing various LiClO₄ salt contents: (a) VP79, (b) VP57, (c) VP47, (d) VP39, (e) VP19.
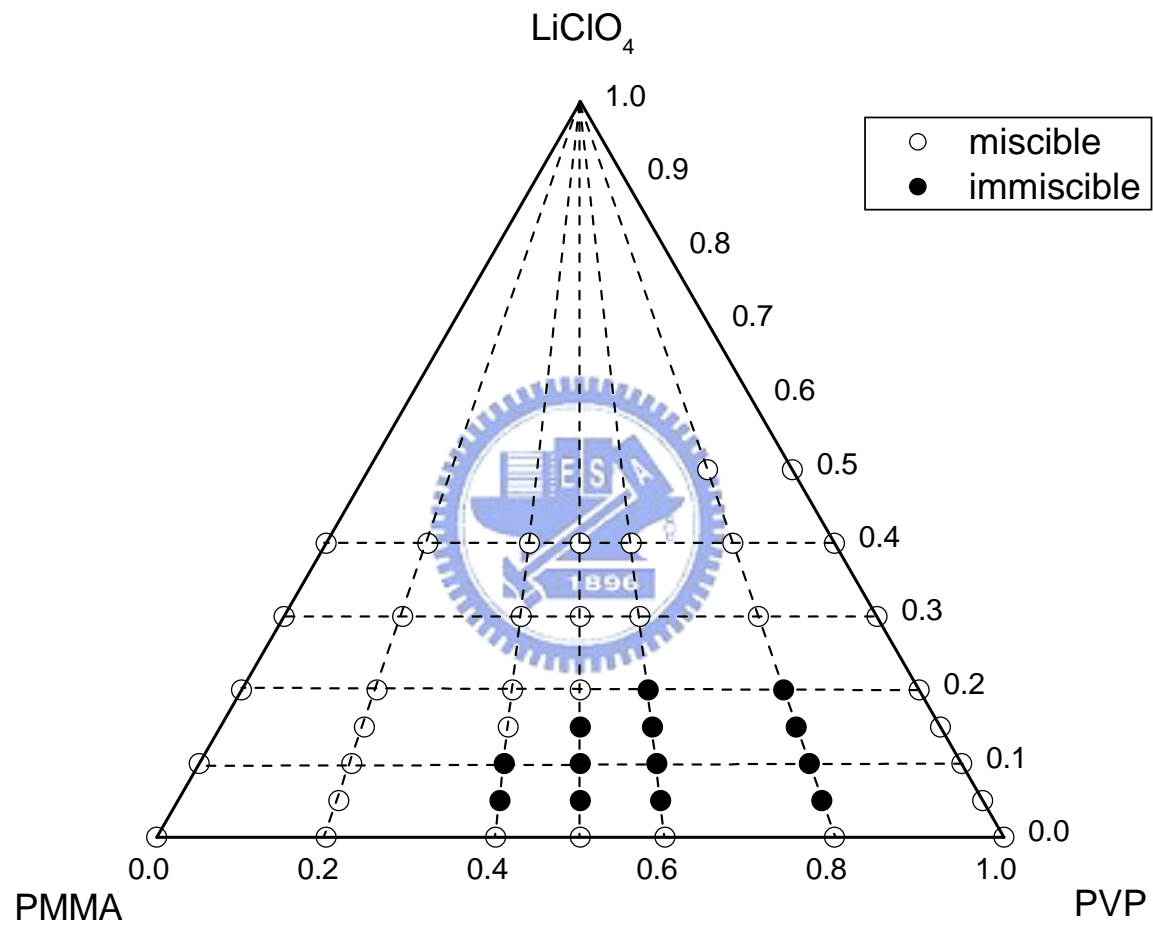
Figure 5-12. Ternary phase diagram of the LiClO$_4$/PVP-*co*-PMMA system. The open circles represent a miscible blend, and the full circles represent an immiscible blend.
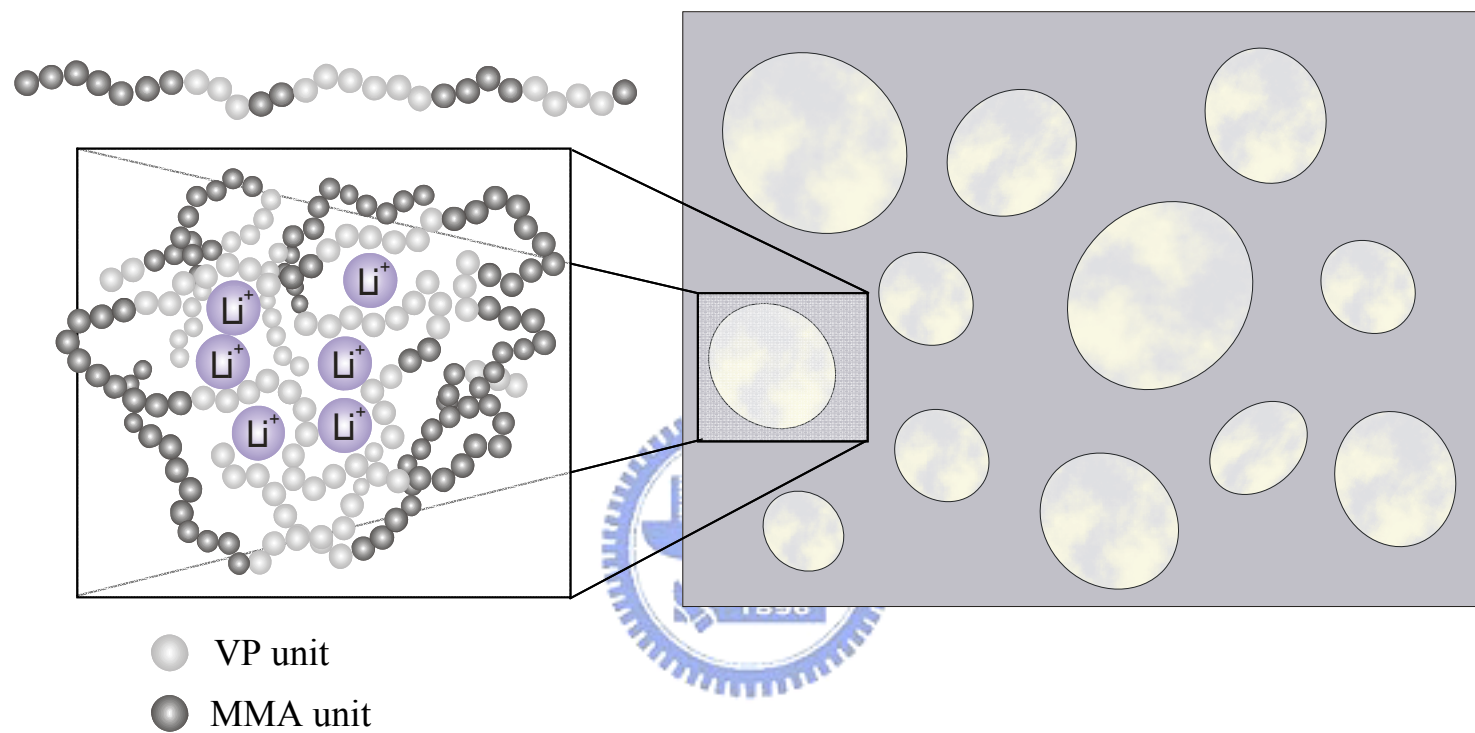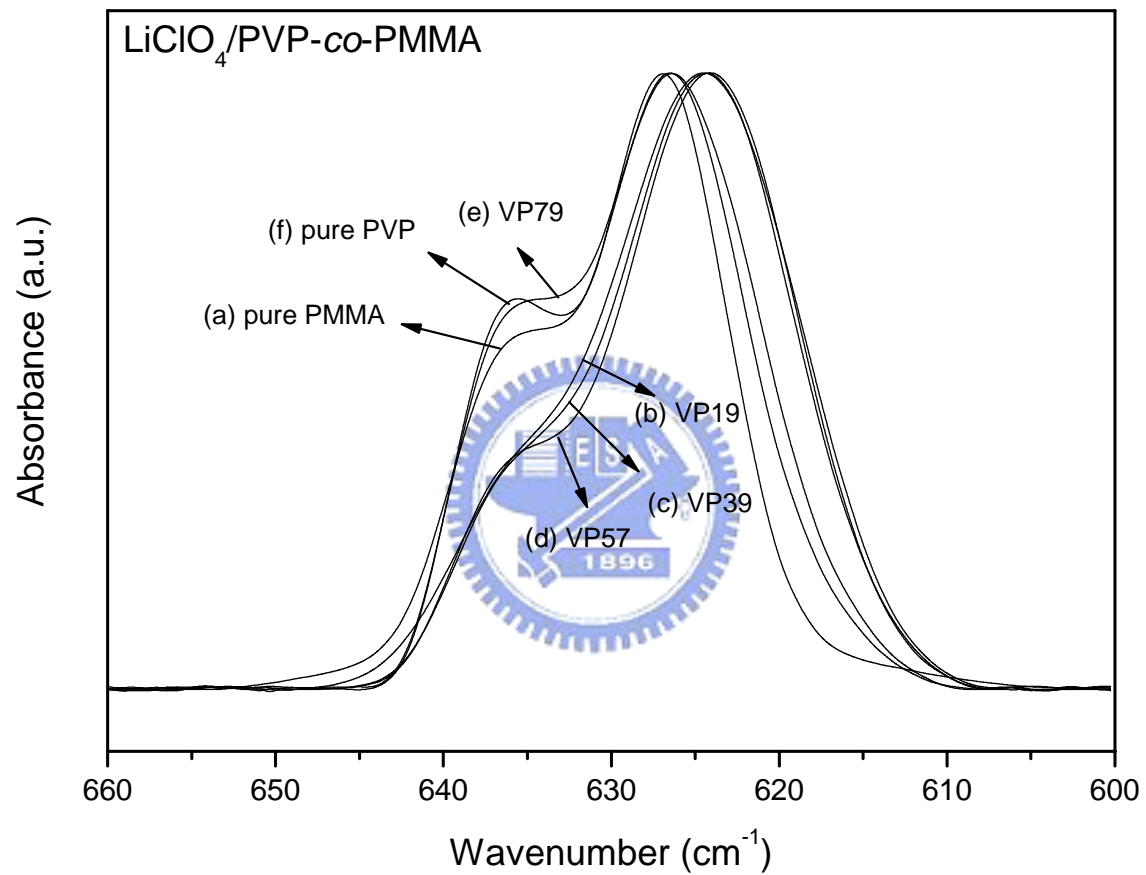
Figure 5-13. Proposed schematic drawing of phase separation occurring in the LiClO$_4$/PVP-*co*-PMMA blend.
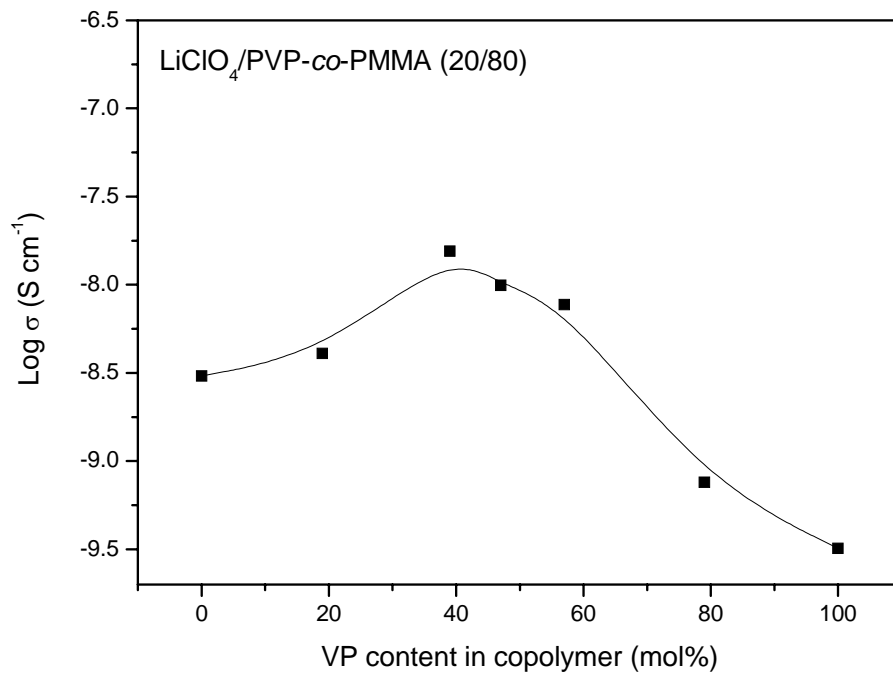
Figure 5-14. Ionic conductivity versus VP content in PVP-*co*-PMMA copolymers plots for LiClO₄/PVP-*co*-PMMA blends at 30 °C.
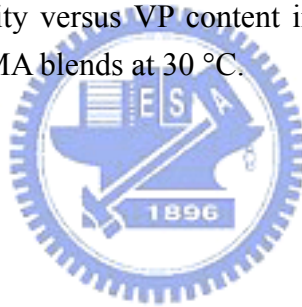
Figure 5-15. Infrared spectra of ν (ClO$_4^-$) internal vibration modes for LiClO$_4$/PVP-*co*-PMMA with various compositions.

CHAPTER 6

General Conclusions

We have described, in this dissertation, miscibility behavior, interaction mechanism and ionic conductivity of $LiClO_4/PEO/PCL$, $LiClO_4/MPEG$-PCL, and $LiClO_4/PVP$-*co*-PMMA blends-based electrolyte systems by using DSC, FTIR spectroscopy, solid-state ^{7}Li NMR, and ac impedance and made some conclusions as follows:

(a) Although each of the three individual binary pairs, in the $LiClO_4/PEO/PCL$ ternary blend, is fully miscible, a closed-loop immiscibility region exists in the ternary blend's phase diagram. Lithium cation more preferably coordinates with ether oxygen atom of PEO rather than with the carbonyl group of PCL. When $LiClO_4$ salt is added to the PEO/PCL binary blend, the PCL component tends to be excluded, which causes the phase separation of these ternary blend. Moreover, the presence of a small content PCL in the PEO phase is able to retard or inhibit crystallization because PEO and PCL are fully miscible in the amorphous phase at all compositions. This factor is responsible for the observed increase in ionic conductivity of $LiClO_4/PEO/PCL$ blend.

(b) The presence of PCL in the MPEG-PCL block copolymer tends to suppress the crystallinity of MPEG as a consequence of the miscibility between MPEG and PCL. Thus, the ionic conductivity of $LiClO_4/MPEG$-PCL blend system at room temperature is higher than that of $LiClO_4/MPEG$-based polymer electrolyte. Besides, raising the concentration of $LiClO_4$ salt or increasing the length of the PCL block in the $LiClO_4/MPEG$-PCL blend increases the relative intensity of stretching band for the "complexed" carbonyl group in IR spectra. However, the relative intensities of the "complexed" carbonyl and "complexed" ether stretching

groups tend to be changed in different directions for some compositions of the LiClO$_4$/MPEG-PCL blend system when the temperature is increased.

(c) A single T_g was observed for PVP-*co*-PMMA random copolymers and implied that these copolymers were miscible. In addition, the negative deviation of T_g of PVP-*co*-PMMA was obtained from DSC analyses because PMMA moiety played an inert diluent role to eliminate the self-association of PVP molecules. For the binary blend of LiClO$_4$/PVP, an unusually phenomenon was observed that the addition of low content of LiClO$_4$ salt tends to reduce the strong dipole-dipole interaction within PVP and leads to the decrease the value of T_g of PVP; then, the further increase of LiClO$_4$ promotes T_g of PVP increasing. Combining the effects of n_i and μ_i on ionic conductivity, consequently, it is reasonable to explain that the maximum ionic conductivity is appearing at LiClO$_4$/VP57 (20/80).

In summary, we found that although a polymer matrix, such as PEO or PVP, is excellent for dissociating lithium salts, the barriers, such as crystallization or strong self-association, may exist to limit the transportation of the dissolved ions. Interestingly, such barriers may overcome by incorporating other polymers like PCL or PMMA, which even possess less ability to dissolve salts than that of PEO or PVP. Whether the method of incorporating polymers is through blending or copolymerizing, the resultant materials tend to increase their ionic conductivity while blending with LiClO$_4$ salt. These phenomena can be evidenced by detecting the miscibility behavior and interaction mechanism using DSC, FTIR, and solid-state NMR techniques. Furthermore, they carry key messages for the ionic conduction process and demonstrate how important it will be in the future to adopt a more fundamental view of solid-state polymer electrolytes.

List of Publications

1. Chen, Hsien Wei; **Chiu, Chun Yi**; Chang, Feng Chih "*Conductivity Enhancement Mechanism of the PEO/Modified-Clay/LiClO₄ Systems*", *Journal of Polymer Science: Polymer Physics Edition* **2002**, *40*, 1342.

2. Chen, Hsien Wei; **Chiu, Chun Yi**; Wu, Hew Der; Shen, I Wen; Chang, Feng Chih "*Solid State Electrolyte Enhancement Based on Poly(ethylene oxide), Poly(oxypropylene) deamine, Mineral Clay and Lithium Perchlorate*", *Polymer* **2002**, *43*, 5011.

3. Chen, Hsien Wei; Jiang, Chang Hung; **Chiu, Chun Yi**; Wu, Hew Der; Chang, Feng Chih "*Hydrogen Bonding Effect on the Poly(ethylene oxide), Phenolic Resin, and Lithium Perchlorate-Based Solid-State Electrolyte*", *Journal of Applied Polymer Science* **2004**, *91*, 1207.

4. **Chiu, Chun Yi**; Chen, Hsien Wei; Kuo, Shiao Wei; Chang, Feng Chih "*Investigating the Effect of Miscibility on the Ionic Conductivity of LiClO₄/PEO/PCL Ternary Blends*", *Macromolecules* **2004**, *37*, 8424.

5. **Chiu, Chun Yi**; Hsu, Wen Ho; Yen, Ying Jie; Kuo, Shiao Wei; Chang, Feng Chih "*Miscibility Behavior and Interaction Mechanism of Polymer Electrolytes Comprising of LiClO₄ and MPEG-block-PCL Copolymers*", *Macromolecules* **2005**, *38*, 6640.

6. **<u>Chiu, Chun Yi</u>**; Yen, Ying Jie; Chang, Feng Chih "*Studying the Effect of Complicated Interaction on the Phase Behavior and Ionic Conductivity of PVP-co-PMMA-Based Polymer Electrolytes*", in modified.

7. Yen, Ying Jie; **<u>Chiu, Chun Yi</u>**; Chang, Feng Chih "*Specific Interaction and Miscibility Behavior in Blends of Octa-Phenol-Polyhedraloligomeric silsesquioxane (POSS) with PVP-co-PMMA Copolymers*", in preparation.

Introduction to the Author

English Name: Chiu, Chun Yi

Chinese Name: 邱俊毅

Birthday: 1978, 10, 07

Address: 412 台中縣大里市東榮路一段 5 號

E-mail: jychiou.ac90g@nctu.edu.tw

Education:

1997, 09 ~ 2001, 06	**B.S.**, Department of Applied Chemistry, National Chaio Tung University, Hsinchu, Taiwan, ROC.
2001, 09 ~ 2002, 06	**M.S.**, Institute of Applied Chemistry, National Chaio Tung University, Hsinchu, Taiwan, ROC.
2002, 09 ~ 2005, 09	**Ph.D.**, Institute of Applied Chemistry, National Chaio Tung University, Hsinchu, Taiwan, ROC.